GENERATION AND CHARACTERIZATION OF FIREBRANDS FROM SELECTED STRUCTURAL FUELS

by

Faraz Hedayati

A dissertation submitted to the faculty of
The University of North Carolina at Charlotte
in partial fulfillment of the requirements
for the degree of Doctor of Philosophy in
Mechanical Engineering

Charlotte

2018

Approved by:

_____
Dr. Aixi Zhou

_____
Dr. Russell Keanini

_____
Dr. Stephen Quarles

_____
Dr. Stuart Smith

_____
Dr. Nenad Sarunac

_____
Dr. Navid Goudarzi

_____
Dr. Mohammad Kazemi

ABSTRACT

FARAZ HEDAYATI. Generation and characterization of firebrands from selected fuels. (Under the direction of DR. AIXI ZHOU and DR. RUSSELL KEANINI)

Over the past few decades, thousands of lives and billions of dollars have been lost due to large open fires. Spotting caused by airborne burning firebrands (or embers) is a fundamental mechanism for fire spread in large fires in wildland, urban, and wildland urban interface (WUI) communities. Firebrands can travel more than a mile from their origin and are understood as the only mechanism that can initiate a fire at long distances.

Spotting by firebrands, or the firebrand phenomenon, can be understood in three major sequential phases: production, transportation, and ignition of the recipient fuel. Numerous studies have been conducted to understand the firebrand phenomenon since the 1960s. Firebrand generation is the first step and the basis for understanding the subsequent processes but has been the least studied phase. A limited number of studies have been devoted to the generation of firebrands from different fuels. Also, firebrand generators have been built to generate firebrands for experimental. Most of the previous researches on firebrand production focused on the experimental design and data collection, with significantly less efforts on a theoretical framework of the phenomena and a systemic analysis of experimental data.

This research analyzes the generation of firebrands from selected structural fuels. Having established this as the main goal, the flowing objectives are achieved. First, the Bayesian statistics is employed to analyze the available data and suggest proper Probability Density Functions (PDFs). Secondly, choosing the standard deviation 0.55 and the margin of error 0.03, a statistical analysis shows that the sample size needs to be

at least 1300. Several tests to generate firebrands from such structural components as wall and corner assemblies and fences were conducted. To be more conservative, at least 1400 samples from each test were collected. Such a large sample size required a more efficient measurement process as opposed to the conventional tedious methods. To address that, thirdly, a new framework to facilitate the cumbersome measurement process is developed. Among several quantities of interest for the measurement, projected area and mass are the most challenging ones. An efficient image processing algorithm is proposed for the former; for the latter, two predictive models are created, which can estimate the mass for each firebrand without physically weighing them. Fourthly, the effects of wind speed on the surface temperature of the smoldering firebrands are monitored with an infrared camera.

The results from chapter two indicated that the bivariate truncated normal and bivariate lognormal distributions had the highest likelihood among other probability density functions. Mass and projected area were strongly correlated, but their correlation with flying distant was either weak or moderate. The predictive models and image processing algorithm presented in chapter three was able to reduce the measurement time for mass and projected area significantly. The mean, standard deviation, and correlation between the parameters can be predicted within 10% error, measuring only 70% of the data (900 instead of 1400 measurements). In chapter five, a statistical analysis of the results concluded that it was more likely that the emissivity of the smoldering firebrands varies between 0.95 and 1. Setting this value on the infrared camera, the temperature reached 1000 degrees C at 6 m/s wind speed. However, the medium wind (3 m/s) may pose a greater threat because the firebrands can burn for a longer period of time.

DEDICATION

To my beloved family, without their support and love, none of this would be possible.

ACKNOWLEDGMENTS

First and foremost, I would like to express my sincere gratitude to my advisor, Professor Aixi Zhou, for his patience, attention, and continuous support. He cares deeply for his students, and as a result, he has made time to guide and to assist me in the research and writing processes. I could not have finished this thesis so efficiently without him.

For insightful comments, time, and plenty of encouragement, I absolutely need to thank the Mechanical Engineering department's contribution to my doctoral committee: Professor Stuart Smith, Professor Russel Keanini, Professor Nenad Sarunac, and Tracy Beauregard department's student specialist. I also give special thanks to Dr. Mohammad Kazemi, the graduate school representative and Dr. Navid Goudarzi for their time and patience.

Equally invaluable, I also thank the Insurance Institute for Business and Home Safety scientists and technicians whose help is much appreciated, I simply cannot express my gratitude in words. My work could not have been accomplished without the monumental support and cooperation of Dr. Stephen Quarles, the chief scientist for wildfire and durability at IBHS.

I express thanks to my fellow lab-mates Dr. Vahid Hemmati, Jacob Kadel, Gregorio Mesa, Noah Bull, Ja'Juan Battle, and Babak Bahrani for their support. I have enjoyed our three years of growing together as friends and scholars. I extend extra thanks to Dr. Hemmati for invaluable intellectual banter and inspiration.

For every person who appreciates a properly placed comma, you will want to join me in thanking Chris Harrington, Caitlin Lejeune, and Dr. Lisa Russell-Pinson, all who were vital to the writing and editing (and re-re-editing) process.

I save my final acknowledgment for my family, particularly my mother, father and sister, for their love and support throughout my graduate endeavors and life aspirations.

Table of Contents

List of Tables

List of Figures

CHAPTER 1: INTRODUCTION

1.1. Problem Statement

Wildfires threaten lives and properties worldwide. In this research, they are defined as fires which have almost unlimited access to the oxygen and fuel. The international Association of wildland fire reports that in the United States, the average number of lost structures in wildfires per decade has grown dramatically over the past 50 years; from 209 in the 1960's to 3000 in the 2000s. Fighting against the WUI fire costs 4.7 billion dollars every year [1-3]. It is apparent that the problem is growing and becoming more severe. This threat is not only limited to the wildland. It is hazardous to urban areas and their interface with wildland, which is often called Wildland Urban Interface (WUI). The WUI is a geographic location where manmade structures meet undeveloped wildland [4].

In open fires, three mechanisms have been renown for spreading of fire: (1) direct flame contact, (2) radiant and convective heat flux, and (3) firebrands. A 2008 study found that the direct flame and radiant/convective heat flux mechanism is relatively weak and ultimately incapable of initiating another fire when the distance is more than 100 feet [3]. Therefore, the first two mechanisms are less dangerous with distance from source. On the other hand, firebrands are capable of initiating spot fires miles from the fire line. Wells reports that firebrands were found 6 miles away from the fire origin near the Lake Michigan [5]. These flying hot objects can be either burning combustible materials (wood) or high temperature non-combustible materials (metals) depending on their origin at which they have been lofted. Given both the firebrands' ignition capabilities at far distances as well as the diversity of the firebrands' origins [6], the natural problem culminates around the

firebrands' potential for catastrophic destruction. Therefore, the primary objective of this research is to investigate and characterize firebrand generation and distribution from selected fuels.

Spotting process by firebrands can be divided into three sequential key phases: generation, transportation, and ignition of the fuel bed. As a result of the abundance of available literature, it is clear that the first two phases have been the areas that the researchers have focused on the least [7]. Limited number of studies have addressed the generation of firebrands, most have focused on explaining the experimental design and firebrand collection method. However, less attention has been devoted to the measurement process, repeatability and reproducibility of the data, and statistical analysis of the results.

Running firebrand generation tests are extremely expensive, financially, time-wise, and labor-wise. Tens of thousands of firebrands are generated in each test and it is not feasible to measure the physical quantities of interests for the entire population. Thus, sampling plays an important role in the measurement process. In the current literature, sample size is typically hundreds of firebrands without any statistical analysis of the sample size. If a statistical test suggests a sample size significantly larger than 500, the efficiency of the current measurement methodology so as to count and measure thousands of firebrands must be explored.

In addition to the above mentioned issues, the surface temperature of the smoldering firebrands has not yet been measured accurately. Temperature is one of the influential parameters in ignition of solids, which needs to be addressed. This could provide a better understanding of ignition potential of the fuel bed.

1.2. Objectives, Goals and Scopes

Considering the issues raised in section 1.1, the main goal of the current research is generating and characterizing firebrand from selected structural fuels. The ignition potential of firebrands depends on several parameters such as: their traveling distance and distribution model, thermal inertia, the surface with which the heat flux transfers to the recipient fuel, and the firebrand surface temperature. In order to investigate these parameters, the following objectives were established;

I. Review previous studies on firebrand generation and development of a Probability Density Function employing Bayesian Statistics
II. Conduct numerous tests to generate firebrands and collect a statistically sufficient sample to characterize
III. Develop a framework to facilitate the measurement by employing machine learning and image processing techniques
IV. Measure the surface temperature of a smoldering firebrand

The following tasks were developed to address the the first objective: (1) collect and categorize all the published experimental data, (2) calculate the fundamental statistical factors (mean, standard division and median), (3) optimize the likelihood function to find the best probability density functions and compare the functions, and, finally, (4) consider the nature of the problem, present the best PDF(s) and discuss the corresponding results.

To accomplish the second and the third objectives, (1) building components made from different materials and different geometries were burned at three different wind speeds in the IBHS research center test chamber, (2) the generated firebrands were collected, dried and characterized by measuring mass, projected area, frequency and the

burning level of the firebrands. (3) The measurement results were applied to deep and shallow machine learning techniques (Gaussian regression process and neural network) to find the trends in the data and provide a framework for future experiments.

To achieve the fourth objective, noninvasive temperature measurement was used. The accuracy of the measurement relies on the emissivity value. Thus; (1) the emissivity value was calculated using the experimental data, (2) the effects of wind speed and moisture content on the surface temperature of two different materials were monitored using an infrared camera.

1.3. Benefits of This Research

More than one million fires were reported in 2015 where 50 percent of them were outside fires [8] and firebrands were understood to be an important fire spread mechanism. This develop our understanding about the size, mass, distribution pattern, and ultimately their threat. The results of this research will benefit federal and state fire managers, foresters, emergency responders, insurance companies and ultimately code and standard organizations. Also, the outcomes of this research can be employed to educate the public and increase the awareness about wildland fires [9].

1.4. Organization of the Dissertation

This dissertation is a three article based where the first chapter provides an introduction to and analysis of the available data. The second chapter reviews and analyzes all the available literature in the field of firebrand production from structural fuels. In this chapter, after summarizing the experimental procedures, the statistical information of the studies is tabulated, the maximum likelihood method is explained, and the best Probability

Density Functions (PDF) presented. Finally, the results based on the finalized PDF are presented and discussed.

The third chapter deals with generating and analyzing new firebrands. The Gaussian regression process regression is employed to generate a model which can predict the mass of each firebrand. Moreover, using neural networks, another predictive model is built and the results are compared. In this chapter a framework to automate the tedious measurement process is proposed.

The fourth chapter deals with the surface temperature distribution of a smoldering firebrand. First a literature review is performed and then the results of the studies are compared. Having explained the measurement procedure for emissivity, the surface temperature for smoldering firebrands is measured.

Finally, chapter five compares the results from the predictive models and summarizes achievements of this research. Its novelty is explained and future research is proposed.

CHAPTER 2: CRITICAL LITERATURE REVIEW AND ANALYSIS OF THE DATA OBTAINED IN PREVIOUS RESEARCHES

2.1. Abstract

This section provides a probability density function (PDF) based statistical approach for the analysis of available experimental data on firebrand production from structural fuels, based on published between 1960 and the present. The Bayesian approach was employed to select the most likely PDF models. While several PDFs may be used to model firebrand generation, inverse normal, lognormal, and standard normal PDFs underestimated the probability of large, heavy, and far traveling firebrands. The truncated normal PDF usually overestimated but provided a conservative estimation of firebrands, had the most reasonable contour plots, and was therefore selected as an example for further statistical analysis. The results showed that that firebrand mass and size were strongly correlated, while the flying distance and firebrand size were moderately correlated. Using a 95% confidence interval for firebrands from outdoor whole building experiments, the flying distance was in the range of 48.3-50.2 meters from the fire location, the projected area was 14.7-17.6 cm^2, and the mass was in the range of 0.6-3.6g. At the same 95% confidence interval, firebrands from indoor whole building experiments had projected area of 2.5-3.2 cm^2 and mass of 0.2-0.3g. This indicated a difference in the size and mass between firebrands produced from outdoor experiments and firebrands generated from indoor experiments. The achievements of this section can provide us with valuable information for the probability of spot fires. The suggested PDFs can also be plugged into different models to predict more realistic firebrand characteristic distributions.

2.2. Introduction and Summary of the Previous Experiments

The growth in the urbanization rate in the United States has been dramatic in the past century; from 39% in 1980 to 75% in 1990 [10]. This leads to the development of wildland for human inhabitants. The Wildland-Urban Interface (WUI), was the magnet for this development in a way that in the United States in the 90s, 60% of the new housing constructions was built in the land categorized as WUI [11]. This interaction between the human daily life and the wildland threatened the lives and properties since they were exposed to wildland fires.

As mentioned in chapter one, there are three known fire spread mechanisms out of these only firebrands can cause a spot ignition miles away from the fire front. Depending on the origin and the characteristics of the firebrands, they can cause different levels of threats. Burning vegetation and trees, interaction of power lines with trees and each other, forestry machinery and hitting rocks are among known origins of the firebrands [6]. In addition to those, they may loft from burning structures-residential or commercial- and are hazardous to both urban and wildland areas.

In this research, we focused on the generation and characterization of the structural firebrands. Chapter one is organized as follows; first the previous studies which considered the generation of firebrands will be reviewed and the employed experimental procedure as well as their results will be discussed. These studies were categorized based on the experiment's conditions. Some of the experiments were real world buildings and they are now labeled outdoor whole buildings (OWB), some were mock buildings ignited under the laboratory conditions which are labeled Indoor Whole Buildings (IWB) and some were only building components labeled Indoor Structural Components (ISC). From that,

theoretical studies will be discussed. This section will conclude with discussion about the knowledge gap and the benefits of the current research. In section 2.3 the raw data related to section 2.2 will be presented and then the data will be statistically analyzed to find the best PDF candidates. Then the results, based on the best PDF will be explained, ending with the conclusions of this chapter.

The materials that are employed in constructions can be classified into two key groups: natural and synthetic. In the U.S., natural materials, customarily wood, are used in residential and commercial buildings are mostly cellulosic based products such as wood, structural sheathing, and particleboards. They may be used in different components of the structure, such as in sheathing, framing, roofing, siding, or decking [12]. Moreover, domestic furniture is typically made out of wood and will also contribute fuel to any burning structure.

The earliest full-scale experiments were conducted by Vodvarka in 1969-1970 [13,14]. Several buildings were ignited, but the generated firebrands were collected and analyzed for only eight of the experiments namely Star Center, Batavia, Heartview and Buildings 68-1, 68-2, 68-3, 69-1 and 69-7. The firebrand collecting method for in his experiments was different than other studies; instead of collecting firebrands in water pans, plastic sheets were laid down downstream of the wind and the hot firebrands would melt through the plastic and leave a footprint on the sheets. The size of the holes were measured and reported as well as the distance they traveled. For the sake of brevity, the testing conditions and the building characteristics are presented in table 2.1. The researchers reported that the damaged structures had access to unlimited oxygen through the openings and the rate of firebrand production was higher than undamaged structures. Moreover, at

the time that the roofs were collapsing, the firebrand production rate reached its maximum. One of the deficiencies of this study was that at closer distances to the fire, the researchers did not quantify the number of, reporting the results with descriptive phrases like “too many” or “too dense”.

For almost 40 years no experiments were performed to study the generation of firebrands, with a focus mostly on the characterization of the firebrands which will be discussed later. In 2012, Suzuki and Manzello et al. [15] reported on an experiment where firebrands were collected a from a controlled burn-down of a two story house in Dixon, California. The burn occurred in a sunny day with mild winds. Water-filled pans were laid down at 4 and 18 meters away from the burning building to collect and quench firebrands. In total 139 firebrands were collected from the pans and their mass and projected area were measured.

Since the real world full-size experiments are very expensive to conduct, smaller scale laboratory tests have been performed to enhance our knowledge of firebrands. Yoshioka et al. [16] was the first to conduct a whole building test in a wind tunnel. In this experiment, the wind velocity, temperature, heat flux, and mass change of the burning house were recorded during the experiment. An ignited wood crib was placed close to the house, which ignited the mock building (some other combustible materials were used as well). Two trays were placed two meters from the building one of which was filled with water to preserve the firebrands shape and mass and the other tray was empty to monitor how long the firebrands burned. The schematic of their setup is shown in figure 2.1.

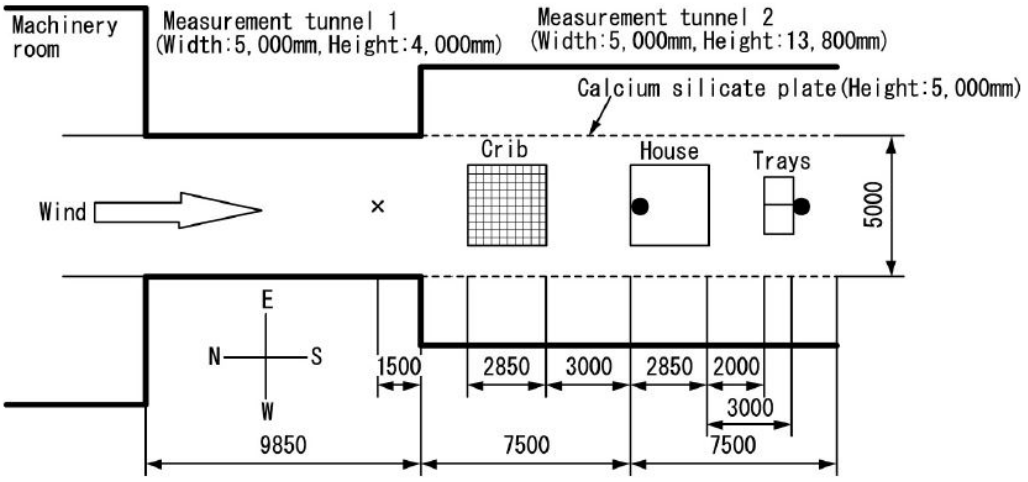

Figure 2-1. Yoshioka et al. experiment layout; taken from *[16]*

Combustion of wood crib and the house, as well as the generation of firebrands were recorded using CCD cameras. Utilizing hotwires and thermocouples, the velocity and temperature were monitored as suggested locations. Heat flux transducers were installed on the brand collectors. Similar to Vodvarka, the researchers concluded that the firebrand production range has a peak at the time the roof collapsed. They also reported that the total number of firebrands and their oven dried weight in the wet tray is about six times greater than that in the dry tray.

Ten years after that, a very similar study was performed by Suzuki et al. [17]. Instead of using only two trays, arrays of water pans were placed downstream of the wind to capture the firebrands. Figure 2.2 depicts the schematic of their setup. There were load cells installed beneath the burning structure to record the mass loss rate and it was observed that for the first 6 minutes, the mass loss rate was almost steady and then it rose sharply. Similar behavior was seen with the temperature variation which was recorded by two

sensors installed, one meter from the ceiling and the other one from the floor. More information about this experiment is provided in Table 2.1.

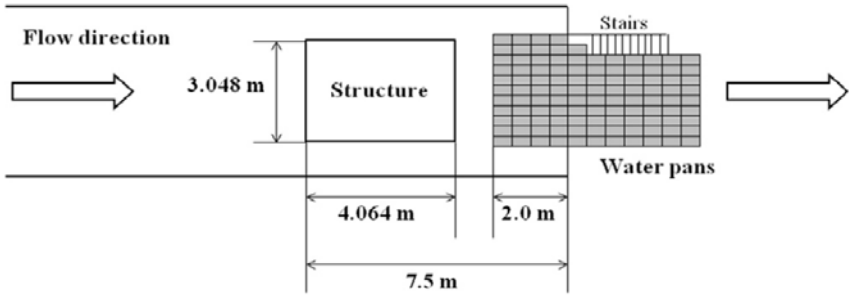

Figure 2-2. Suzuki et al experimental layout *[17]*

The third category include the experiments which considered firebrand generation form the Indoor Structural Component (ISC). The earliest one was performed in 1969 and reported by Waterman [18]. The effect of building height, wind speed and roof type. Since the tests were done at small scale, in order to compensate for the effect of size on material strength, Waterman purposely used butted pieces for 50 percent of the sheathing. The experimental setup did not allow the firebrands to fly for a long distance and as soon as they left the assembly, they were caught by mesh screens. Thus, the firebrands did not have enough time to burn while they were flying and this would affect their size distribution. He reported that most of the firebrands were glowing rather than flaming. It was observed that covering the roof with more shingles can help to keep the roof integrated reduces the number of the generated firebrands. However, if the pathways of air get blocked by overusing the shingles, the pressure beneath the roof increases which causes a more intense firebrand production.

To determine whether burning simple structures can provide realistic information about the characteristics of the real world firebrands, Suzuki et al. [19], conducted a study

to evaluate the generation of firebrands from real scale building components in a wind tunnel; burning wall and re-entrant assemblies were exposed at a wind speed of 6 and 8 m/s. Ultimately, 156 firebrands sampled from a burning wall at 6 m/s wind and 155 and 154 firebrands from a corner assembly at 6 and 8 m/s wind were collected respectively. The experimental setup is very similar to the researchers' previously explained study [17] and thus the setup layout is not provided again.

Suzuki and Manzello [20], studied the effects of siding treatments on similar structural components at 6 and 8 m/s wind speed where 414 and 290 firebrands were sampled from the population for analysis. It was observed that siding treatments do not heavily affect the size and mass range of the firebrands from wall assemblies; however, the distribution has been changed.

Beside the mentioned studies, there has been several reports which focus on generation and collection of firebrands originating from burning vegetation, both in the laboratories and real world forest fires [21,22]. The process of collecting the data was basically the same, however, the burning sample was different types of vegetation. In addition, there have been efforts to build a firebrand generator which can provide information about the size and mass distribution of a firebrand shower; the most well-known one is the NIST firebrand generator often called the Dragon [23-25].

The firebrand phenomenon has been studied from the theoretical point of view as well, with most studies focusing on vegetative fuels. Having taken turbulence into account, Himoto and Tanaka [26], have solved the coupled conservation equations of momentum and angular momentum numerically to obtain the traveling distance of a firebrand. These

research reported that the lognormal probability density function best estimated for firebrand distribution in the longitudinal direction.

Barr and Ezekoye [27], developed a simple mechanical model based on the yielding stress of branches under aerodynamic and weight forces. The breakage model has ultimately coupled with a plume model to explain the transport and mass loss rate of the vegetative fuel. More recently, Tohidi et al. [28] developed another simple model to predict the mechanical failure of the vegetative fuel and generation of a firebrand. Using QQ plots, a lognormal regression was chosen as the input to the Monte-Carlo simulation [29] to predict actual spot fires. In addition, it was determined that the surface area of the firebrand was proportional to its mass by the power of two thirds.

Table 2-1. Summary of firebrand generation experiments using structural fuels

Experiment in Literature	**Structure ID**	**Testing conditions[1]**	**Height[2]**	**Collection Method**
Vodvarka, Star Center **[13]**	OWB1	5.3-8.9 m/s, 1.6 ˚C, 89%	2	Plastic sheets
Vodvarka, Batavia **[13]**	OWB2	4.4-8 m/s, 21.1 ˚C	1	
Vodvarka, Heartview **[13]**	OWB3	8.9-11.1 m/s, 4.4 ˚C	1	
Vodvarka, Building 68-1**[13]**	OWB4	0.9-1.7 m/s, 28.8 ˚C, 65%	2	
Vodvarka, Building 68-2**[13]**	OWB5	0.4-1.3 m/s, 30 ˚C, 70%	1.5	
Vodvarka, Building 68-3**[13]**	OWB6	2.6-3.5 m/s, 28.3 ˚C, 70%	1.5	
Vodvarka, Building 69-1**[14]**	OWB7	< 2.2 m/s, 21.1 ˚C, 75%	2.5	
Vodvarka, Building 69-7**[14]**	OWB8	2.2-15.6 m/s, 13.8 ˚C, 45%	2	
Suzuki et al, at 4m **[15]**	OWB9a	5.7 m/s, 25 ˚C	2	Water pans
Suzuki et al, at 18m**[15]**	OWB9b	5.7 m/s, 25 ˚C	2	
Yoshioka et al., wet**[16]**	IWB1a	2-4 m/s	1	Water pans
Yoshioka et al., dry**[16]**	IWB1b	2-4 m/s	1	
Suzuki et al. **[17]**	IWB2	6 m/s	1	
Waterman **[18]**	ISC1	6.9-15.6 m/s	N.A.	Mesh screen
Suzuki et al., walls**[19]**	ISC2	6 m/s		Water pans
Suzuki et al., corners**[19]**	ISC3a	6 m/s		
Suzuki et al., corners**[19]**	ISC3b	8 m/s		
Suzuki et al., corners**[20]**	ISC4a	6 m/s		
Suzuki et al., corners**[20]**	ISC4b	8 m/s		

1. Testing condition information includes wind speed, temperature, and relative humidity. 2. Building height in stories.

Parallel to the mentioned stream of research, which focused on the generation of firebrands specifically, some other scientists focused on other characteristics including flight path, mass loss, and surface temperature. Only the last parameter, surface temperature, was of interest to the current research. Thus, the studies which focused on the other parameters will not be reviewed here. Rigorous readers can find information about those elsewhere [30-37].

One may notice that there has been huge investments-both financially and timewise- to study the firebrand phenomenon. However, our understanding in this field is still inadequate. The first gap that comes up to the author's mind is that the focus of all the mentioned studies was to develop a repeatable experimental procedure. Typically, most of the publications were dedicated to explaining sample preparation and experimental approach which were followed by a short statistical analysis. Mosely, the statistical analysis section reported the mean and sometimes not even the standard deviation [38] of the collected sample accompany with a busy mass versus project area plot [17,20,19,15]. Often histograms of the mass and size distributions were plotted which could have been plotted more accurately. As a rule of thumb, the number of the bins in a histogram needs to be greater than the square root of the sample size which has not been considered in numerous previous studies on this topic. [24,17,20,19,15]. Most the studies in this field employed graphical methods to suggest a distribution [24]. Graphical tests were qualitative and strongly depend on the opinion of the observer. For example, changing the bin size in a histogram can easily change the histograms appearance and influence how one intents to suggest a distribution. Also, in QQ plots the straightness of the line was the measure to determine the distribution. That "straightness" is also a very qualitative measure. Thus, no

solid statistical background was used to propose a proper PDF. Such a study would (1) provide an understanding the characteristics of produced firebrands from a statistical perspective, (2) assist future theoretical studies since, the results of this study could be used in any statistical approach, such as Monte Carlo simulations, (3) help improve experimental design and procedures in future firebrand production research and (4) provide reliable information to modify the experimental procedures to make realistic, repeatable and reproducible data.

2.3. Raw Data and the Statistical Analysis

The stochastic nature of the firebrand phenomenon, including production, transport and ignition, suggests the statistical-based approach should be favored here for this phenomenon. Whenever a system includes numerous particles, like the firebrand phenomenon, studying each particle individually is somewhat difficult.

It is common sense that larger firebrands are more likely to ignite a material since their thermal inertia is typically higher and a single one of them can be hazardous. This does not mean, however, that smaller firebrands cannot be lethal since they can penetrate through small openings to a house, and if the fuel bed on which they land on is easily ignitable, like carpets, may be extremely dangerous. In addition, the accumulation of small firebrands is also understood as a great threat [39]. Thus, the distribution pattern-mean, standard deviation and the skewness- of the firebrands is very important. The distributions can predict how fatal a firebrand shower can be.

Hence, it is necessary to obtain a probability density function (PDF) that can model the size and mass distribution as well as the traveling distance. The benefits and applications of the PDFs include; (1) as discussed earlier, depending on the geographical

location, small or large firebrands can cause different threats. Thus, the estimating the probability of the different size of the firebrand would be helpful. This goal can be achieved by integrating the probability density function between the specific boundaries. (2) One of the criteria that has been suggested for ignition of solids is the critical heat flux [40]. Since calculating the heat flux for each firebrand is not practical (typically large sample size), estimating how the heat flux may vary with the mass or surface area of the firebrands, employing PDFs, the total energy of a firebrand shower can be estimated as follows:

$$\langle E \rangle = \int_{-\infty}^{\infty} \int_{-\infty}^{\infty} \ldots \int_{-\infty}^{\infty} E_{one-brand}\,(x,y\ldots)\; PDF(x,y\ldots)\; dxdy\ldots \qquad (2.1)$$

where *x, y* and *z* can be different quantities of interest such as mass, projected area, or any other parameter. The PDFs can be plugged into different statistical simulators such as Monte Carlo to predict locations of spot fires. For details, see [28].

(3) The effects of all the important parameters in firebrand generation are embedded in statistical concepts including mean, median and standard deviation from which the PDFs are constructed. It is already known that wind speed, moisture content of the fuel, heat release rate of the burning material etc. affect the generation and distribution of the firebrands. However, there are several unknown influential parameters that have not are understood. The indeterminate approach takes those into account as well. In order to build a PDF, the mean and standard deviation of each experiment needs to be calculated.

2.3.1. Raw data extraction

Table 2.2 represents the mean, median and standard deviation of all the previous researchers. The IDs are defined in table 2.1. For older studies (before the year 2000), the

data is extracted directly from the sources, for more recent studies, we contacted the authors and, requested the raw data from their studies. When the raw data could not be obtained from the authors, the data reported in the original sources were employed. These data are necessary to build any PDFs. An “N.A.” in a cell indicates that this parameter could not be obtained because an analysis could not be performed due to unavailable or insufficient data. Since the sample size is larger than 40 in all the studies, we constructed a confidence interval to have an estimation of the variation range of mass and projected area in the last column.

It should be mentioned that some of the data in table 2.2 is constructed has been slightly modified. In the original Vodvarka’s report [14] ,for OWB7 and 8, addresses both the radius and the angle of the collecting sheets. In order to be consistent with other studies, only flying distant was used in our analysis. Moreover, there are cases in the original studies where the quantity of firebrands were labeled as “uncountable” or “many”; these were not included in the calculations. For OWB1, at 800 ft (243.84 m), the size of the firebrands were not well defined. It was assumed that we only had one firebrand with the mentioned dimension and 39 brands with the area of 2.5×2.5 inch (6.35×6.35 cm). For OWB2, due to insufficient data, we assumed that the size of all the firebrands smaller than 1×1 were normally distributed. Wherever it was necessary, the C size was transformed to cm based on Vodvarka 1969 [13].

Table 2.2 also provides the correlation between different parameters. As mentioned earlier, the influential parameters in the generation of firebrands were correlated which suggesting that there should be a correlation between the characteristics of the firebrands

as well. The primary investigations showed that there was a strong correlation between the mass and projected area. Also, a moderate correlation was observed between projected area and flying distance. Correlations basically defined how the growth in one parameter affected the variation in another. Their value can vary between -1 and 1. If the correlation between two parameters is one, it shows that they are in perfect relation with each other and the growth in one leads to growth in the other one. The Opposite trend can be interpreted for minus one correlation. Zero correlation means the variation of the parameters do not affect each other [41]. Considering the correlations is necessary if they exist, otherwise important terms in the statistical model is neglected which will be explained later. Neglecting the correlations is equivalent to $(x_1 + x_2)^2 = x_1^2 + x_2^2$! Hence the firebrand phenomena needs to be modeled with a multivariate PDF.

Table 2-2. Statistical parameters in each experiment

ID	Sample size	Flying Distance x (m)			Projected Area a (cm^2)			Mass m (g)			$\rho_{x,a}$	$\rho_{m,a}$	Range of 95% C.I.
		μ_x	σ_x	$\tilde{x}$	μ_a	σ_a	$\tilde{a}$	μ_m	σ_m	$\tilde{m}$			
OWB1	212	210.91	32.88	182.88	71.96	60.44	58.06				-0.49		
OWB2	182	29.51	31.41	15.24	14.70	22.60	6.45				0.38		
OWB3	170	103.27	32.73	76.20	24.66	25.71	25.80				-0.11		
OWB4	551	30.14	12.43	21.33	2.22	4.41	1.35				0.13		48.3<x<50.2
OWB5	529	49.81	11.11	50.29	1.88	3.49	1.35		N.A.		0.04	N.A.	
OWB6	236	46.07	12.62	45.72	1.10	1.22	0.45				0.03		17.4<a<17.6
OWB7	1,180	56.10	32.40	38.1	6.34	8.32	2.71				-0.15		
OWB8	1,107	45.04	22.06	47.24	2.85	1.02	2.71				-0.04		
OWB9a	89				2.03	2.70	1.23	0.06	0.10	0.03		0.89	1.9<a<2.8
OWB9b	50				4.50	11.25	1.92	0.12	0.16	0.04		0.51	0.06<m<0.1
IWB1a	368				0.83	0.57	0.62	0.01	0.02	0.01		0.96	
IWB1b	62				1.50	1.26	0.62	0.06	0.07	0.02		0.99	2.5<a<3.2 0.2<m<0.3
IWB2	475				3.26	4.93	1.74	0.29	0.67	0.07		0.98	
ISC1	430,303		N.A.			N.A.		0.12	0.05	0.11	N.A.	N.A.	m ≈0.12
ISC2	156				2.27	2.87	1.31	0.16	0.33	0.05		0.59	
ISC3a	155				3.13	3.19	2.18	0.30	0.44	0.17		0.94	3<a<3.6 0.3<m<0.4
ISC3b	154				4.52	4.08	3.11	0.56	0.72	0.30		0.86	
ISC4a	414				5.66	12	1.33	0.41	1.79	0.04		0.81	3.1<a<4.5
ISC4b	290				1.16	3.28	0.44	0.06	0.25	0.01		0.95	0.16<m<0.37

2.3.2. Statistical analysis of the available data

In this section, the raw data (project area, mass and traveling distance) of the studies from the previous chapter are employed to build different PDFs. Table 2.1 represents all of the studies in which a quantitative report about the size/mass/projected area of the firebrands were reported.

The generation and distribution of firebrands is a complex natural phenomenon which depends on both of fire characteristics and environmental conditions. Fire characteristics itself, depends on construction characteristics [14] (i.e. structure height and material type (heat of combustion), geometry of the structure (i.e. roof type and area), etc. which determines the fire size and fire convection column. Some of the environmental characteristics are wind speed, humidity, temperature and the barriers in the wind flow. Many of the mentioned parameters are strongly correlated to each other and it is very unlikely that modeling a firebrand shower can be accomplished without simplifications. Common ways to model firebrand phenomenon include physical (deterministic), statistical (probabilistic) and/or the combination of these two. In the first approach, the momentum and energy balancing equations for the firebrands and/or the air are considered. An order of magnitude analysis can be utilized here to neglect some terms in the balancing equations, which simplifies the analytical or numerical procedure.

For instance, environmental characteristics, such as wind, and construction features, like the openings and windows affect, the oxygen supply for a burning building. The burning fuel has its own combustion characteristics including heat release rate and the parameters that form the convection column. The convection column play a major role in the generation and distribution of firebrands [33] which needs to be considered in

deterministic approach. Typically, in a deterministic approaches, one may nondimensionalize the equations in order to find a general pattern for the firebrand distribution. This approach is more reliable when parameters which affect the distribution pattern are known. Often, not all the influential parameters in a phenomenon are known and this can affect the accuracy of a model. Employing a deterministic approach, three studies considered the firebrand formation from vegetative fuels. Since it is beyond the scope of the current study, the reader is referred to the original papers [26-28].

As explained in section 2.2, in all the studies in this field, the PDFs are chosen based on the graphical tests such as histograms and QQ plots which are incapable of providing a reliable statistical background. In order to provide a more solid statistical background to select a PDF, in this section, a method will be explained which can help us to develop different PDFs more reliably.

The fundamental statistical concepts that have been provided in section 2.2 are applicable to all the PDFs in different ways. In order to find the most appropriate PDF, the Bayesian Maximum Likelihood Method was employed. The maximum Likelihood Method estimates the best way to employ the fundamental statistical concepts (mean and standard deviation) to maximize the probability of fitting of the model. The Bayesian Information Criterion (BIC) [42] can help us in this regard, which can be calculated as follows:

$$BIC(s) = -2\log(\mathrm{L}_n\,\theta(\mathrm{s})) + \nu(\mathrm{s})\log(\mathrm{n}) \qquad (2.2)$$

where $\mathrm{L}_n\,\theta(\mathrm{s})$ is the likelihood function, $\nu(\mathrm{s})$ is the number of components in the model, and *n* is the sample size. Having calculated the BIC scores for a set of known PDFs, the PDF corresponding to the lowest BIC score can be presented as the most probable

function to occur [43]. Generally speaking, if the difference in BIC scores is larger than 10, then there is strong support that the models are different [44].

More than 200 PDFs exist in statistics and calculating the BIC score for all data set is not feasible. In this research, we tested 18 of the most common models that are available in computational engineering software such as MATLAB and R. The statistical distributions are as follows: Beta, Birnbaum-Saunders, Exponential, Extreme Value, Gamma, Generalized Extreme Value (GEV), Generalized Pareto, Inverse Normal (or Gaussian), Logistic, Log-logistic, Log-normal, Normal (or Gaussian), Rayleigh, Rician, t Location-Scale, Weibull, and Poisson. Moreover, since most of the physical quantities of interest like mass and projected area cannot have a negative value, for the cases that the mean value was small enough that some parts of the curve could be negative, the truncated normal distribution was included in the statistical distributions, as a modifier of the standard normal distribution. The truncated normal distribution is a common distribution in many engineering problems [45]. The standard normal distribution needs to be modified by setting the values in the negative range to zero and normally scaling up the PDF in the positive domain of physical quantities in such a way that the total integral equals unity. Table 3.3 represents the selected five values of BIC scores among all 18 for all the studies tabulated in Table 3.1.

For each experiment the corresponding BIC scores for the first ranked model, along with the three models that were used before [28,26,24] are reported. Due the reasons already explained, the truncated normal has also been included in the Table 2.3.

Table 2.3. Ranking of the distributions based on the BIC score

Experiment	Rank	Distribution name	BIC for distance/ mass	Rank	Distribution name	BIC for area
OWB2	1	Generalized Pareto	-3963	1	Generalized Pareto	-4558
	4	Inverse Gaussian	1546	4	Inverse Gaussian	1147
	6	Lognormal	1567	6	Lognormal	1186
	13	Truncated Normal	1710	11	Truncated Normal	1547
	14	Normal	1780	14	Normal	1671
OWB4	1	GEV	4385	1	Generalized Pareto	-1420
	2	Inverse Gaussian	5457	4	Inverse Gaussian	-390
	4	Lognormal	5466	5	Lognormal	-343
	11	Truncated Normal	5659	13	Truncated Normal	1150
	12	Normal	5662	14	Normal	1156
OWB5	1	Birnbaum	5286	1	Generalized Pareto	-13777
	2	Inverse Gaussian	5286	3	Inverse Gaussian	-478
	3	Lognormal	8288	4	Lognormal	-445
	7	Truncated Normal	5315	13	Truncated Normal	493
	9	Normal	5317	14	Normal	863
OWB7	1	T Location scale	1531	1	Generalized Pareto	-44870
	5	Inverse Gaussian	10606	5	Inverse Gaussian	6010
	6	Lognormal	10617	6	Lognormal	6079
	14	Truncated Normal	11433	11	Truncated Normal	7800
	15	Normal	11533	13	Normal	8360
OWB8	1	Truncated Normal	9924	1	Generalized Pareto	-63550
	2	Generalized Pareto	9928	2	Lognormal	1300
	4	Normal	9969	3	Inverse Gaussian	1468
	12	Lognormal	10425	12	Truncated Normal	3205
	17	Inverse Normal	10670	13	Normal	3210
OWB9	1	Inverse Gaussian	-451	1	GEV	472.69
	2	Generalized Pareto	-445	2	Inverse Gaussian	474
	3	Lognormal	-441	3	Lognormal	479
	12	Truncated Normal	-251	12	Truncated Normal	618
	15	Normal	-171	16	Normal	678
IWB2	1	Inverse Gaussian	-594	1	GEV	1909
	2	Generalized Pareto	-569	2	Inverse Gaussian	1915
	4	Lognormal	-564	3	Lognormal	1928
	12	Truncated Normal	820	12	Truncated Normal	2597
	14	Normal	984	14	Normal	2875
ISC2	1	Lognormal	-340	1	Inverse Gaussian	547
	2	Birnbaum	-338	2	Lognormal	547
	3	Inverse Gaussian	-334	3	Birnbaum	549
	12	Truncated Normal	-7	11	Truncated Normal	660
	14	Normal	114	14	Normal	781
ISC3a	1	Generalized Pareto	-80	1	Inverse Gaussian	627
	2	Lognormal	-75	2	Lognormal	630
	7	Inverse Gaussian	-55	3	Generalized Pareto	630
	12	Truncated Normal	142	11	Truncated Normal	718
	14	Normal	198	16	Normal	806

The histogram of mass, projected area and traveling distance are included with the fitted curves for selected studies (studies with larger sample size) are depicted in figures 2.3-2.8. As a rule of thumb, the minimum number of the bins is the square root of

the sample size. As seen in the mass/projected area plots, the lognormal and inverse normal curves are very similar in all the cases where they overestimate the frequency of the smaller firebrands and underestimate the frequency of larger ones. The truncated normal, however, underestimate the frequency of smaller firebrands and overestimate that of the larger ones. It was noted that the log-normal and inverse normal models tended to overestimate the frequency of smaller/lighter firebrands and underestimated the frequency of larger/heavier ones. Moreover, the frequency of the firebrands landing at closer distances was also over predicted by the log-normal and inverse normal models.

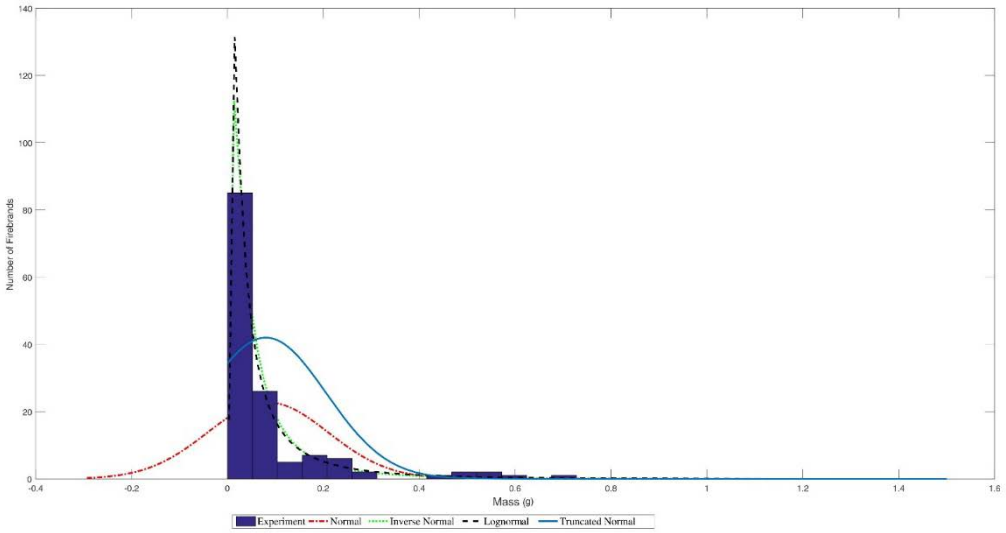

Figure 2-3. Histogram and selected curve fits of mass for OWB9

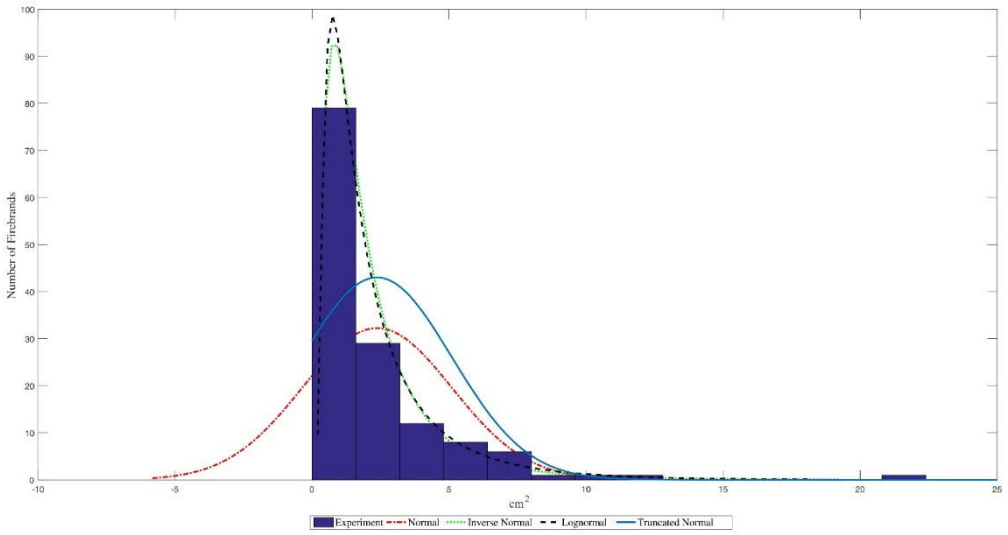

Figure 2-4. Histogram and selected curve fits of projected area for OWB9

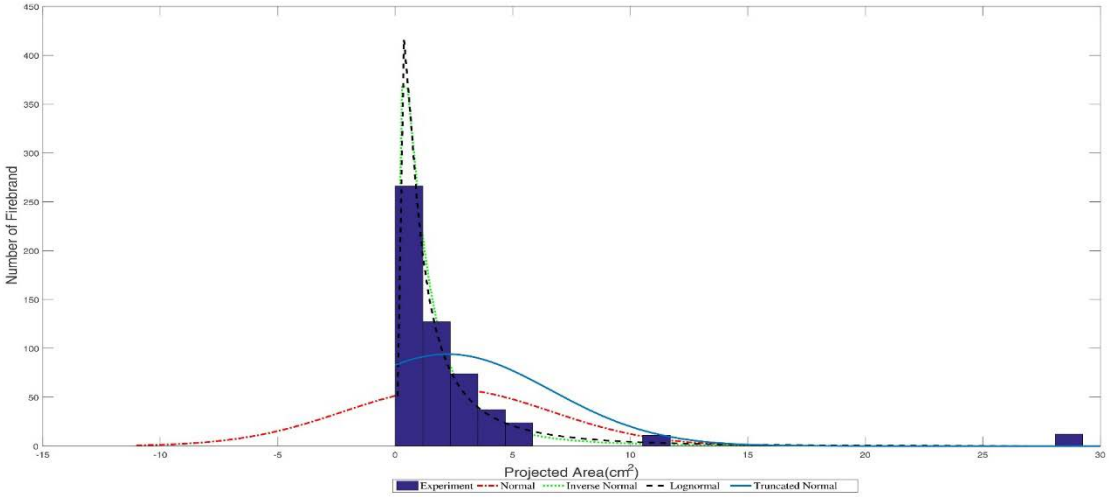

Figure 2-5. Histogram and selected curve fits of projected area for OWB4

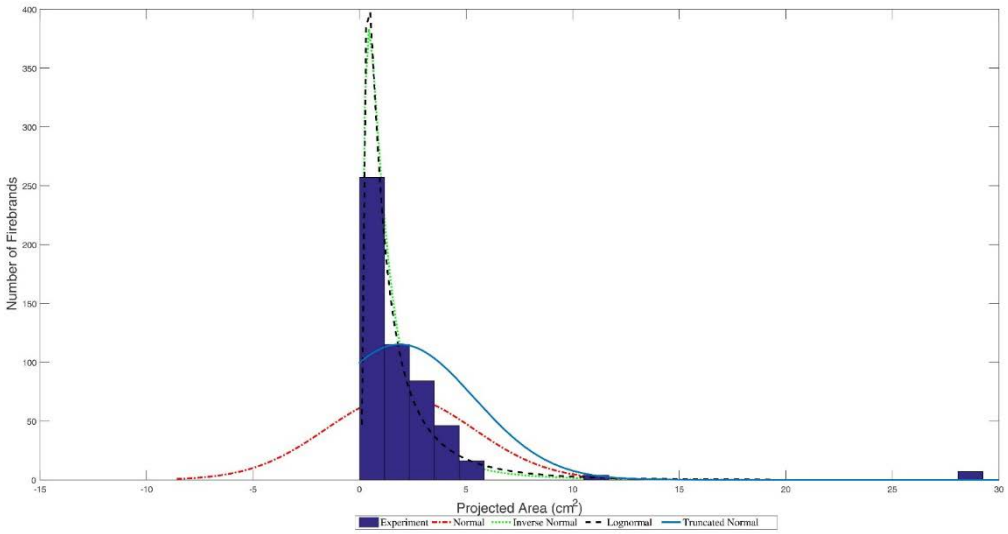

Figure 2-6. Histogram and selected curve fits of projected area for OWB5

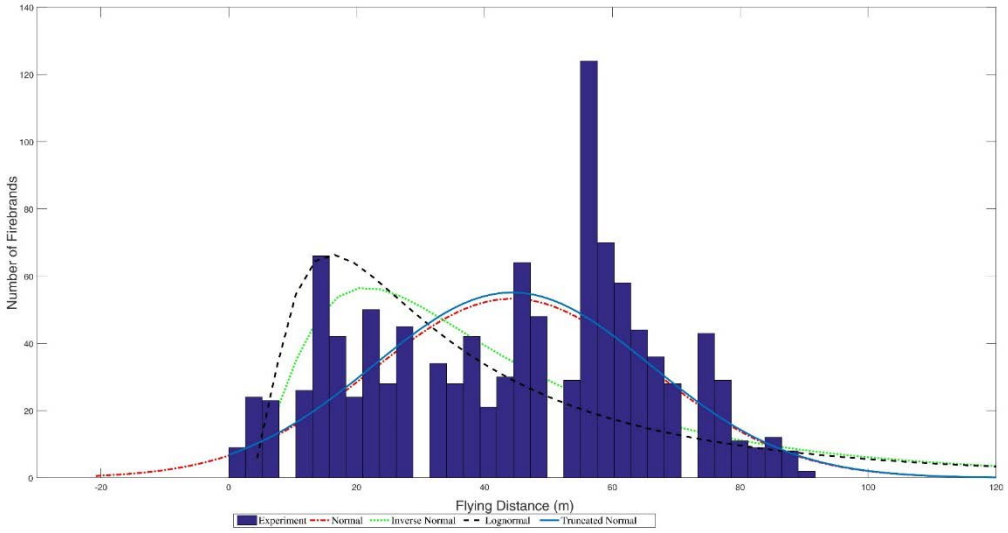

Figure 2-7. Histogram and selected curve fits of traveling distance for OWB9

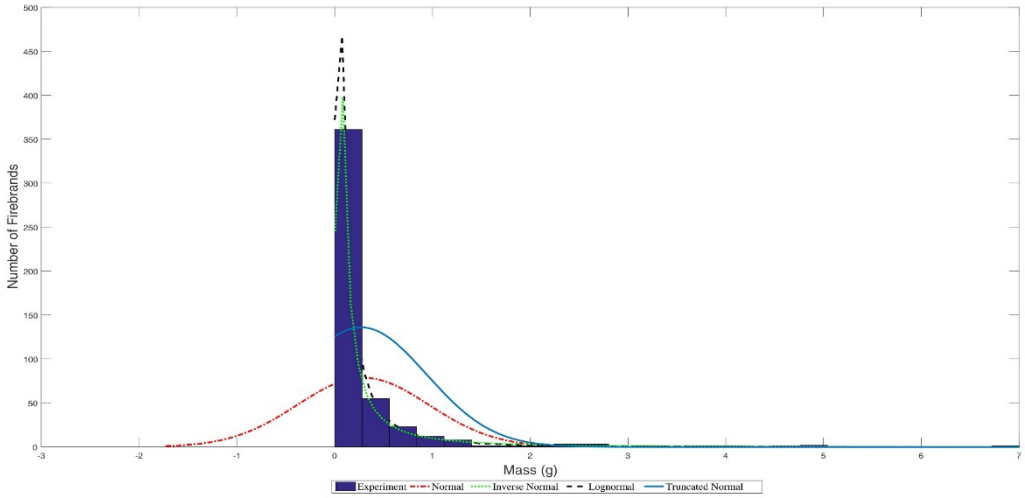

Figure 2-8. Histogram and selected curve fits of projected area for IWb2

As explained in section 2.3, the correlations between the variables take us to higher probability dimensions. Considering the list of the distributions in Table 2.3, one needs to employ higher dimension of the suggested PDFs. Since the raw data only provide us with one set of correlations, the bivariate distribution of the truncated normal, lognormal and inverse normal are presented, respectively.

$$P(x_1,x_2) = Ae^{\left\{\frac{-1}{2(1-\rho^2)}\left[\frac{(x_1-\mu_1)^2}{\sigma_1^2}-\frac{2\rho(x_1-\mu_1)(x_2-\mu_2)}{\sigma_1\sigma_2}+\frac{(x_2-\mu_2)^2}{\sigma_2^2}\right]\right\}}$$

$$\rho = cor(x_1,x_2) = \frac{cov(x_1,x_2)}{\sigma_1\sigma_2}$$

$$A = \frac{1}{2\pi\sigma_1\sigma_2\sqrt{1-\rho^2}\left(\int_0^\infty\int_0^\infty e^{\left\{\frac{-1}{2(1-\rho^2)}\left[\frac{(x_1-\mu_1)^2}{\sigma_1^2}-\frac{2\rho(x_1-\mu_1)(x_2-\mu_2)}{\sigma_1\sigma_2}+\frac{(x_2-\mu_2)^2}{\sigma_2^2}\right]\right\}}dx_1dx_2\right)} \quad (2.3)$$

Where μ is the mean, σ is the standard deviation, x_1 and x_2 are variables to studied, and ρ is the correlation factor representing how strong the two variables are correlated [45,46].

$$P(x_1,x_2)=\frac{1}{2\pi x_1 x_2 \sigma_{y_1}\sigma_{y_2}\sqrt{1-\rho^2}}e^{(\frac{-q}{2})}$$

$$q=\frac{1}{1-\rho^2}\left[(\frac{\ln x_1-\mu_{y_1}}{\sigma_{y_1}})^2-2\rho(\frac{\ln x_1-\mu_{y_1}}{\sigma_{y_1}})(\frac{\ln x_2-\mu_{y_2}}{\sigma_{y_2}})+(\frac{\ln x_2-\mu_{y_2}}{\sigma_{y_2}})^2\right] \qquad (2.4)$$

$$\sigma_{y_i}=\sqrt{\ln(1+\frac{\sigma^2{}_{x_i}}{\mu^2{}_{x_i}})}$$

$$\mu_{y_i}=\ln(\mu_{x_i})-\frac{\sigma^2{}_{y_i}}{2}$$

Where μ_{y_i} and σ_{y_i} are the mean and standard deviation of $Y_i=\ln X_i$ and μ_{x_i}, σ_{x_i}, ρ are the mean, standard deviation and the correlation coefficient of the samples [47].

$$P(x_1,x_2)=\sqrt{\frac{\lambda_1\lambda_2}{4\pi^2 x_1{}^3 x_2{}^3}}\;e^{\left(-\left(\frac{\lambda_1(x_1-\mu_1)^2}{2\mu_1{}^2 x_1}+\frac{\lambda_2(x_2-\mu_2)^2}{2\mu_2{}^2 x_2}\right)\right)}\times \left(1+K\left(x_1-\mu_1\right)\left(x_2-\mu_2\right)\;e^{\left(-\left(\frac{\lambda_1(x_1-\mu_1)^2}{2\mu_1{}^2 x_1}+\frac{\lambda_2(x_2-\mu_2)^2}{2\mu_2{}^2 x_2}\right)\right)}\right) \qquad (2.5)$$

Where $\lambda_i=\frac{\mu^3{}_i}{\sigma_i{}^2}$ is the shape parameter, μ_i is the mean and $K=\frac{8\rho}{\sigma_1\sigma_2}$ where ρ is the correlation coefficient and σ_i is the standard deviation of each data set [48].

The plots regarding the equations 3 through 5, for selected samples, are shown in Figures 2.9-2.14.

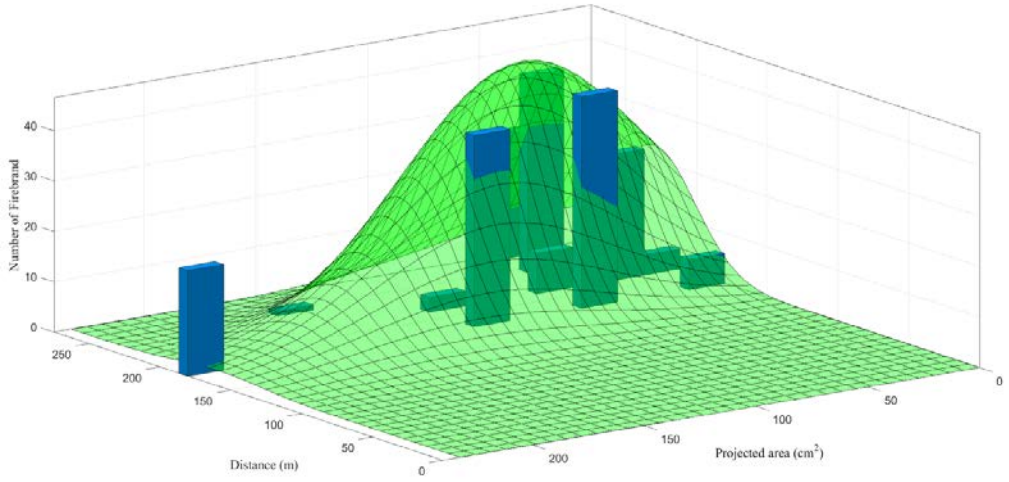

Figure 2-9. Bivariate Truncated Normal and the associated histograms for OWB1

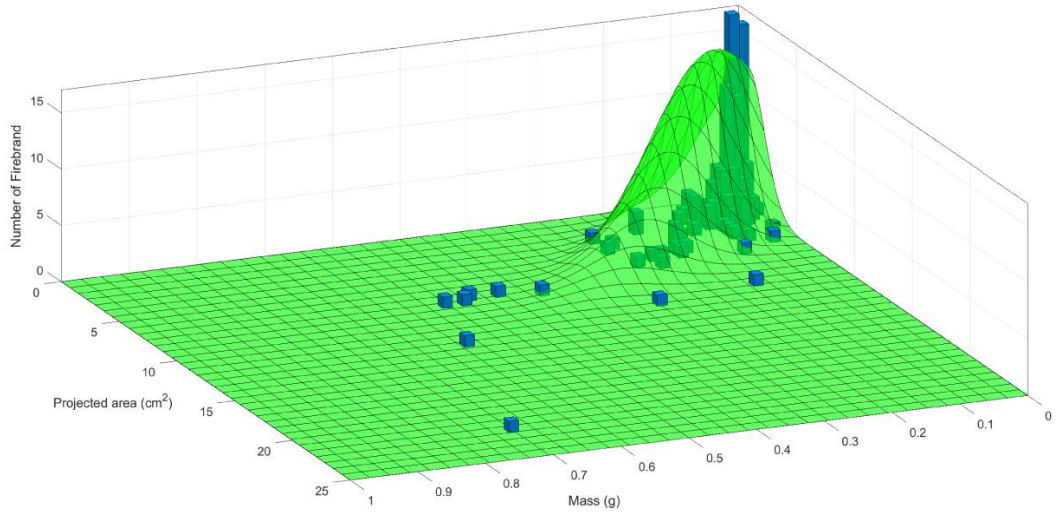

Figure 2-10. Bivariate Truncated Normal and the associated histograms for OWB9

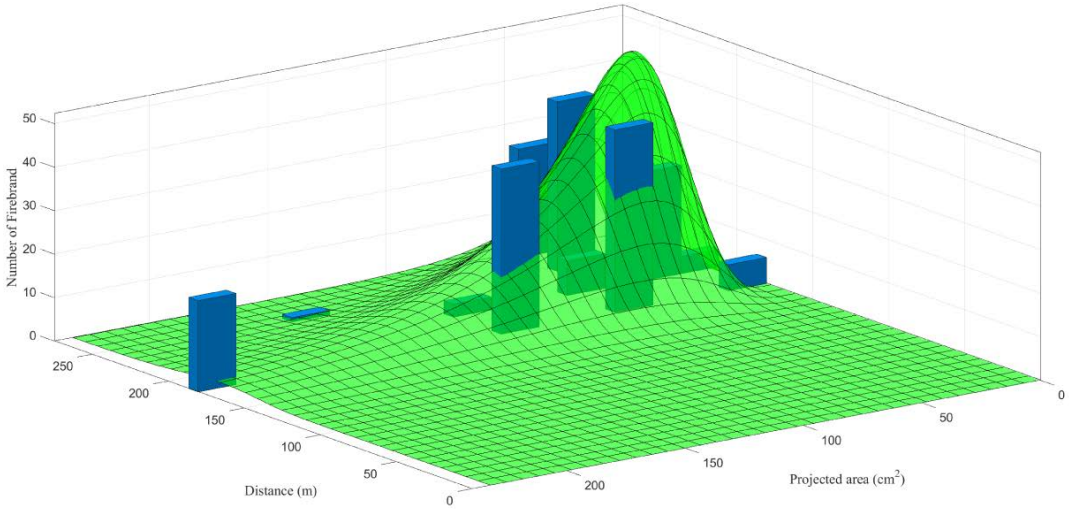

Figure 2-11. Bivariate Lognormal and the associated histograms for OWB1

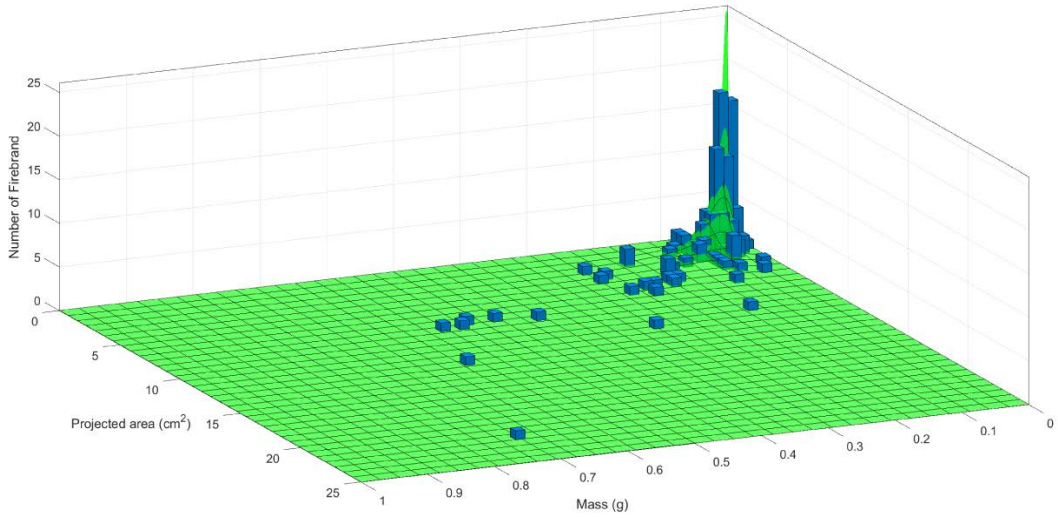

Figure 2-12. Bivariate Lognormal and the associated histograms for OWB9

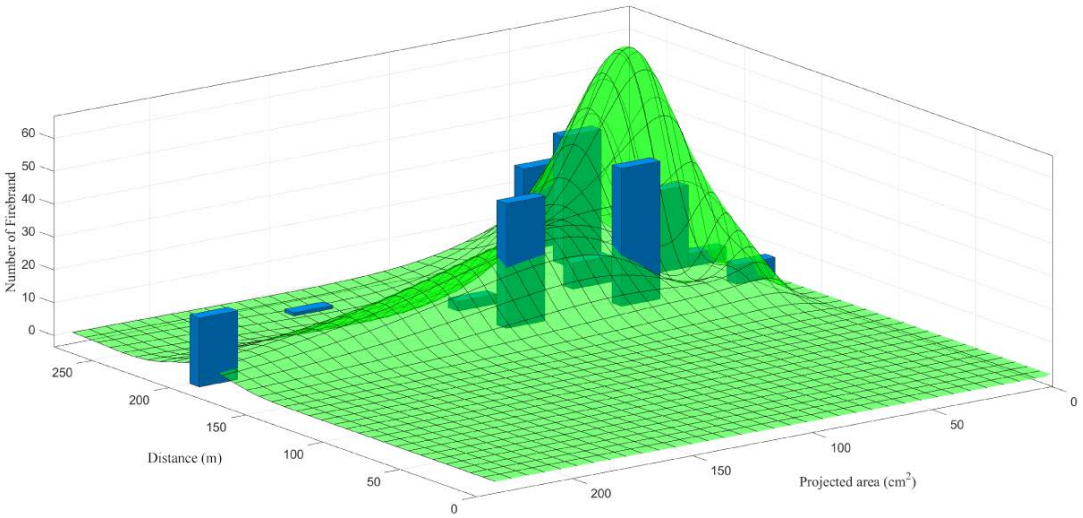

Figure 2-13. Bivariate Inverse Normal and the associated histograms for OWB1

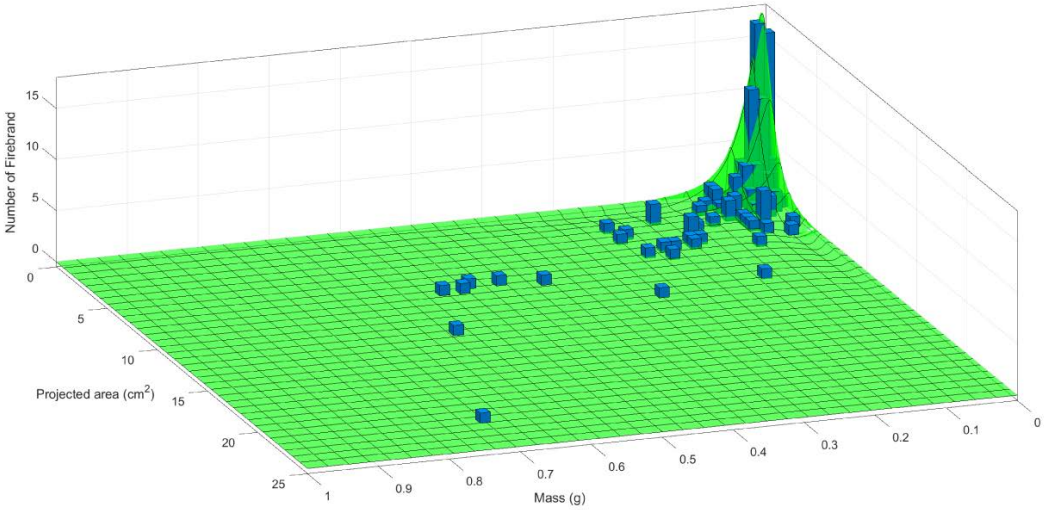

Figure 2-14. Bivariate Inverse Normal and the associated histograms for OWB9

As can be seen, none of the models provided a perfect fir to the data. Truncated normal over predicted the mean value as well as the frequency of the larger firebrands. Log-normal and Inverse normal distributions can appropriately predict the smaller firebrands but were incapable of predicting the frequency of larger firebrands. The contour plots for the experiments OWB1, 2 and 8 were plotted.

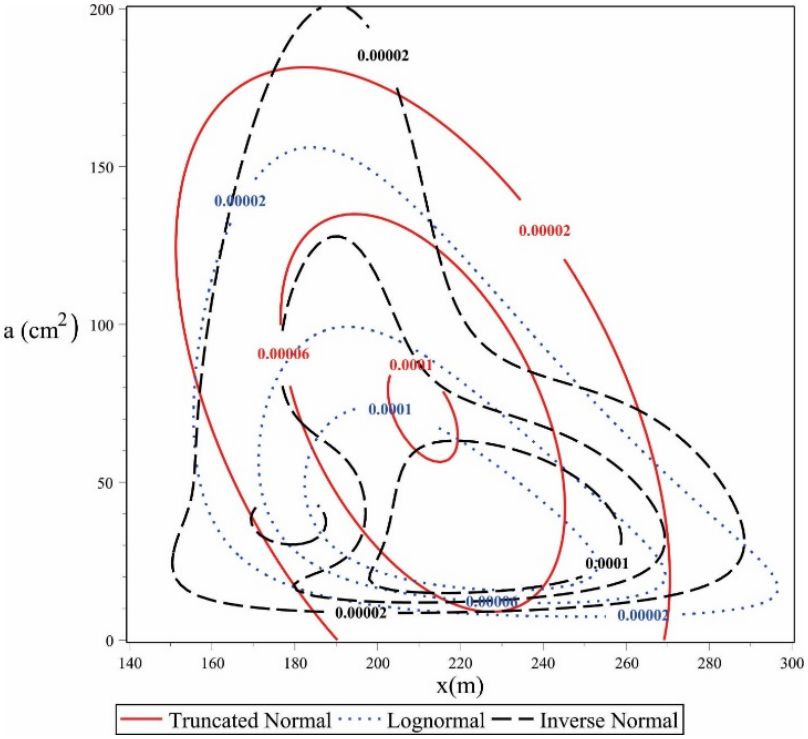

Figure 2-15. Contour plots of the three bivariate distributions using OWB1

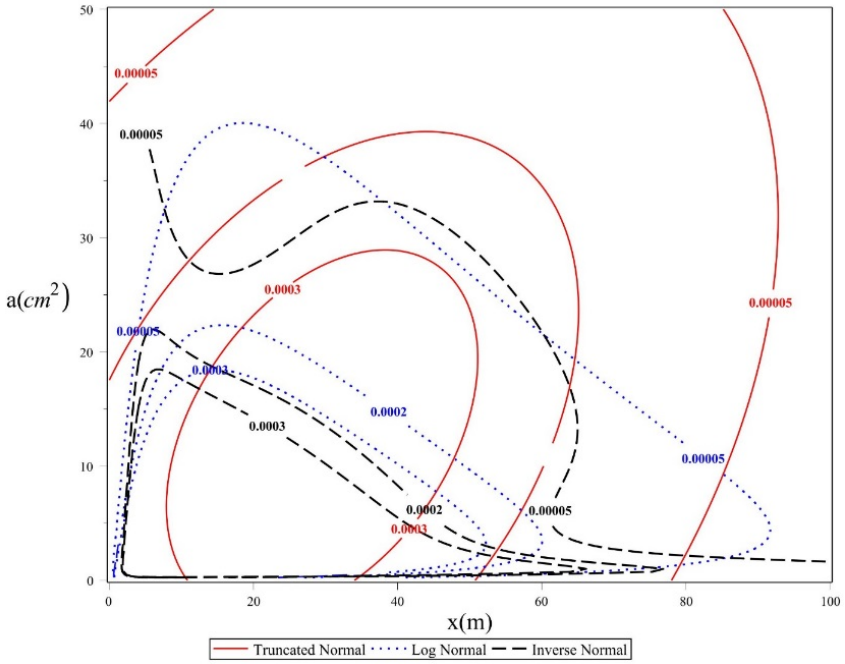

Figure 2-16. Contour plots of the three bivariate distributions using OWB2

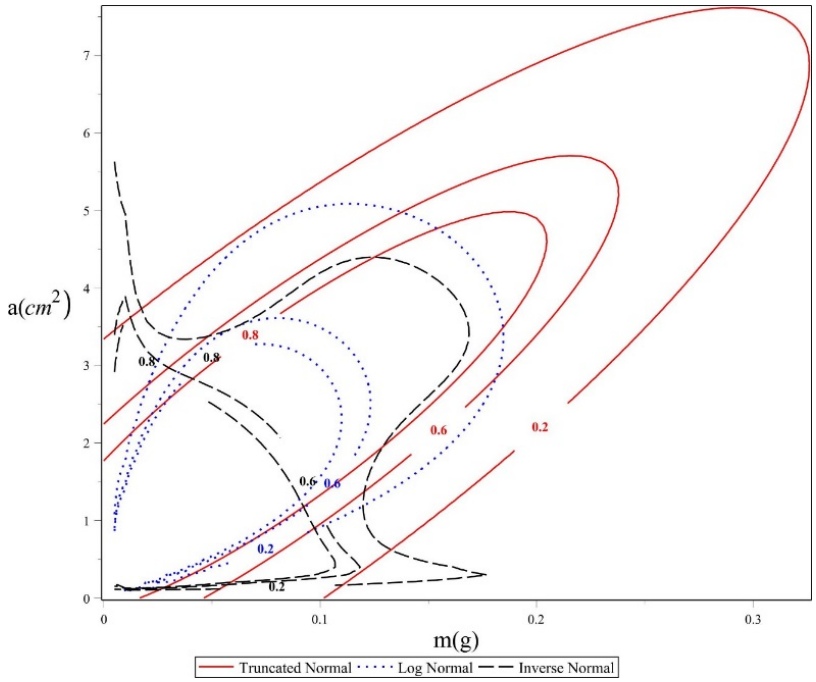

Figure 2-17. Contour plots of the three bivariate distributions using OWB9 data

Considering the histograms, Table 2.3 and the contour plots, there were several reasons that the truncated normal distribution was selected for further analysis in this research. (1) Figures2.15-2.17 showed that the variations of the inverse normal, for which

BIC scores were among the lowest, happened rapidly, which was probably not close to what would happen in reality. For example, in figure 2.17, at lower projected areas, mass had an abrupt change which typically does not happen in nature, (2) based on the Central Limit Theorem, if the sample size grows, the distribution of any phenomenon get closer to Normal distribution, (3) the quality of the available data was questionable since there is no report about the sampling techniques and sample size. For example, for OWB9, only 140 firebrands were collected at 4 meters and 18 meters. The sample size was too small and the distance from the fire looked random. Assuming normality makes the computations much easier and also provided us with numerous useful tools, including confidence intervals, ANOVA and some machine learning techniques, without which one would not be able to do much [49]. It should be mentioned that assuming normality for non-normal data is a common assumption. The phrase "assuming normality" brings up more than 10,000 results on Google Scholar. George Box, a famous statistician, once said: "Essentially, all models are wrong but some are useful."

2.4. Results

As can be seen in Table 2.2, the experiments recorded the projected area and also either flying distance or mass. Thus, the obtained bivariate truncated normal distribution for some studies was a function of mass and projected area and for some was a function of flying distance and projected area. Instead of plotting 3D graphs, the contour plots of those were depicted, similar to figures 2.15-2.17, since it was easier to observe the trends. For OWB studies, variation in the plot axis was quite different and it was not possible to plot all in a same figure. Along a contour line the probability stays constant and the inner loops were associated with higher probabilities. A positive slope of the major axis of the

ellipse indicated a positive correlation and zero and infinity slopes corresponded with no correlation. The length of the minor diameter represented how strongly the variables were correlated. The shorter the length, the stronger the correlation. The behavior of each contour plot can be analyzed based on the above mentioned explanations. To avoid repetitions, only selected ones will be discussed; the rest can be explained in a similar way.

2.4.1. Experiments considered projected area and flying distance

As can be seen in figures 18-20, the correlation values between the flying distance and projected area varied. For OWB1 there was a moderate negative correlation (approximately -0.5), which implied that the firebrands' projected area at longer distances were higher than those close to the fire. On the other hand, the correlation value for OWB2 shows an opposite trend. For the other experiments, correlations were smaller. This observation suggests that more experiments need to be conducted to figure out how surface area and flying distance affect each other.

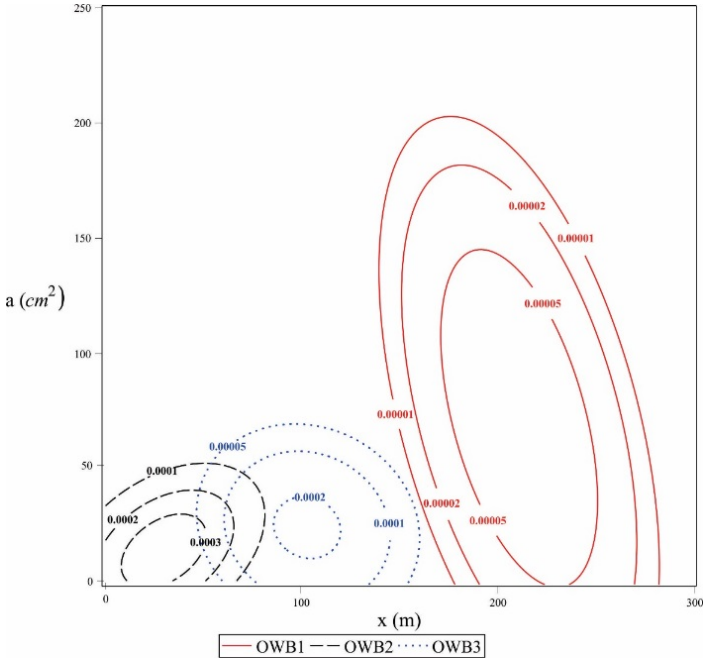

Figure 2-18. Bivariate Truncated Normal PDF Contour plots for OWB1-3

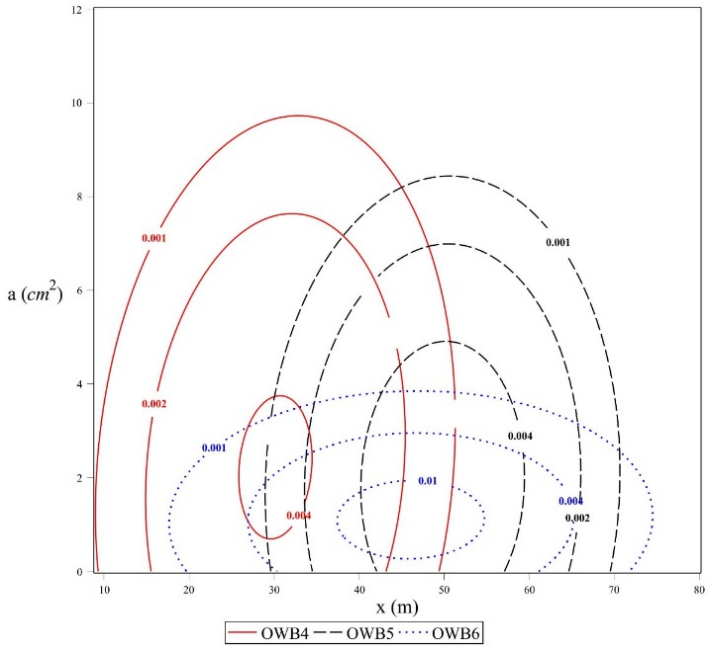

Figure 2-19. Bivariate Truncated Normal PDF Contour plots for OWB4-6

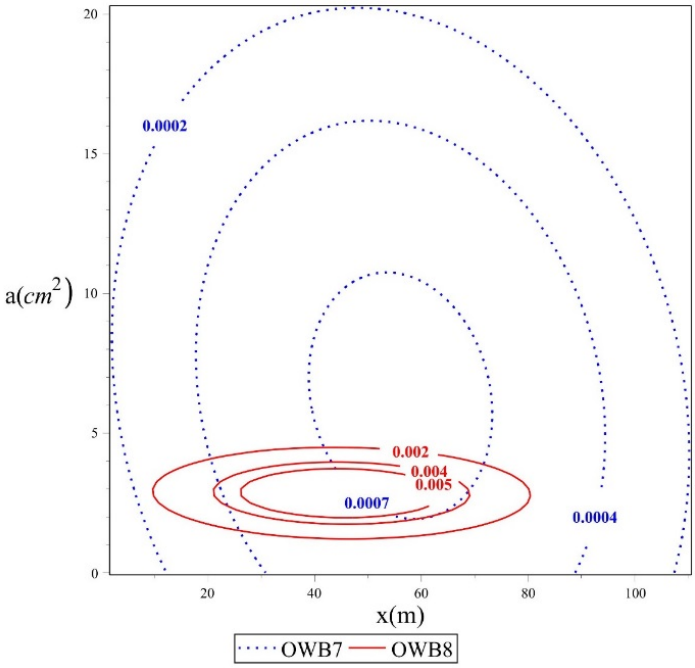

Figure 2-20. Bivariate Truncated Normal PDF Contour plots for OWB7 and 8

2.4.2. Experiments considered projected area and mass

Figures 2.21-2.24 showed that mass and projected area had stronger correlations than flying distance and projected area, which provided evidence that larger firebrands were also heavier. Figure 2.21 indicated that the correlation between mass and projected

area was stronger at closer distances to the fire-4m vs 18m-. Moreover, more variability in mass and projected area can be seen at 18 meters compared to that of at 4 meters.

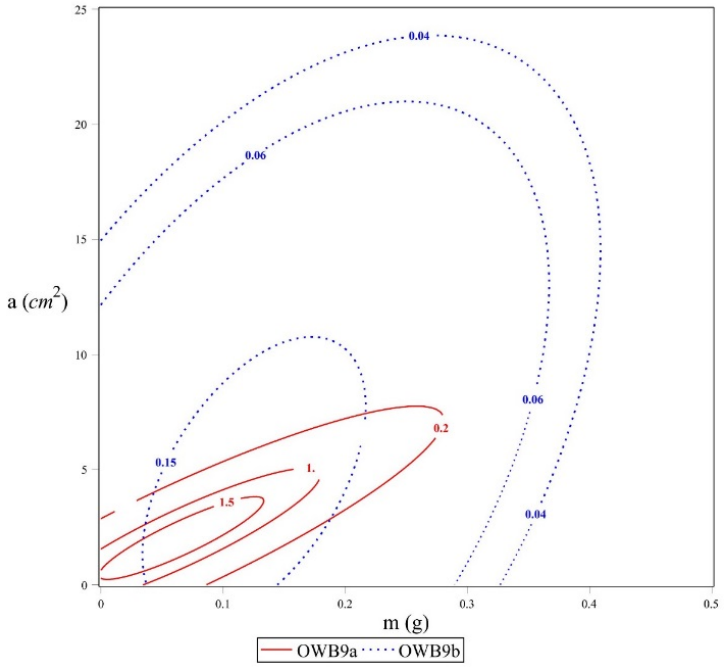

Figure 2-21. Bivariate Truncated Normal PDF contour plots for OWB 9

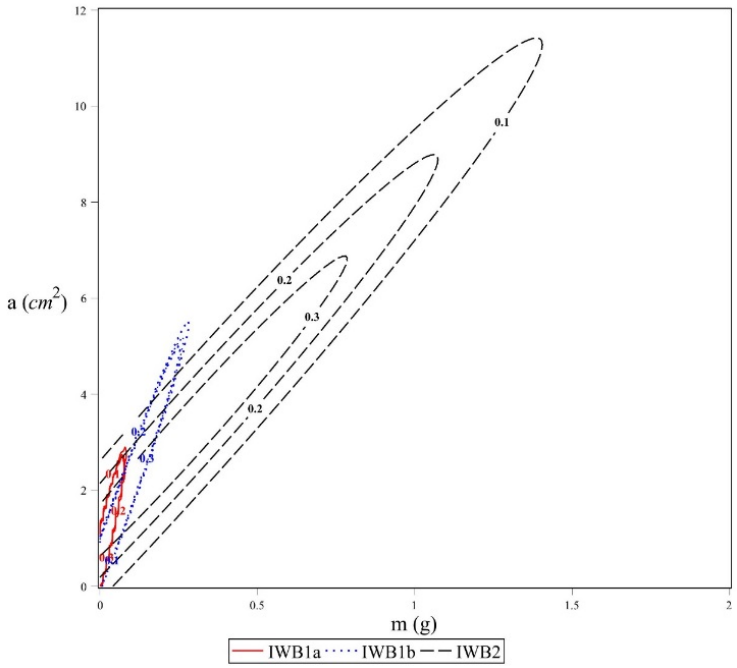

Figure 2-22. Bivariate Truncated Normal PDF contour plots for IWB1a-b & IWB2

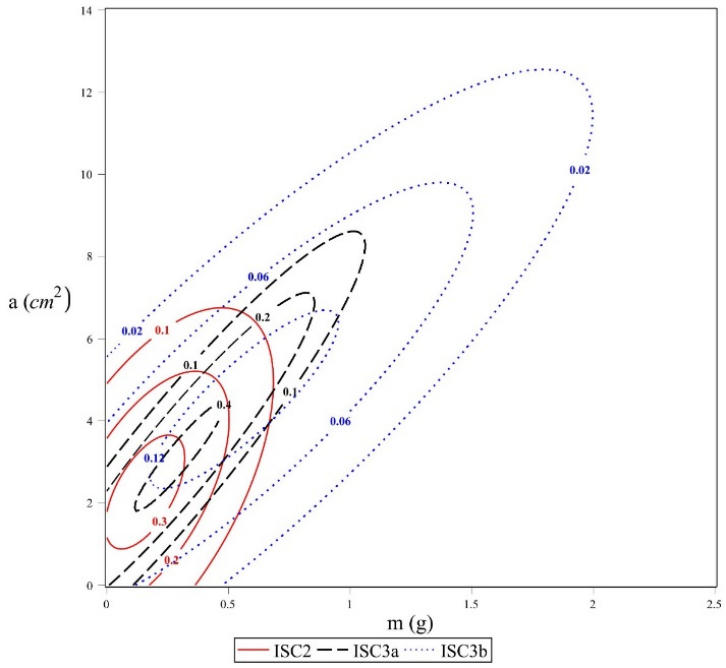

Figure 2-23. Bivariate Truncated Normal PDF contour plots for ISC2 & ISC3a-b

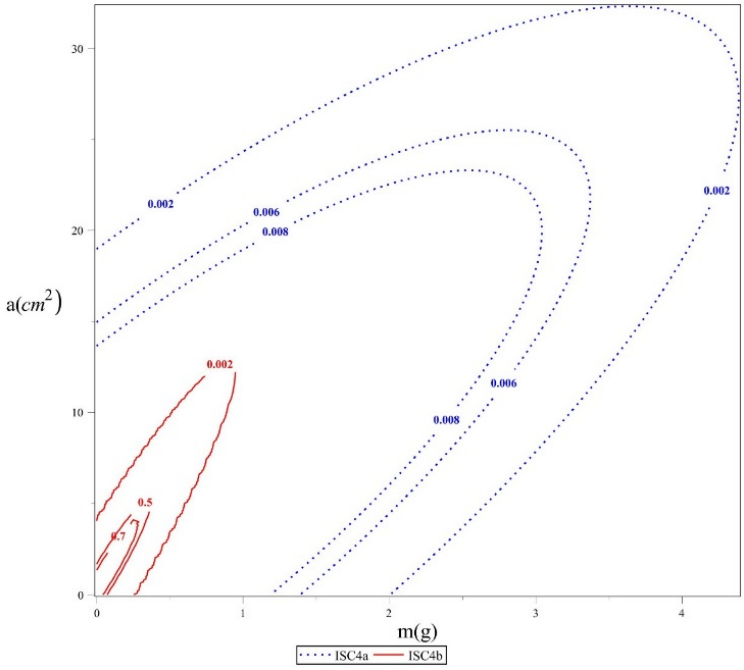

Figure 2-24. Bivariate Truncated Normal PDF contour plots for ISC4a & ISC4b

Comparing the contour plots of ISC2 and ISC3a, it can be seen that the firebrands lofted from the corner assembly had a larger variation range for mass and projected area. Moreover the correlation is much stronger in ISC3a. This may suggest that corner assemblies are able to produce more lethal firebrands comparing to walls, which should

be considered in the construction of buildings. Comparing ISC3a and ISC3b in figure 2.23, also revealed that higher wind speed generated larger brands given the stronger correlations between mass and projected area. This can also be seen in figure 2.24. In the latter figure, the variation range in the contour plots is smaller, which may be a result of siding treatments [20].

Waterman's experiment [18] only reported the mass of the firebrands so it was not possible to calculate a correlation coefficient. Table 2.4 presents the details of this experiment. This table shows that smaller sheets generated fewer firebrands except the last line of the table. In order to facilitate to investigate the effect of wind pressure on, the experiments were categorized into two parts; the low pressure group from 0.13 to 0.15 inch (0.33-0.38 cm) of water and the high pressure group 0.49 to 0.59 inch (1.24-1.49 cm) of water. Considering the average of the frequency of the generated firebrands, it was concluded that higher pressure increased the firebrand generation. On average, there were 19,967 firebrands for the high pressure group versus 6,344 for the low pressure group. Also, higher pressure leads to generation of heavier firebrands; the average mass at lower pressure is 743.30 grams which increases to 2389.10 at higher pressure.

Table 2-4. Summary of ISC1 firebrand information

Sheet area (m^2)	**Frequency of Associated sheet**	**Total number of generated brands**	**Brand per unit area**
8.45	8	202740	2999
6.41	2	3177	248
5.94	24	220527	97
5.66	3	9952	586

2.4.3. Comparing the results

In order to compare the variation range of mass and projected area of the data obtained from different experiments, the 95% confidence intervals of the experiments that were conducted at 6 m/s are plotted in figure 2.25. In addition to the mentioned studies, the firebrands generated from the NIST firebrand generator [24,38] have also been included in this plot.

Figure 2.25 shows that the firebrands generated from the only outdoor real world experiment (OWB9) were lighter than that of generated from the indoor full structure tests or components. However, the projected area of OWB9 was consistent with ISC2, IWB2 and ISC3a. The firebrands from the ISC4a were heavier and larger than most of the firebrands in other experiments which may be the effects of siding treatments. The NIST firebrand generator data (left bottom corner) was not in agreement of the other experiments. However, a huge improvement can be seen in the revised version of the apparatus.

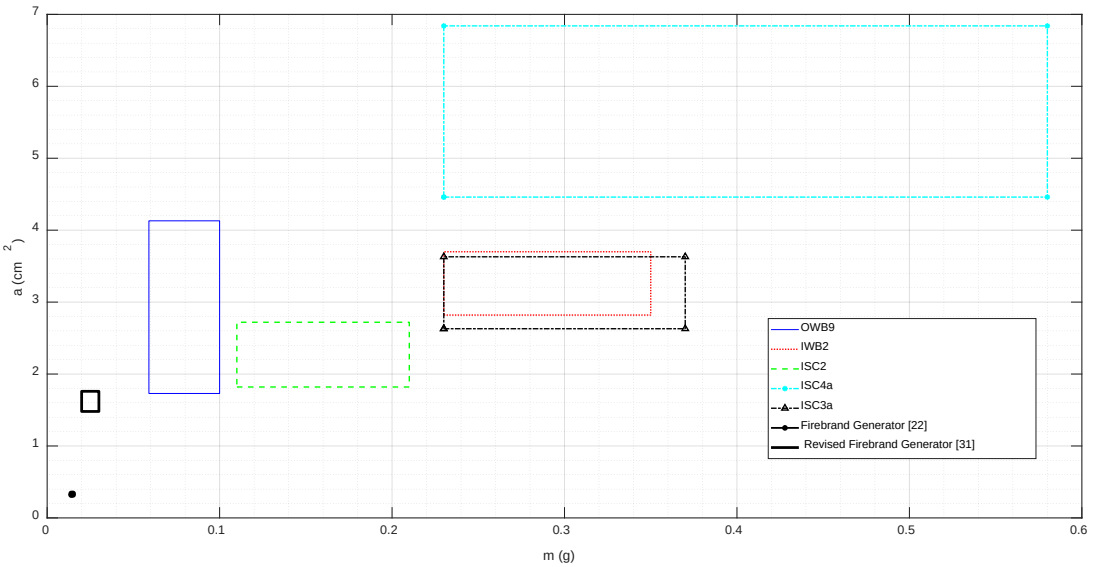

Figure 2-25. 95% confidence interval range for mass and projected area

2.5. Summary and conclusion

In this chapter, all the studies reporting on the generation of firebrands from structural fuels were summarized, and the associated experimental data were gathered. The experiments were categorized based on how the firebrands were generated; (1) Outdoor Whole Buildings (OWB), Indoor Whole Buildings (IWB) and Indoor Structural Components (ISC). After plotting the histograms to visually observe the data, the Maximum Likelihood Method was employed to find the best Probability Density Function candidates (PDF). The Bayesian Information Criterion (BIC) score was also calculated for each PDF. The BIC scores were listed, and based on the lowest BIC scores and the results of previous experiments, three PDFs were chosen for further analysis namely Lognormal, Inverse Normal and Truncated Normal. Distribution's contour plots indicated that the variation of the inverse normal distribution happened very rapidly, which does not sound realistic. Both of the lognormal and truncated normal distributions sound reasonable, but as the Central Limit Theorem suggests, and the simplicity and the tools that truncated normal distribution provides, bivariate truncated normal distribution was finalized for further investigation. The contour plots based on the chosen model were depicted and each one was discussed. Finally, a confidence interval analysis was conducted to calculate the range of variation in the mass and projected area for each experiment. It was observed that the NIST firebrand generators' data was not in agreement with other experiments. Moreover, there was a strong correlation between mass and projected area and a moderate/weak correlation between the flying distance and projected area. It was also observed that the firebrands which were lofted from corner

assemblies were typically larger and heavier than the ones lofted from flat wall assemblies.

CHAPTER 3: A NOVEL FRAMEWORK TO CHARACTERIZE FIREBRANDS

3.1. Abstract

The objective of this study was to (1) provide a statistically adequate firebrand sample size and (2) develop a framework to reduce the labor in the tedious measurement process of the firebrand experiments. For the first objective, several tests were conducted at the IBHS research center to generate and collect firebrands from burning OSB/cedar siding corner assemblies that were ignited at three different wind speeds. A statistical analysis suggested a sample size of at least 1300; however, a more conservative sample size of 1400 was chosen. Measuring the physical quantities of interest, including mass, projected area, flying distance and, the burning levels, for such a large sample size (3*1400), required an efficient measuring process. To achieve the second objective a unique image processing algorithm was developed to calculate the projected area. Moreover, to facilitate the weighing process, a Gaussian process regression was employed to predict the mass based on other parameters. It was observed that having measured 70% of the firebrands, the model could predict the mass of the remaining unseen 30% of the data within 5% error. Employing this predictive model, the sample size could be reduced by 30% (900 instead of 1400 firebrands) and the mean, standard deviation and correlation between the parameters can be predicted within 10% error. The model can also provide information about mass/size of the firebrands at the locations were not covered with pans during the experiment.

3.2. Introduction

Three principal ways have been identified that cause fire spread in a Wildland Urban Interface (WUI): direct flame contact, radiant heat, and burning firebrands [4,35,22,50]. It has been reported that firebrands are capable of igniting a spot fire at distances more than 60 meters away from the fire [3]. Heat flux from flames is not high enough to initiate a fire at further distances. Depending on the size and rate of spread of the wildfire, spotting often overpowers fire suppression efforts and becomes the dominant fire spread mechanism [51]. The firebrand process includes three components; generation, transportation, and ignition of the recipient fuel. The generation phase is probably the least developed area [52,53].

The ignition potential of a firebrand depend on the susceptibility of the fuel bed and environmental conditions. The physics of ignition can help to identify influential parameters in each category. Thermal mass and thermal flux exchange are the two important parameters in the first category (fuel properties), which can be estimated by the mass and projected area of the firebrands. It was reported that re-flaming was observed for firebrands with some unburned material [54]. Thus, the burning level of a firebrand at the time of lofting was influential to determine the thermal flux exchange.

Wind speed can be considered to be as the most important environmental parameter since the transport mechanism and area under threat by firebrands heavily dependent on the wind speed. In addition, the aerodynamic shape of the firebrand is important in the transport since the drag and lift coefficients are strong functions of the shape.

Several studies have been conducted to obtain a better understanding of the firebrand generation in structural fires. Typically, these experiments are extremely expensive (time and labor) to run. For example, in full scale tests [13,14], structures were set on fire, and plastic sheets were laid out downstream of the structures. As a result, hot firebrands melted through the sheets, and by measuring the size of the remaining hole, the projected area and traveling distance of the firebrands were determined. One potential problem of this method was that, in case where firebrands were not hot, there would not be melt plastic and the results would not be accurate. A more common technique has been to distribute water pans [55,38,56,39,17,20,19,15,24] downstream of the burning structure. Quenching firebrands preserved their mass and shape, which provided valuable additional information to compare to plastic sheet test results. In this method, the center of each pan was considered to be the landing position for each ember which was not what happened. Thus, inevitably, the data was treated as discrete rather than continuous.

In these experiments, the firebrand measurement process can be more time consuming than running the tests. To measure the mass, the firebrands need to be oven-dried first, then weighed individually. In order to measure the surface area, various approaches have been employed, among which digital image processing has been the most effective [9,13]. The traveling distance of the firebrands have been determined by the location of the pans in which they were collected.

In full-scale experiments, thousands of firebrands were generated, so extracting information for the entire population was not practical. Therefore, sampling techniques play a pivotal role in the validity of the measurements. The sample of the full-scale building component experiments conducted in the past 20 years varied between 50 and

500 firebrands [38,39,20,15]. The vital question is how many firebrands are needed to sufficiently quantify the characteristics of entire population of firebrands in an experiment. If the answer suggests a sample size far larger than 500, the feasibility of the current measurement methodology to count and measure thousands of firebrands must be explored. Furthermore, it is not practical to cover the entire area downstream of the wind with water pans to catch all the firebrands. Therefore, no information can be obtained at the uncovered locations. There is a need to find a way to determine (or at least estimate) different characteristics of the firebrands at those locations were pans are not located.

In order to address the above-mentioned issues, two key goals were established for this chapter:

(1) Determine a statistically acceptable sample size for each experiment, based on the desired confidence interval, margin of error, and standard deviation.

(2) Improve the efficiency of the labor intensive measurement process employing machine learning and image processing techniques. The predictive model, also enables us to estimate different characteristics of the firebrands locations not covered by water pans.

To achieve the first goal, a statistical analysis was conducted which suggested that the sample size for each experiment needed to be at least 1300 (the details will be presented subsequently). To this end, numerous tests were conducted at the Insurance Institute for Business & Home Safety (IBHS) to generate firebrands from several materials and assemblies ignited an burned at different wind speeds. To be even more conservative, at least 1400 firebrand from each test were randomly chosen and measured. To satisfy the second goal, a framework to automize the tedious measurement process is

proposed. Given that measurement of mass and projected area were the two difficult tasks, an efficient image processing algorithm was developed to minimize the human effort in these measurement. Moreover, Employing shallow and deep machine learning techniques, the Gaussian regression process and neural network, two models were built to predict the mass of a firebrand without physically weighing it. These models were also capable of predicting the mass or surface area of the firebrands where no water pan was laid down. A comprehensive uncertainty analysis for all the measurements will be presented.

The structure of this chapter is as follows: 1. the experimental procedure is explained. 2. A discussion about the measurement process is presented, 3. The predictive models based on the Gaussian regression process and neural network are introduced, and 4. The results are analyzed, including the prediction errors (between the measured and predicted vales).

3.3. Experimental Procedure

The experiment procedure was divided into three section: pre-test, test, and post-test. Pre-test included material selection, experiment design, and sampling. Testing included details about running the tests and collecting the firebrands. Finally, details regarding the measurement process is covered in the post-test section.

3.3.1. Material selection

Several parameters were considered in the experimental design, including material type, geometry, layout of the pans and wind speed. In a set of experiments, several full-scale geometries with different materials were designed and tested under different environmental conditions. This study only include the corner assemblies at three

different wind speeds. The corner assemblies were built from typical residential construction materials. All the samples were conditioned to reach a nominal moisture level of 6%. The schematic and dimensions of the corner assemblies are plotted in Figure 3. 1. The OSB sheathing was covered with 0.5 inch gypsum on the non-fire and 1.25 inch western red Cedar on the fire side.

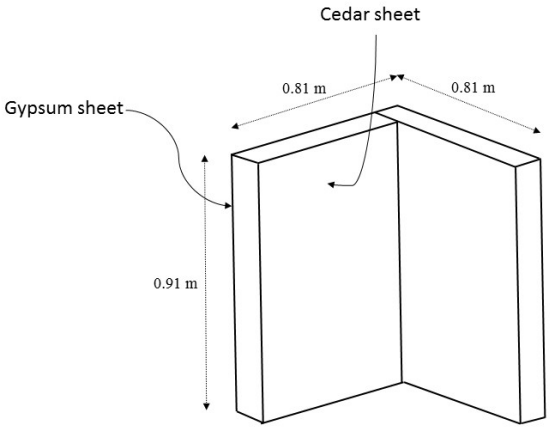

(a)

(b)

Figure 3-1. The Corner assembly (a) dimensions (b) during a test

3.3.2. Pan layout

The layout of the water is an important role in post-test analysis. As mentioned earlier, it is not practical to cover the entire downstream with water pans and consequently, only a fraction of the generated firebrands can be collected in the water pans. This inevitably affects the randomness of the sample. More discussions will be presented subsequently about sampling. In previous studies, a rectangular area of approximately 2×15 meters downstream area was covered completely with water pans[24]. If a model can predict different characteristics of the firebrands at the uncovered locations, spacing out the water pans can help to collect a more diverse sample that helps maintain randomness. Considering the dimensions of the test chamber at the IBHS research center, a more scattered water pan pattern was designed for the experiments. The test chamber floor area and the pan layout pattern are shown in Figure 3. 2. Since the wake flow behind the wall assembly is strong, four column of pans were placed at closer distances to cover a wider range. After that, assuming a symmetrical distribution, only one side of the center line was covered with water pans in each row to be able to cover a longer range. In total, 46 water pans with dimensions of 0.65×0.45 meter were placed downstream of the wall assembly.

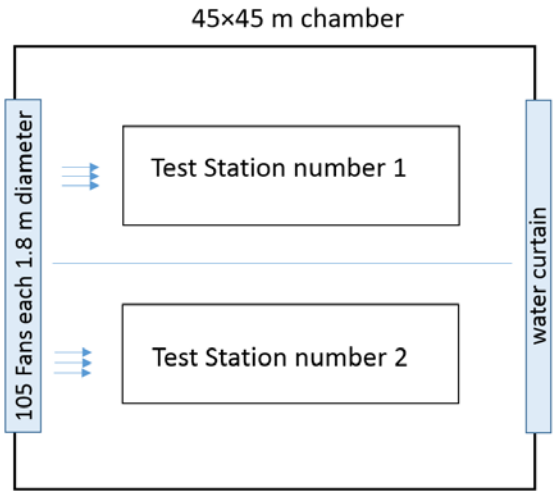

(a) Test chamber

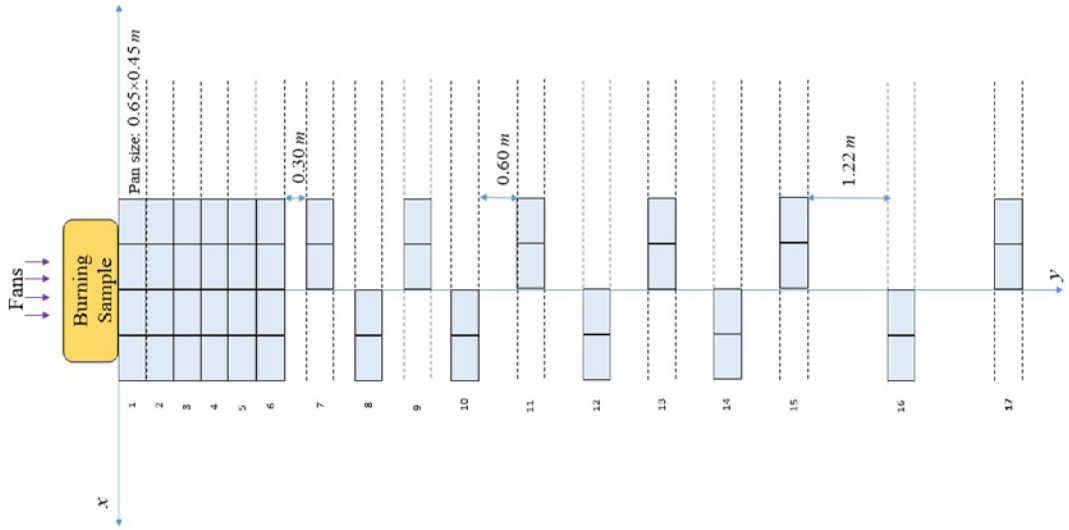

(b) Pan layout

Figure 3-2. Test chamber and the playout of the pans

3.3.3. Sampling

Sampling has probably been the least focused area in pre-test section. During a firebrand production experiment, the number of firebrands in the complete sample (or the whole firebrand population) is often very large. This makes the complete collection and characterization of the entire firebrand population impractical or impossible. Thus,

statistical sampling should be used, i.e., collecting a subset of manageable size should be used to represent the whole firebrand population. This procedure must follow statistical principles for sampling, because statistical values will be calculated from the collected firebrands, and further statistical analyses as well as extrapolations from the collected firebrands to the whole population will be made. Ideally, a firebrand collection process should result in an unbiased representative group of firebrands. In practice, only firebrands larger than a certain size can be collected as, very small firebrands cannot be collected and measured. For example, in some early firebrand studies, expressions such as “too small to be counted” appeared in reports [13,14]. When water pans were used in some firebrand studies, the collection of minute firebrands is not possible [24]. In strict terms, firebrand collection was not a random sampling process. Therefore, the sampling of firebrands is a nonprobability sampling procedure because some firebrand (i.e., the very small ones) of the population will not be selected. This exclusion bias is a source of uncertainty and brings limits on how much information a firebrand sample can provide about the population, which makes it difficult to extrapolate the results from the collected firebrands to the whole population. On the other hand, these minute firebrands usually do not have sufficient heat energy to ignite a recipient fuel on which they land, and thus they are not a threat and a concern (or population of interest) in the firebrand phenomenon. Given the limitations, a common practice to address this issue is to use a so-called consecutive sampling (or total enumerative sampling) technique, e.g., to collect firebrands that are large enough until the required sample size is achieved. This leads to an important question: what is the appropriate sample size for a firebrand production experiment so that meaningful statistical extrapolation can be made?

The number of samples in previous full-scale studies varied between 50-500 firebrands. If the purpose of sampling is to describe/estimate characteristics of the entire population, random sampling should be employed. Two types of random sampling were considered: simple and stratified. Stratified is often used when there are different groups in the population [57]. Since each of the experiments was considered a separate group, stratified sampling was chosen for this research. Choosing the conservative values for standard deviation of the sample equals 0.55 and 0.03 as the margin of error; therefore, the recommended sample size, based on statistical analysis, was 1300 [58]. To become more confident in this study, at least 1400 firebrands from each test were randomly chosen for further analysis. This study only considers the firebrands lofted from the corner assemblies, which were made of cedar/OSB at three different wind speeds. In total, 4415 firebrands were analyzed (1400, 1520, and 1495 at idle, medium, and high wind speed, respectively).

3.3.4. Test procedure

Before starting a test, in each pan a mesh screen was put and then the pans were filled up with water. An arrow shaped burner was manufactured for these tests, which winds were 0.71 meters long. The burner was placed adjacent to the wall for each test and kept “on time” for 10 minutes. The wind tunnel and burners turned on at the same time where the samples were exposed to three different wind speeds namely 5.36 m/s (idle), 11.17 m/s (medium) and, 17.88 m/s (high). After 30 minutes the test was stopped and firebrands collected from the pans. The firebrands were placed inside an oven for 24 hours to reach zero moisture content level.

3.4. Firebrand Characterization

Boxes of oven-dried firebrands were taken to the Flammability Lab at UNC-Charlotte, where a group of undergraduates and graduate students carefully analyzed them. Each box contained numerous sealed bags, each bag belonging to a specific pan from a given test. Four parameters for each firebrand were evaluated, including traveling distance, charring level (charred or partially charred), mass, and projected area. The first three were fairly straight forward to measure and are grouped together in Section 3.1. The latter measurement, however, involved a more complicated process and is discussed separately.

3.4.1. Traveling distance, charring level and mass of the firebrands

Traveling distance was calculated by applying the Pythagorean Theorem over the pan row and pan column, where the origin was set on the burning wall assembly. See Figure 3.1 for details.

Since firebrands containing unburned material have greater tendency to switch to re-flaming phase [54], and it seemed beneficial to determine the charring level of the firebrands. In this study, it was observed that firebrands may have different charring levels as depicted in Figure 3.3. We counted the firebrands whose surface was not completely charred (black). However, since quantifying the charring level is complicated and out of the focus of this study, it was included in the statistical analysis. One possible criteria to define the charring level could be the density of each firebrand. This would an interesting future research subject.

Measuring mass were the most tedious parts of the measurement process. A digital balance (Sartorius H51) was used to weigh the firebrands.

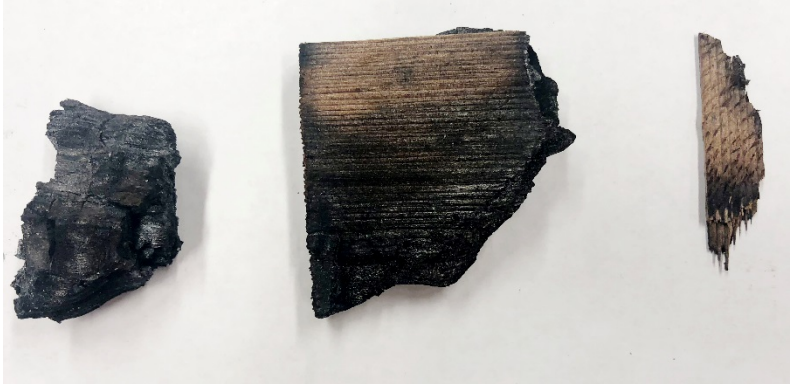

Figure 3-3. Charred and partially charred firebrands (from left to right)

3.4.2. Projected area

To determine the projected area, the randomly chosen firebrands from a given bag were scattered on a white sheet. A photo was taken using a digital camera (Nikon D5600+18-55 VR kit lens), placed perpendicular to the sheet. Three light sources provided adequate lighting from three directions (120 degrees interval) on the sheet to avoid shadows. Limited detailed information is available in the literature about the calculation of the surface of a firebrand [38,56,39,20]. Typically, the camera is fixed on a tripod and positioned over the center of the sheet. However, the sheet may be tilted from the desired position, and this could cause delay in the measurement process if a user wanted to rotate and crop the image manually. Furthermore, placing each firebrand on the sheet added significant time to the measurement process compared to just scattering them. These manual processes increased the overall measurement procedure time, especially with larger sample sizes. As the goal was to minimize the labor in measuring the projected area of the firebrands, a MATLAB code was written utilizing the algorithm described below:

The firebrands were placed on a white paper regarding to the bag they belonged to and then using a digital camera, positioned perpendicular to the sheet, an image was

taken. There was adequate lighting on the sheet to avoid making any shadows. The images were processed with MATLAB Image Analysis Toolbox. The input of the code is a noisy image Figure 3.4.a. Stretching the histogram of the colors of the image, in the first step, the contrast of the image is increased (Figure 3.4.b). Then considering the increase in the intensity of the colors the edge of the sheet is detected (Figure 3.4.c) and the equation of the line, edge of the sheet, is calculated. After that, the tilt angle of the sheet is calculated and then the image is rotated by the same angle (Figure 3.4.d). The image is then cropped from the borders (Figure 3.4.e) and the noise is removed (Figure 3.4.f). Finally the borders are cleaned (Figure 3.4.g), the holes in the boundaries are filled (Figure 3.4.h), and the objects are labeled (Figure 3.4.i). The number of the pixels of the objects is counted for each image and with respect to the ratio that is defined by the rectangle, the projected areas are transferred to an Excel Spread sheet.

Using this method, counting and calculating the projected area of hundreds of firebrands can be accomplished in seconds.

3.4.3. Results

In a sample, the expected value of a parameter represents the most probable value. For firebrands, the mean value (of any parameter) is an indicator of the accumulation of the firebrands. In addition to accumulation, the ignition potential of a firebrand storm depends on individual large firebrands whose thermal inertia are high. These larger firebrands cause the probability distribution function (PDF) to be asymmetric, which is measured by the skewness.

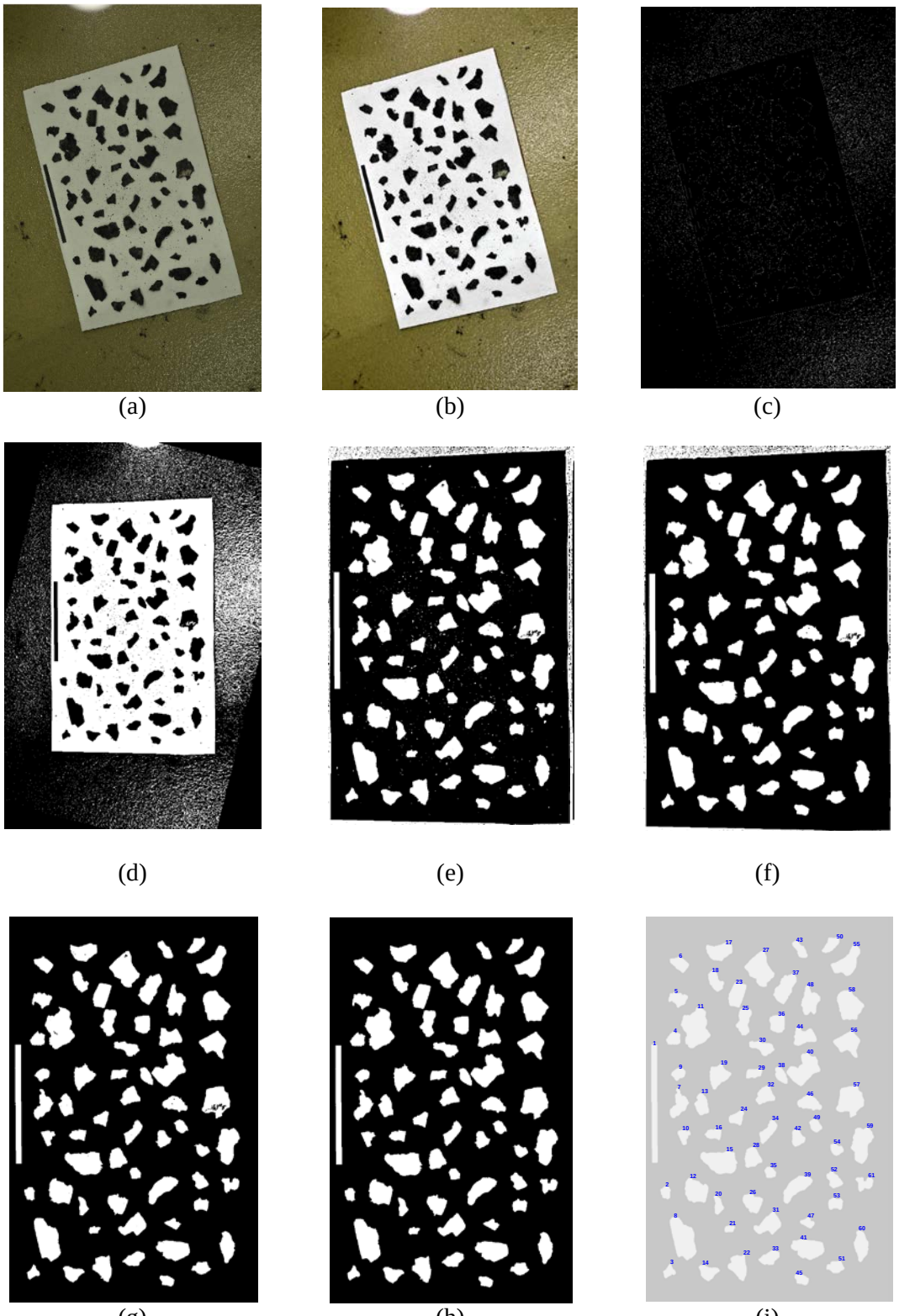

(a) (b) (c)

(d) (e) (f)

(g) (h) (i)

Figure 3-4. Detailed steps to calculate the projected area

Table 3.1 tabulates the skewness of each parameter, including the mean, standard deviation, and correlation values between each parameter. The closer the correlations are to unity, the stronger the parameters grow with each other. When the correlations are closer to minus one, an increase in one parameter results in a decrease in another. Obviously, zero correlation means no relation between the parameters exists.

Table 3.1 also showed that the mean and median for all the quantities of interest increased with increasing wind speed. Moreover, the standard deviation of the parameters increased with wind speeds, which implies that the range of variation in the size and mass of the firebrands was larger at stronger winds. As observed in previous studies [59], there is a strong correlation between mass and projected area but the value of the other two correlations (mass and flying distance/projected area and flying distance) were moderately small.

Table 3-1. Summary of the measured parameters

Physical quantity	**Statistical quantity**	**Idle (5.36 m/s)**	**Medium Wind (11.17 m/s)**	**High wind (17.88 m/s)**
Flying Distance (m)	Mean	2.71	3.2	5.07
	S. D.	3.72	3.24	3.88
	Skewness	0.47	0.52	0.27
	Median	1.11	1.99	3.20
Projected Area (cm^2)	Mean	2.10	3.90	4.87
	S. D.	2.72	6.48	7.87
	Skewness	5.17	6.62	13.47
	Median	1.26	2.08	2.99
Mass (g)	Mean	0.09	0.25	0.38
	S. D.	0.24	1.28	1.44
	Skewness	7.63	25.37	21.99
	Median	0.02	0.06	0.14
Mass and Area Correlation		0.83	0.72	0.90
Mass and Flying Distance Correlation		-0.20	-0.11	-0.07
Area and Flying Distance Correlation		-0.24	-0.20	-0.10

3.4.4. Uncertainty in the measurement

Uncertainty in the measurement of mass and traveling distance may be easily determined by looking at the catalog of the devices. In order to investigate the uncertainty of the projected area, different geometries have been plotted on a sheet with known pixel numbers and areas. As Photoshop plots with three significant digits (0.01 cm^2 resolution), the calculations also presented three significant digits. Miscounting the pixels typically happens at the borders of an object, which depend on the user-defined binary image threshold. The threshold defines how sensitive the code should be when it converts different shades of gray in an RGB image to a binary one. In order to investigate the effects of thresholding, objects with tilted sides and known surface areas were plotted, see Figure 3.5a. The object in the top left corner represents the edges with 45 degrees. The middle rectangular represents edges with 0/90 angles. Moreover, in order to study the curvature, a circle was also plotted. The right bottom corner rectangular is to check the validity of the code. As depicted, setting the thresholding value (α) to 0.20 results in loosing numerous pixels in counting. Conversely, setting the thresholding value to 0.9 leads to identifying any dark point on the sheet as an object.

In order to find the proper range for thresholding value, alpha was increased from 0.1 to 1 with 0.1 intervals. It was observed that the minimum error (difference between the column number 1 and 2-4) happens when $0.6 < \alpha < 0.8$ which numerical values are shown in Table 3.2.

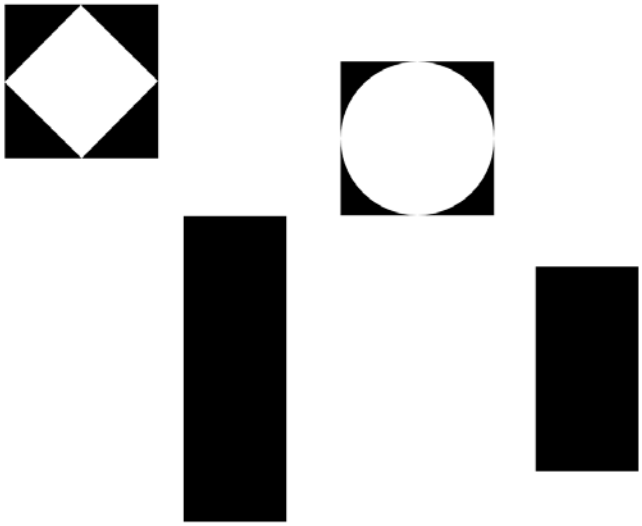

(a)

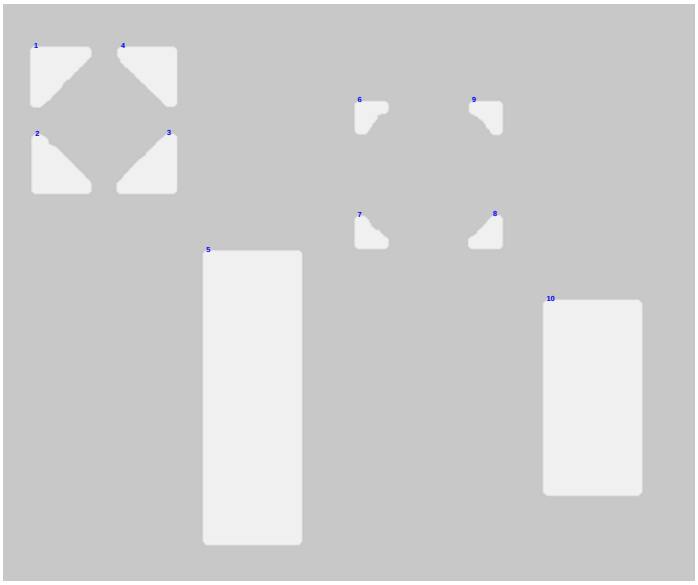

(b)

Figure 3-5. Effects of thresholding; (a) original (b) low (c) medium (d) high

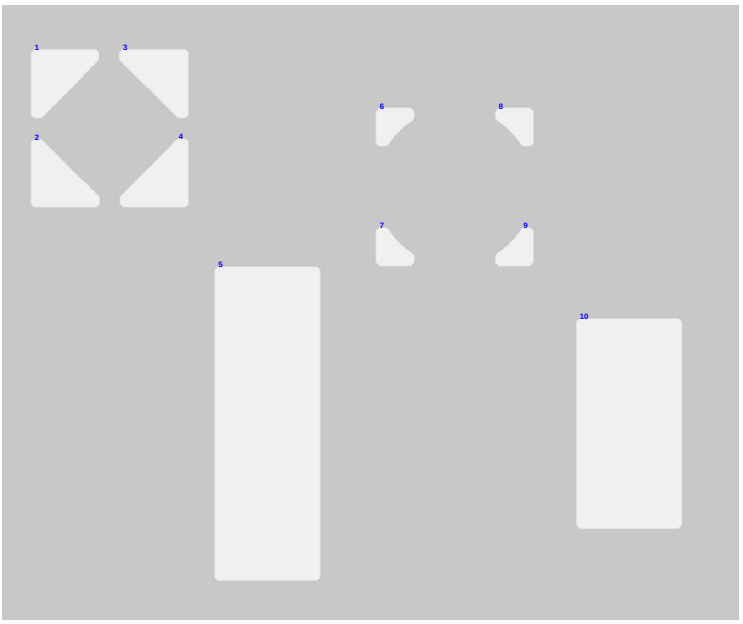

(c)

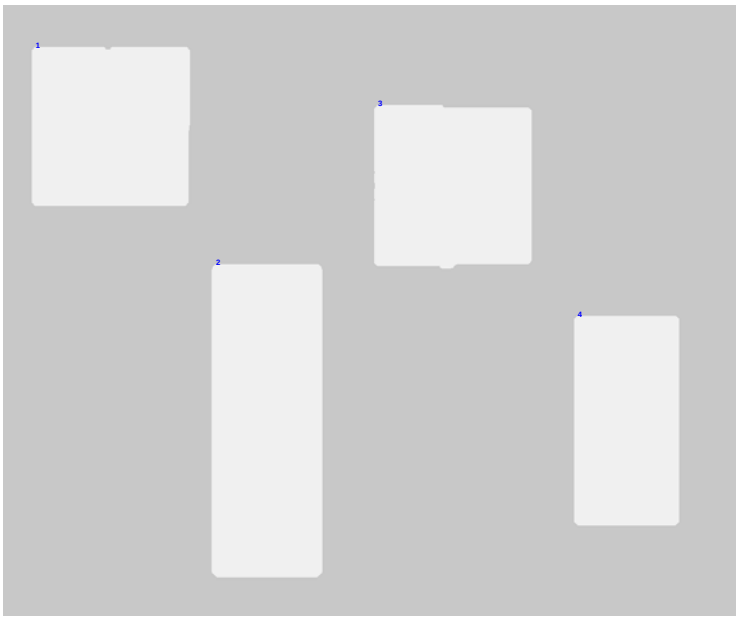

(d)

Figure 3.5. Continued

Table 3-2. Relative Error calculation

Best Estimation	α=0.3	α=0.6	α=0.8	Error α=0.3	Error α=0.6	Error α=0.8	Max-Min
1.81677	1.71437	1.74800	1.74891	0.05636	0.03786	0.03735	0.0345
1.81677	1.69634	1.73638	1.73760	0.06629	0.04425	0.04358	0.0413
1.81677	1.74188	1.77428	1.77673	0.04122	0.02339	0.02204	0.0348
1.81677	1.73394	1.76114	1.76847	0.04559	0.03062	0.02658	0.0345
19.35480	19.35480	19.35480	19.35480	0.00000	0.00000	0.00000	0.0000
0.77880	0.57676	0.60274	0.60396	0.25943	0.22607	0.22450	0.0272
0.77880	0.57034	0.60304	0.60365	0.26767	0.22567	0.22489	0.0333
0.77880	0.58256	0.60274	0.60335	0.25197	0.22607	0.22528	0.0208
0.77880	0.57095	0.60274	0.60274	0.26688	0.22607	0.22607	0.0318
12.90320	12.92887	12.92887	12.92887	0.00199	0.00199	0.00199	0.0000
Average				0.1257	0.1042	0.1033	0.0258

The average difference between the minimum and maximum proper thresholding values is 0.026 which may be chosen as the uncertainty for this method. In practice, however, there are several sources of uncertainties which can affect the uncertainty which are demonstrated in Figure 3.6.

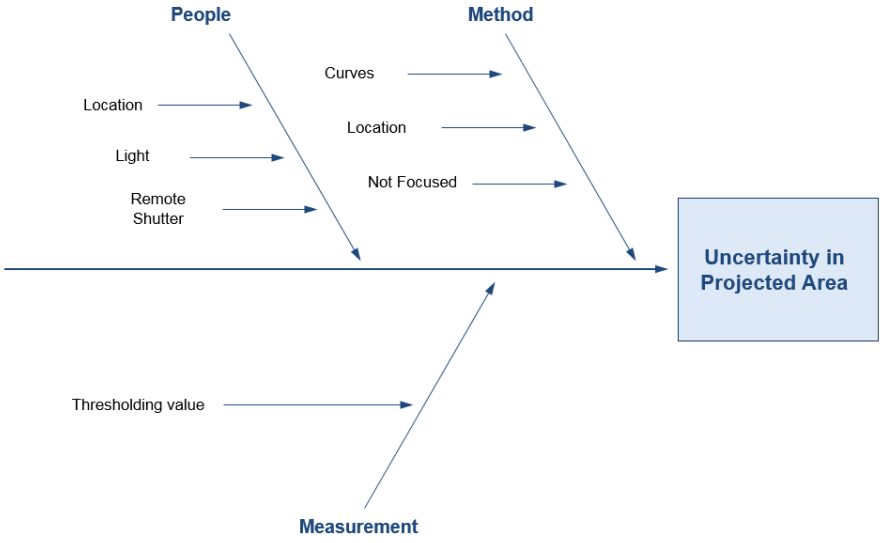

Figure 3-6. Fishbone diagram for uncertainty

Figure 3.6 shows the major influential parameters of uncertainty in measuring the projected area of firebrands. For example, if the central points of the camera and the sheet were not aligned or there was inadequate light on the sheet, shadows may be created that

leads to increasing uncertainty. Moreover, blurry images can lead to miscounting the pixels which can be minimized by employing camera's auto focus tool. Aligning the sheet center with the camera, providing adequate light, and using a remote shutter, the uncertainty sources can be minimized.

In order to address the effect of thresholding, 27 real-world firebrands over a range of sizes were scattered on a sheet and the complete measurement process was performed at two different thresholding values similar to the third and fourth columns in Table 3.2. Table 3.3 tabulates the numerical results based on two thresholding values (0.6 and 0.8). The last column in this the difference between the two middle columns.

The average of the differences of the last two columns (0.04 cm^2) in Table 3.3 can be cosnidered as the uncertainty value in this measurement. However, the maximum value (0.11 cm^2) is selected in order to be extremely conservative.

The standard uncertainty, standard error, of the measurement can be calculated by dividing the standard deviation by the square root of the sample size. The standard uncertainty of the measured mass, travel distance, and projected area are equal to 0.0037 grams, 0.05 meter, and 0.05 cm^2, respectively.

Table 3-3. Effects of thresholding in measurement

Firebrand Index	α=0.6	α=0.8	Difference
1	1.7774	1.8033	0.0259
2	1.4041	1.5001	0.0961
3	0.6840	0.7430	0.0590
4	0.5803	0.5937	0.0134
5	1.1888	1.2415	0.0527
6	0.4161	0.4438	0.0277
7	0.9574	1.0128	0.0554
8	0.8936	0.9302	0.0366
9	1.3351	1.4228	0.0876
10	0.9822	1.0324	0.0502

11	0.5187	0.5665	0.0478
12	0.6789	0.7055	0.0265
13	0.7376	0.7644	0.0267
14	0.6787	0.7227	0.0440
15	0.7063	0.8179	0.1116
16	0.5943	0.6193	0.0250
17	0.2311	0.2652	0.0341
18	0.4419	0.4685	0.0267
19	0.2911	0.3196	0.0285
20	0.3136	0.3483	0.0347
21	0.8540	0.8996	0.0456
22	0.4611	0.4817	0.0206
23	0.5152	0.5886	0.0734
24	0.1578	0.1827	0.0250
25	0.8899	0.9414	0.0515
26	0.3452	0.3983	0.0531
27	0.3137	0.3737	0.0600

As already mentioned, skewness is an important parameter in studying PDF asymmetry. In order to assess the uncertainty in measuring the reported value of skewness (Table 1), the uncertainty budget first needs to be determined. Equation 1 shows that the uncertainty in skewness depends on the uncertainties of the mean and individual firebrands:

$$b = \frac{\frac{1}{n}\sum_{i=1}^{n}(x_i - \overline{x})^3}{\left[\frac{1}{n-1}\sum_{i=1}^{n}(x_i - \overline{x})^2\right]^{3/2}} \quad (1)$$

Thus, its uncertainty can be calculated as:

$$u_c = \sqrt{(\frac{\partial b}{\partial \overline{x}}u(\overline{x}))^2 + (\frac{\partial b}{\partial x_i}u(x_i))^2}$$

Where $u(x_i)$ and $u(\bar{x})$ have already been calculated as 0.11 and 0.05, respectively.

Taking the partial derivative with respect to x_i and $\bar{x}$ we have:

$$\frac{\partial b}{\partial \bar{x}} = \frac{\left(\frac{A}{4414}\right)\left(\frac{A}{4413}\right)^{\frac{3}{2}} - \frac{3}{2}\frac{\sqrt{A}(B)}{4413}\frac{A}{4414}}{\left(\frac{A}{4414}\right)^2}$$

$$\frac{\partial b}{\partial x_i} = \frac{\left(\frac{(B)\left(\frac{A}{4413}\right)^{\frac{3}{2}}}{4414} - \frac{3}{2}\frac{A\sqrt{\frac{A}{4413}}(B)}{4414\times 4413}\right)(n-1)^3}{A^3}$$

Where

$$A = -4414\bar{x}^3 + \sum_{i=1}^{4414}(3\bar{x}^2 x_i - 3\bar{x}x_i^{\,2} + x_i^{\,3})$$

$$B = -3\times 4414\times \bar{x}^2 + \sum_{i=1}^{4414} 6\bar{x}x_i - 3x_i^{\,2}$$

The numerical values for the derivations are:

$$\frac{\partial b}{\partial \bar{x}}\Big|_{\bar{x}=3.62, n=4414} = 1.06$$

$$\frac{\partial b}{\partial x_i}\Big|_{\bar{x}=3.62, n=4414} = 0.01$$

Finally, the numerical value for the combined uncertainty for skewness reduces to 0.05 cm^2. Employing a similar approach, the uncertainty in measuring the skewness for mass and traveling distance are 0.005 and 0.2, respectively.

3.5. Mass Predictive Models

As explained earlier, among all measured values, projected area and mass were more time consuming to measure. However, employing the suggested technique discussed in this chapter, measuring the projected area has become a straightforward task. Measuring the mass, on the other hand, still remains a tedious task because each of the 4415 firebrands must be weighed individually. This sparked the process to begin brainstorming how to make the weighing process less labor intensive.

To shorten the time needed to weigh firebrands, machine learning (a type of artificial intelligence that enables the computer to predict or classify a set of data [60]) can be employed. There are two major categories in machine learning, shallow and deep learning [61,60,62,63] and each one contains several different algorithms in order to predict a variable. From the first category (shallow learning), the Gaussian process regression was selected for this study. This type of regression works well for continuous regressed values, such as mass [64,65]. This method provided the best estimated value for the prediction as well as a probabilistic range that defined the certainty about the predicted values. From the deep learning category, feed-forward neural network was selected. This technique works best when the sample size is relatively large and the relationship between the predictors (input) and response (output) can be defined with a mathematical relation. The mathematical formulation of the Gaussian process regression and neural network is beyond the scope of this paper; however, the method has been subsequently explained in a narrative and explanatory way.

3.5.1. Gaussian regression process

The idea of Gaussian process regression [66,67] is the extension the probability distribution of numbers to the probability distribution of functions. In this study four

different measurements were conducted for each firebrand, where the obtained data set can be analyzed in two different ways. The conventional way is to see all the points in four dimensional space. The alternative look is to consider them as the values of a function sampled at four points. In the first perspective, points can be chosen from a probability distribution which are typically determined by a mean vector and a covariance matrix. In the second analyzation, we can have a probability distribution of functions determined by mean and covariance functions. This covariance function depends on the Kernel function which describes the influence of each point to its neighbors.

In order to predict the value of an input that the model has not yet seen before (validation subset), Gaussian regression built a multidimensional normal distribution with the seen data (training subset). In other words, in order to regress the $n+1th$ value, an n dimensional normal distribution is built. Having conditioned (sliced) the multivariate PDF, the dimensions of the PDF reduces and ultimately the most probable value, as well as a probabilistic range for the prediction, can be estimated [65]. The probabilistic range depends on the covariance function between the inputs that the user provides for the algorithm.

Before moving on to neural network section, it was necessary to address the effects of the training and validating subsets on the model. The training subset is used to build a model to predict the response value and the validation set was used to assess the accuracy of the build model based on the training data set. Typically 70% of the data is implemented to train the model and 30% is held out for the validation set [68]. The accuracy of the model, however, heavily depends on how the data is split and trained. Although one may have chosen the subset elements randomly, it would be more accurate

if the division process was repeated multiple times in a random way in order to minimize the dependency of the model on the subsets. This process is known as cross validation [69]. In this method, the data would randomly be divided into *k* sets. *K-1* of the sets would be used to train and 1 will be saved for validation. This process continues until all the subsets have been employed for validation at least once [69]. The larger the *k* is, the more computational efforts we will have but the model will be more robust.

3.5.2. Back-propagation neural networks

Three tasks can be done with neural networks: clustering, classification and regression. The latter one is the desired goal in this research. The major difference between regression and the other two applications is the number of neurons in the output layer. Unlike regression, in clustering and classification multiple neurons can exist in the output layer.

The fundamental concept of neural networks is to identify the key characteristics of human brain and mimic these into a form of computer model. In the human's brain, a large number of neurons are interconnected by electrical pathways. Information flows between the neurons in form of impulses, get processed and then flows out. This enables the brain to react based on previously observed patterns. The same idea is employed to create an artificial interconnected neural network. The impulses in a human brain are modeled with numerical values known as "weights". Adjusting the weight values trains the network to achieve the desired outcome.

The back-propagation algorithm consists of two major processes: forward and backward propagating. In forward propagation the network typically learns the pattern

and in backward propagation the errors are minimized employing an optimization technique.

The neurons are arranged in three discrete layers: input layer, hidden layer and output layer. Each neuron is connected to all the other neurons in the previous layer. Information is passed through the neurons via a numerically weighted value. The larger the values are, the stronger the connections are between the neurons. The values of the neuron in the previous layer, multiplying by the associated weight between the neurons forms an input for the transfer function for that layer. The transfer functions are typically simple mathematical relations which determine the relationship between the inputs and the outputs. The output of the transfer function is the input for the next layer of neurons. When training starts, usually the weights are distributed randomly at first and outputs are calculated. Then, the errors between the estimated outputs and the training data are calculated. At this point, the role of back-propagation appears. The error goes back to the network and the optimization algorithm changes the initial numerical weights to minimize the error. This procedure keeps repeating until the minimum error achieves. Figure 3.7 graphically depicts the process. As can be seen, the weights (arrows) and organization of the hidden layer keep changing until the difference between the regressed value and the desire one (training data set) is small.

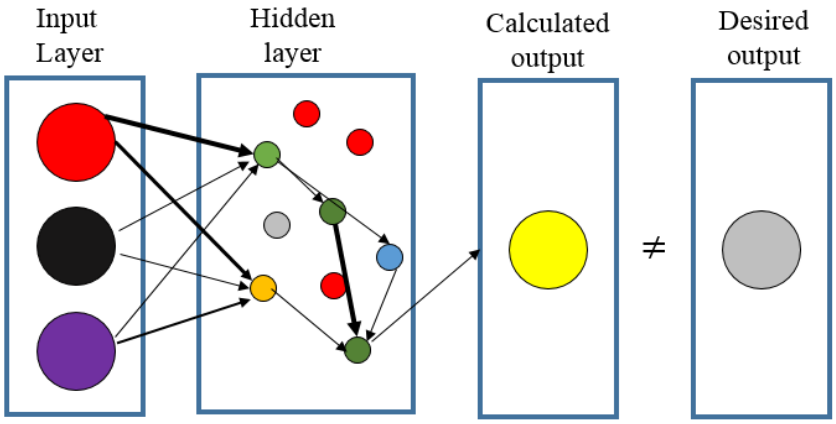

(a)

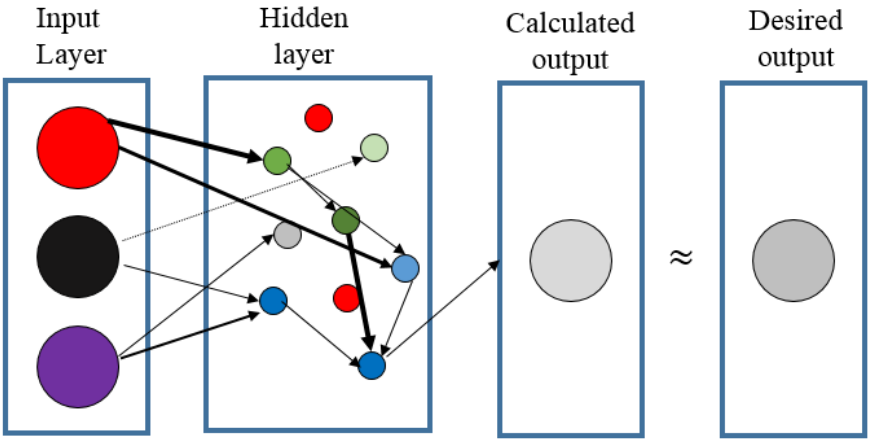

(b)

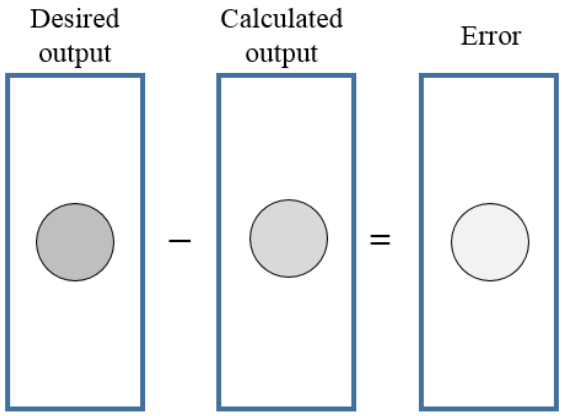

(c)

Figure 3-7. Neural network algorithm

Several parameters can be manipulated to minimize the network error such as weights, learning rates, and number of neurons. Thus, it would not be difficult to

minimize the error by overfitting the data. In this case, the predictive model may work perfectly for a seen set of data but is not applicable for a new data set. Thus, the optimizing algorithm needs to stop before reaching the over fitting status.

In neural networks the entire data set is divided into three groups: training, validation and testing. The validation partition is extracted from data to avoid overtraining. During the training phase, the validation set is evaluated and once the validation error begins to increase the optimization algorithm stops. A numerical example will be explained in section 3.6.

3.6. Regression Results

In order to evaluate the influence of different inputs on predicting the mass of each firebrand, a decision tree model was built based on the inputs. The main idea behind the decision tree is that it considers the different attributes in the data and uses them to split the data into subsets [70]. The obtained split subsets are called “pure” if all the elements in that subset are homogenous and called “impure” vice versa. Once all the predictors have been split, the algorithm starts to split each subset in order to find the purest subset. Needless to say, clustering the data into an absolutely “pure” subsets rarely happens.

The importance of the predictors in estimating the response value is measured by the magnitude of a fraction; the nominator is the purity of each branch and the denominator is the number of binary decisions to reach the final step in each subset. The larger the ratio, the more significant that parameter in predicting the response.

Figure 3.8 represents the important parameter in predicting the mass for each firebrand. As can be seen, projected area, distance, and wind speed are the three important

predictors. In order to reduce the complexity of the model, the three most important predictors mentioned above were chosen to build the model with. Having employed 3/2 Matérn kernel function and used a cross validation factor of five, *(k=5)*, a Gaussian regression was built over the training set.

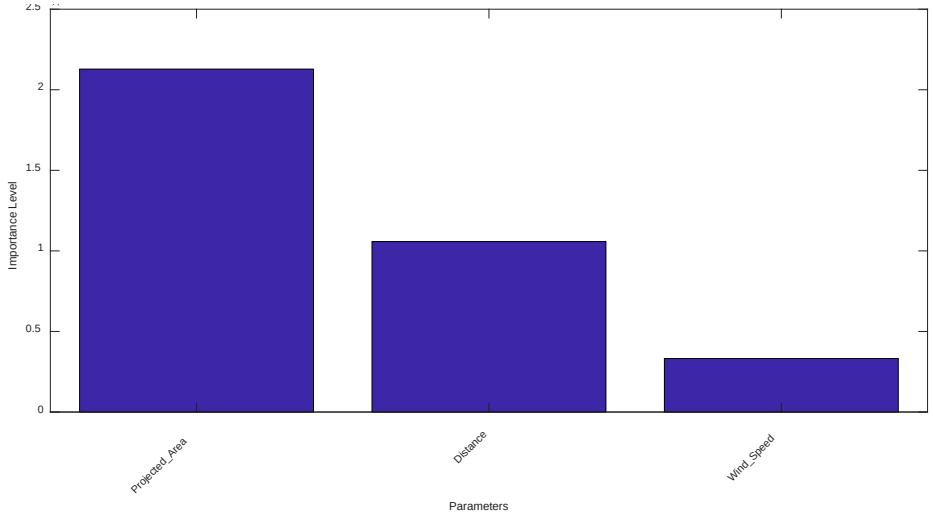

Figure 3-8. Predictor Importance

3.6.1. The Gaussian process regression results

Figure 3.9 depicts the results of the prediction of the mass for idle, medium, and high wind speed experiments. In the figures, the red dots depict the measured mass, and the blue circles illustrate the values from the predictive model. The dotted line shows the maximum probabilistic range for what the mass of a firebrand could be based on a given surface area, traveling distance, and wind speed. This will be helpful to simulate the worst case scenario and monitor how large/heavy a firebrand can be at any desired distance or wind speed.

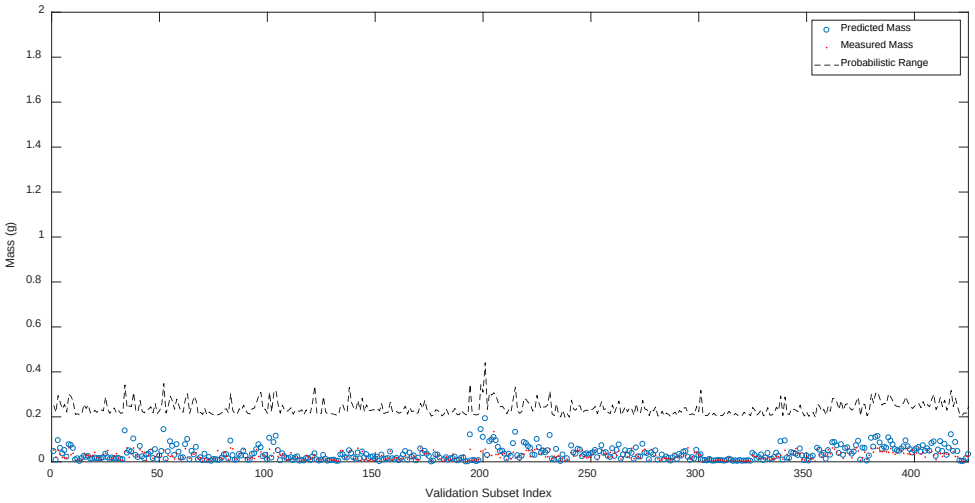

(Idle)

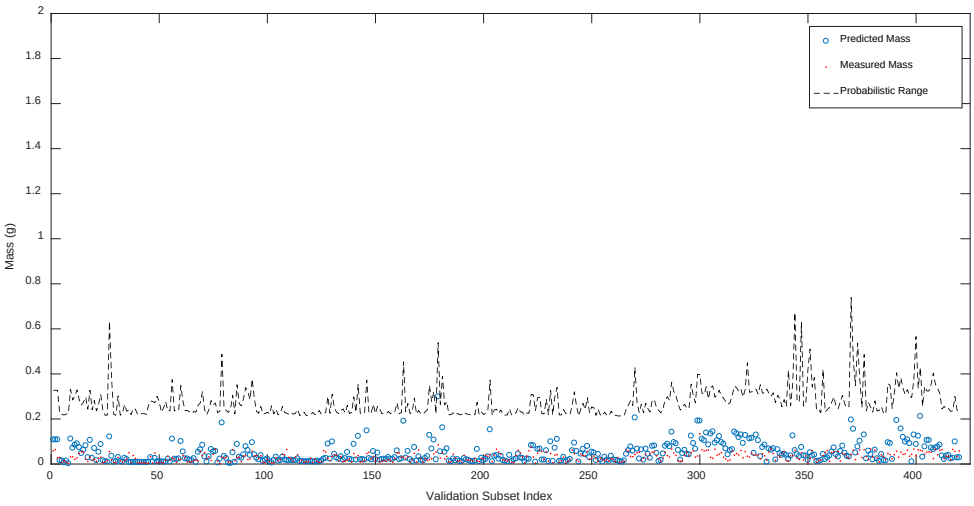

(Medium wind)

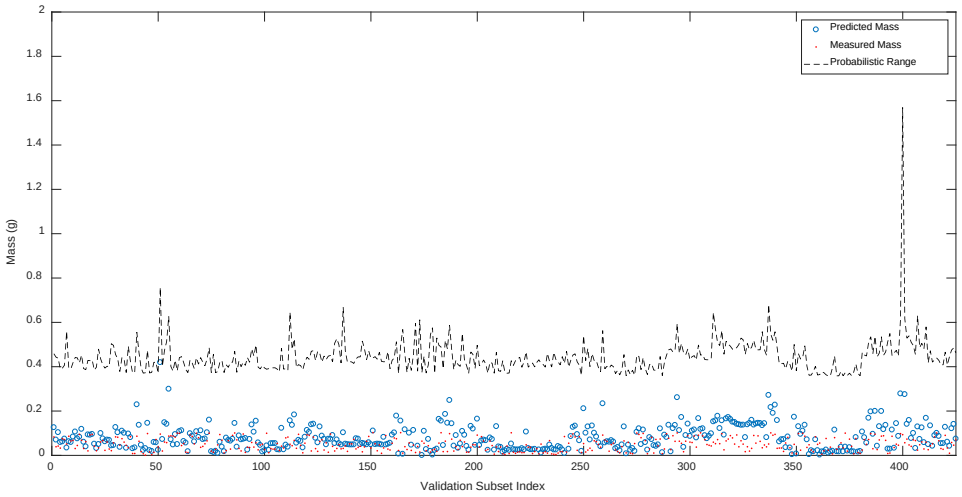

(High wind)

Figure 3-9. Results of predictive model with the upper limit estimation

In order to visualize the relative error between the predicted and measured values, the validation subsets were plotted for each firebrand (Figure 3.10). Referring to the figures, the model was able to predict mass within 7 percent. It must be noted that although the individual values for mass have been predicted sufficiently accurate, the individual values do not play an important role when one intends to create a PDF based on the data.

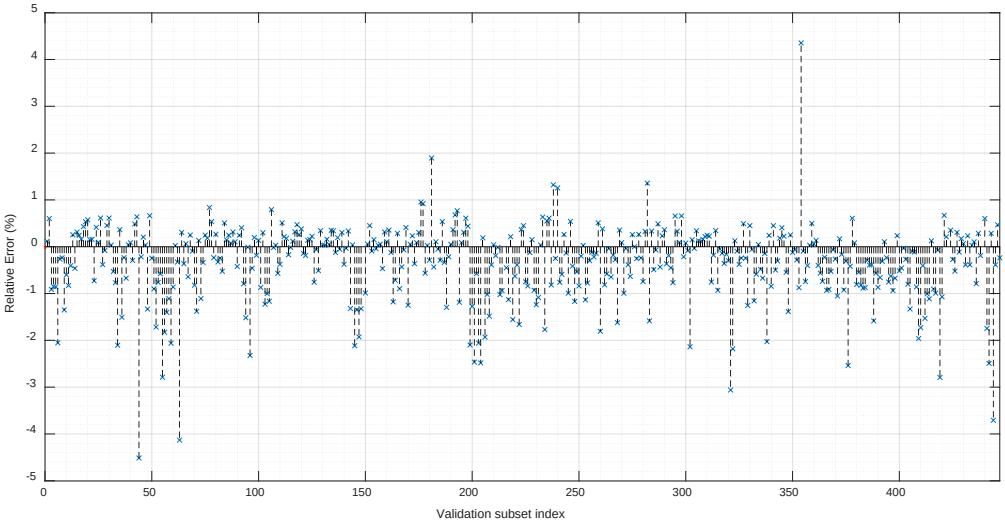

(Idle)

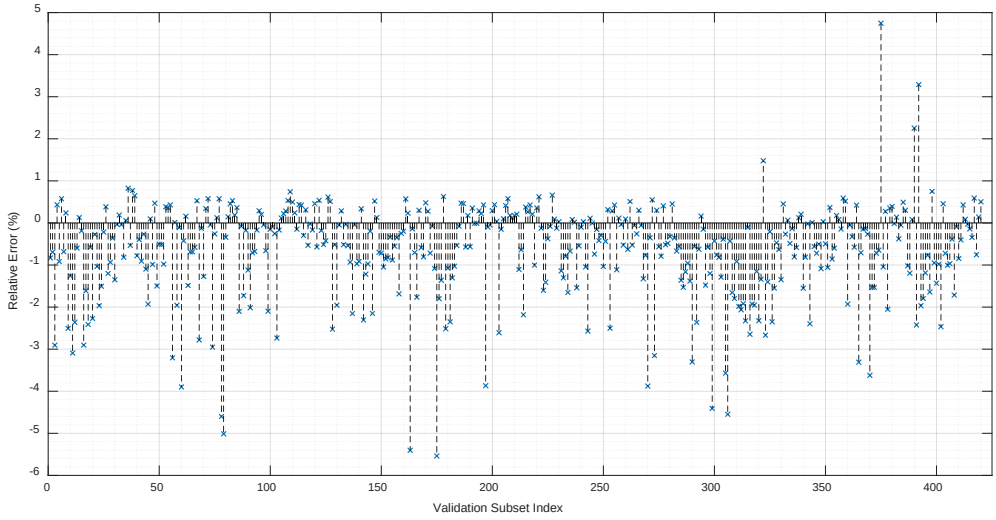

(Medium wind)

Figure 4.10. Individual error for each prediction

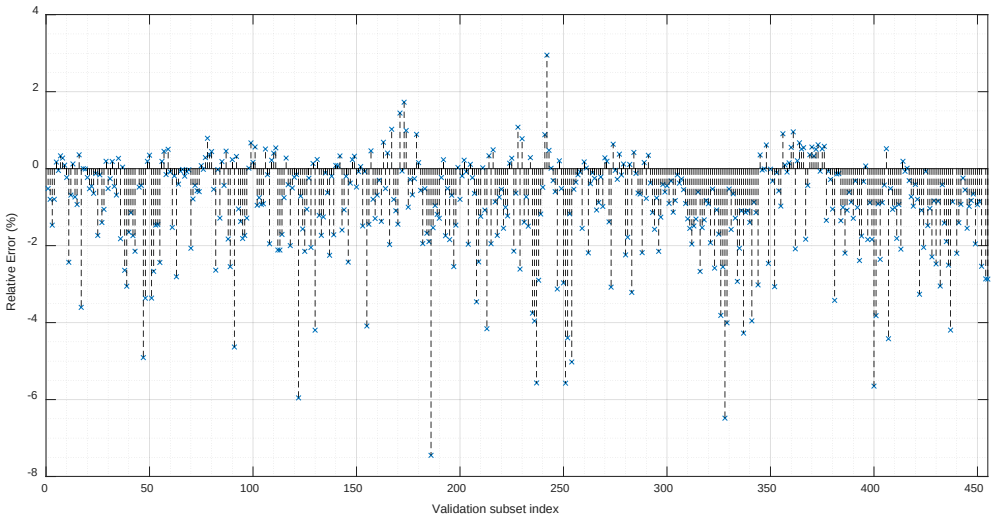

(High wind)
Figure 4.10. Continued

Regardless of the underlying PDF for a statistical model, all of them require the mean, standard deviation and correlations between the parameters. Bearing in mind that the statistical analysis suggested a sample size of 1400, the relative error of mean, standard deviation, and correlations versus the training size are plotted in Figure 3.11-13. In each Figure, 5 and 10 percent error bars were plotted with red dotted lines. What stood out in these figures was when setting the training size of 700, the model can predict the mean, standard deviation and correlations of the mass with less than 10 percent error. In other words, employing this model, the results that one may obtain by counting 700 firebrands was less than 10 percent deviated from counting 1400 firebrands. Hence, employing this technique can significantly reduce the labor involved with the measurement process.

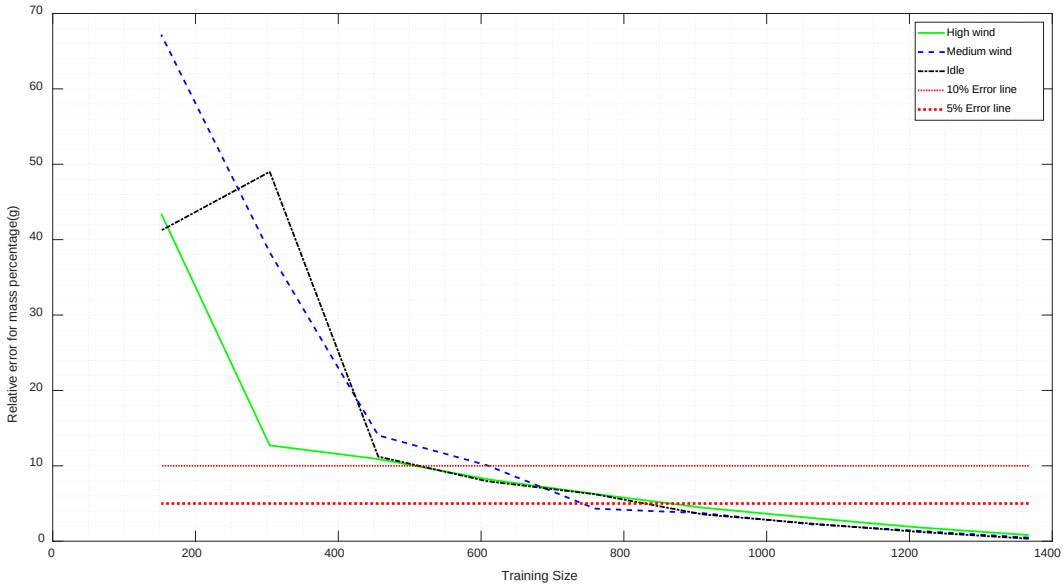

Figure 3-10. Variation predication of mean for mass with sample size

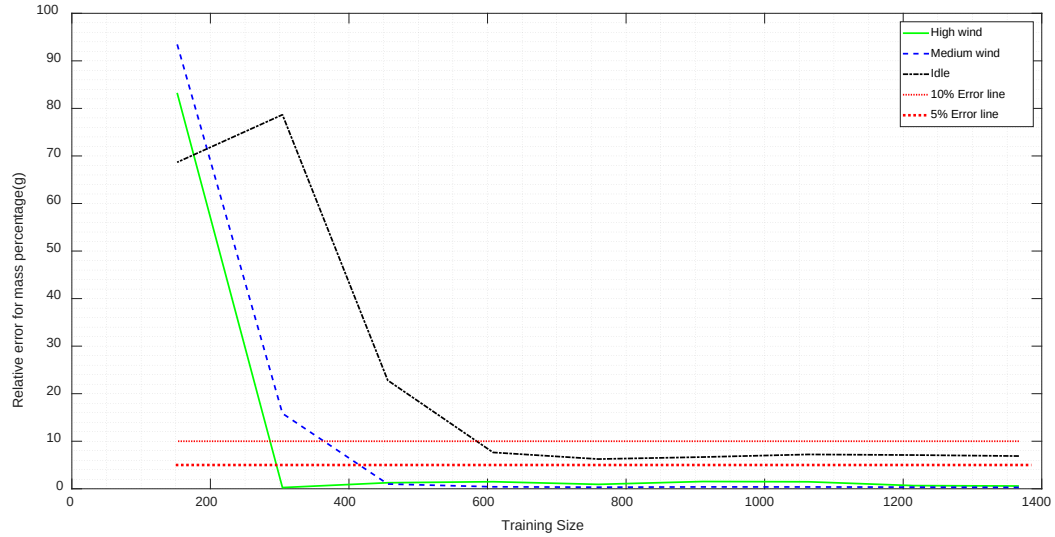

Figure 3-11. Variation predication of standard deviation for mass with sample size

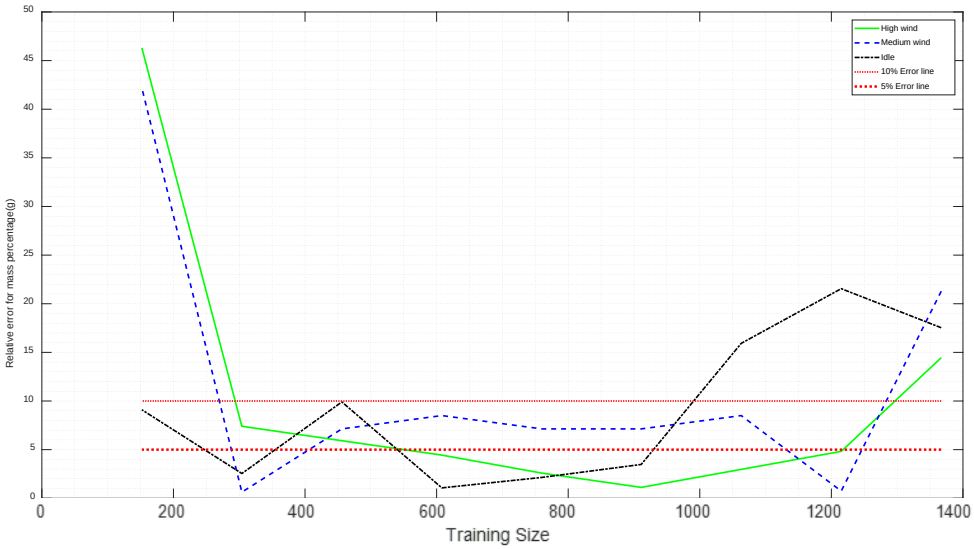

Figure 3-12. Variation predication of mass and area correlation with sample size

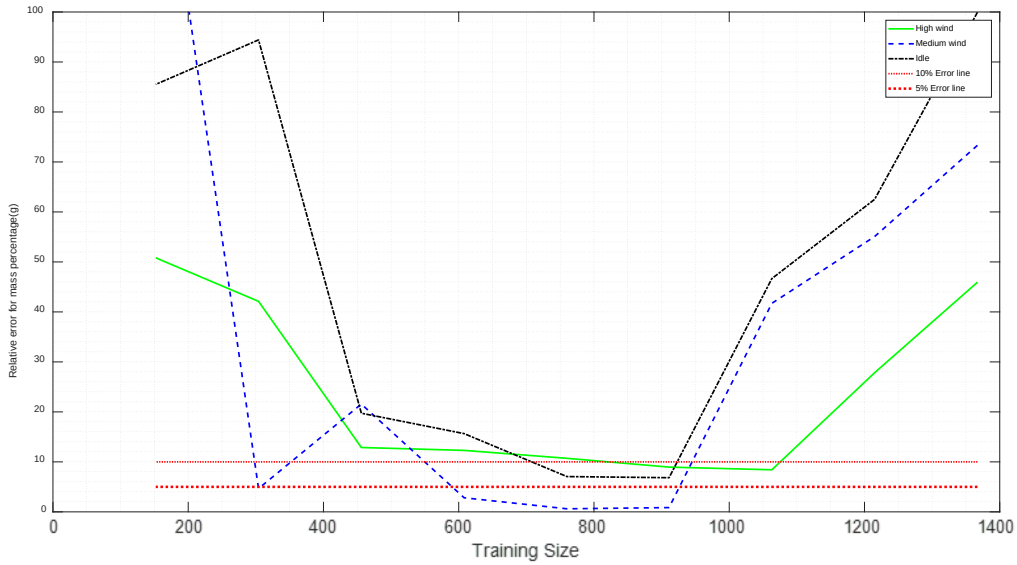

Figure 3-13. Variation predication of mass and distance correlation with sample size

As seen in Figures 3.12 and 3.13, unlike 3.10 and 3.11, the relative error increases when the training size gets larger than approximately 900 samples. The explanation originates from overtraining the model. In any regression problem, if the complexity of the model increases, it is very likely that the model is not capable of predicting the validation set very well [71]. If the model touches every point in the training set exactly, it involves the fluctuation and noise in the training set and will be trained without any

uncertainty for the prediction. However, the model will lose the ability to predict a response value for a new unseen point. In Figures 3.10 and 3.11, since the concept of the mean and standard deviation was to subtract each point from the mean value, the noise in the data set goes away. Conversely for correlations, Figures 3.12 and 3.13, when the training size gets larger than 900, the model losses its accuracy to predict the mass and then the relative error in calculating the correlations increases. It should be mentioned that in the tests, we have no other option but to take the center pans as the landing position of the firebrand. Thus the data is inevitably being manipulated. Considering this fact, the calculated correlation between the mass and flying distance may have less degree of accuracy comparing to other presented parameters.

3.6.2. Neural network results

The results of neural network prediction is depicted in Figure 3-14 for idle, medium and high wind. Ten hidden layers were used for this prediction. As can be seen, the model can predict the mass for more than 200 firebrand in each wind speed with the maximum error of 6%.

In addition to the current models, a model was created using random data from different the wind speeds. In total, 4415 firebrands were collected at three different wind speed. Using 70% for training, 15% for validation and 15% for testing, it was observed that the mass for approximately 650 firebrands were estimated within 10% error. See Figure 3.15 for details). The histogram of the error is plotted in Figure 3.16 where the majority of the errors fall in the vicinity of zero.

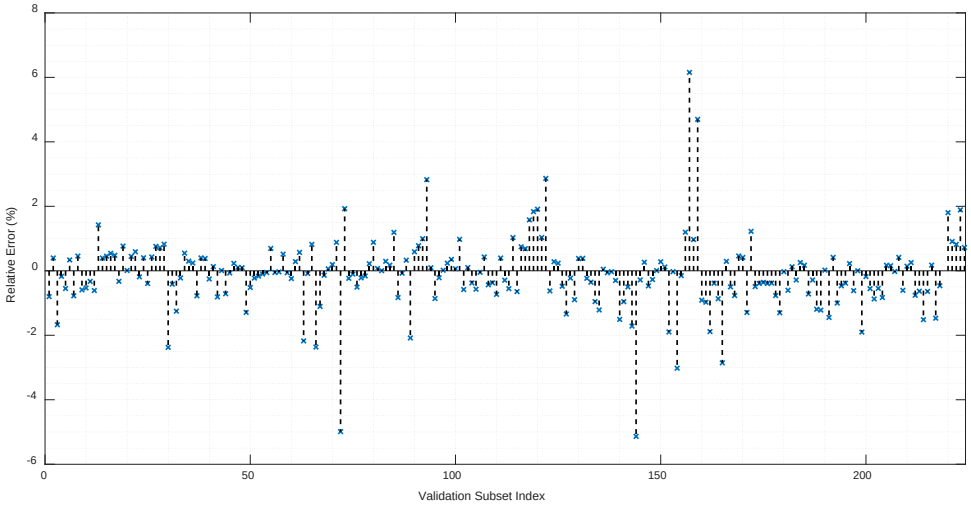

Idle

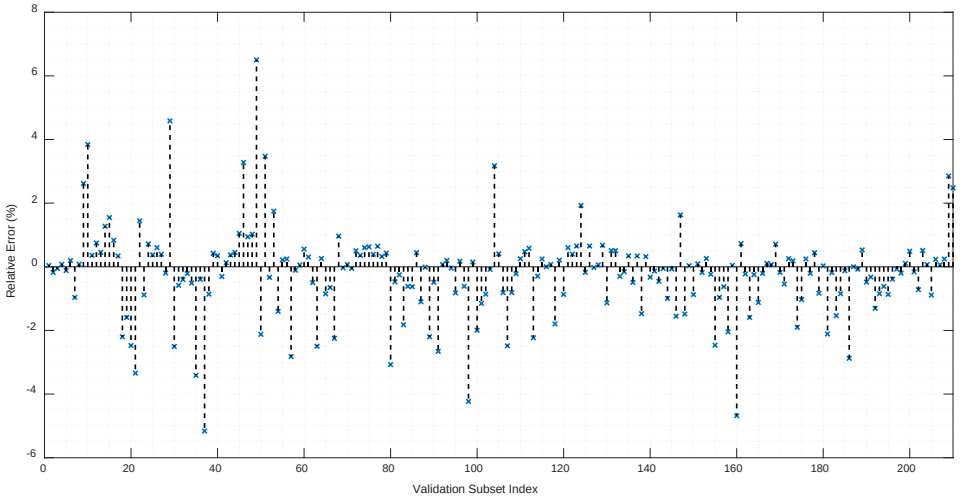

Medium wind

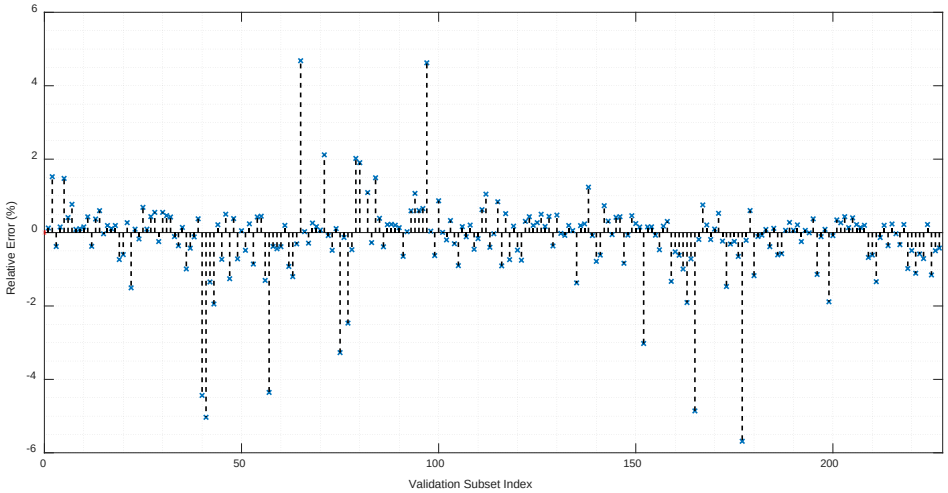

High wind

Figure 3-14. Error of regression with neural network

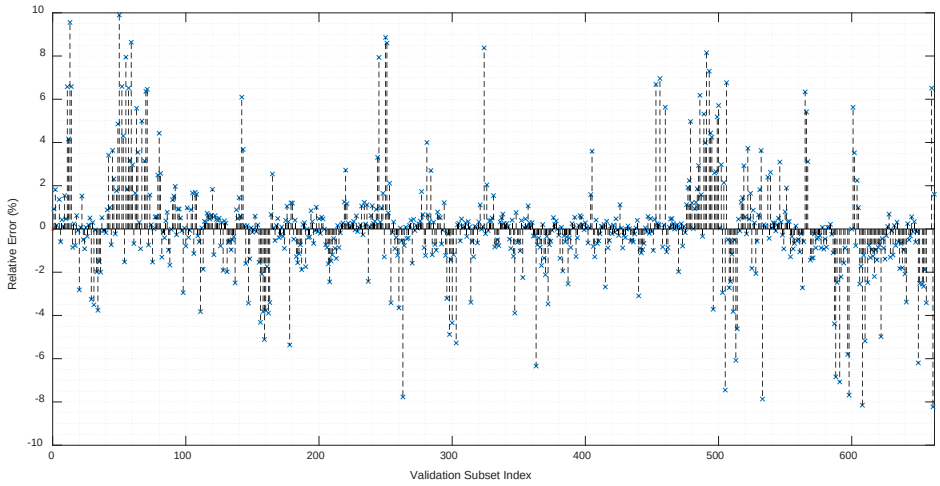

Figure 3-15. Error of over-all regression with neural network

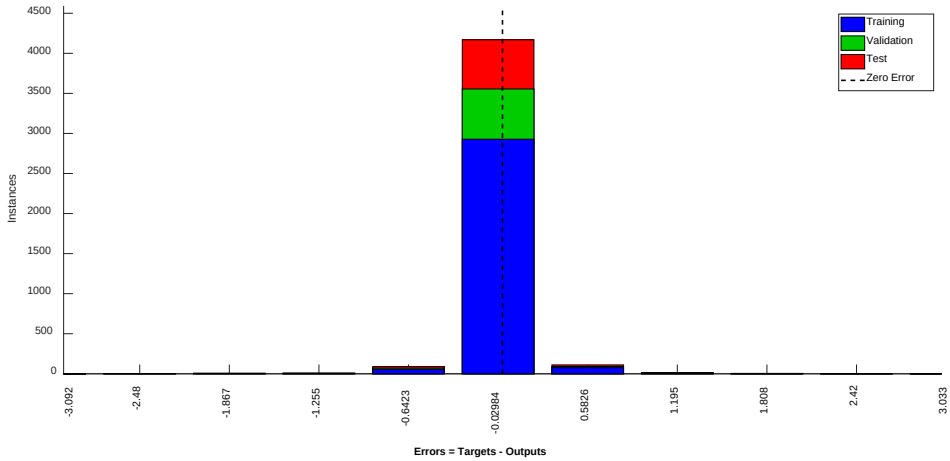

Figure 3-16. Histogram of errors in figure 4.15

In section 3.5.2, overfitting phenomenon in deep learning was addressed. Figure 3-17 depicts this issue graphically. The network parameters, weights and biases, can be adjusted in order to derive the regression error o minimum. However, this may lead to lose the robustness of the model. One way to avoid this is to stop the iteration before the error in validation subset falls into its local minimum. After each iteration on the training set, the current network regresses the validation subset and the error is calculated. Once the error started to increase, the network stopped generalizing accurately, providing evidence of overfitting. As can be seen in Figure 3.17, at the 10^{th} epoch best validation

performance was seen. An epoch describes the number of times that the algorithm sees the entire data within the three subsets.

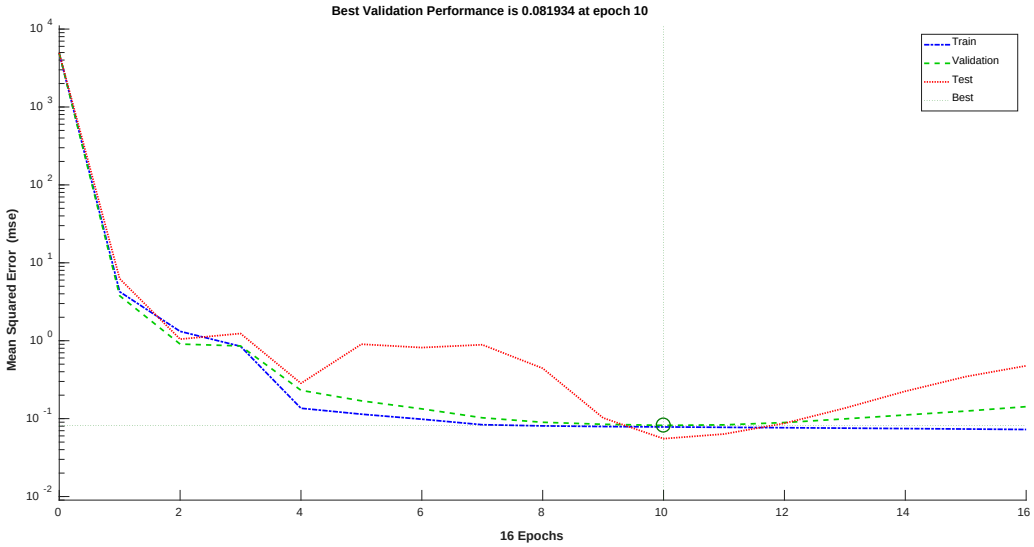

Figure 3-17. Over training threshold

3.6.3. Comparing the methods and conclusion

The essence of Gaussian process regression and neural networks differ significantly. The former one is a parametric technique and the latter one is a non-parametric one. In parametric methods, a probability distribution is considered as the underlying statistical model and based on that, a finite number of parameters are needed to completely define the PDF. The number of parameters to define a non-parametric model is unlimited. Thus, comparing the result of the two models may be unfair. Both methods are helpful in different scenarios which are discussed subsequently.

The Gaussian process regression maximizes the marginal likelihood function which provides us with an uncertainty in the regression. In firebrand studies, this can be beneficial to determine the lethality of the larger/heavier firebrands-worst-case scenario- by considering the upper limit. Moreover, employing different kernels enables

the user to effortlessly improve the accuracy of the regression. This method involves with a few user defined parameters which helps the users to employ the whole algorithm as a black box. On the other hand, the Gaussian process loses its efficiency at larger dimensions; if the number of predictors exceed 10, the efficiency of this method decreases [72,73].

As previously discussed, neural network is a non-parametric technique. When the number of the hidden layers approaches infinity, this non-parametric technique becomes more similar to a parametric ones [74]. In neural network, most of the network parameters such as learning rate, biases, initial values, and weights need to be defined by the user which act as a double-edged sword. It can lead to a proper regression if they are tuned properly. On the other hand, failing to match these parameters can damage the regression heavily [75,76].

In order to compare the results of shallow and deep learning, root mean square error (RSME) at each wind speed was compared and tabulated in Table 4.4. As can be seen, the errors associated with the Gaussian process regression are smaller than that of the neural network.

Table 3-4. Root mean square error for both models

Experiment	**Gaussian process regression**	**Neural Network**
Idle	0.02	0.11
Medium	0.04	0.22
High	0.08	0.27
All combined	0.08	0.36

CHAPTER 4: SURFACE TEMPERATURE OF SMOLDERING FIREBRANDS

4.1. Abstract

Accurately measuring the surface temperature of a smoldering firebrand has been challenging. Different techniques have been employed for this task, such as contact method using thermocouples and noncontact method using infrared cameras. The infrared (IR) devices, in theory, are more convenient because they allow the user to analyze a large area, compared to thermocouples, which only measure the contact point. In other words, one IR image contains information equal to hundreds of thermocouples. In practice, however, the IR devices requires the user to accurately set radiative emissivity, which can be challenging. In order to determine the proper range for emissivity, ASTM E1933 is used. One spot on the firebrand was monitored with thermocouples, pyrometer, and IR camera. Then, the emissivity was adjusted to minimize the difference between the three recordings. It was observed that the emissivity varied between 0.95 and 1 with 99% confidence. Setting the emissivity value to 0.97, the surface temperature of smoldering firebrands ranged from 100 to 1000 degrees C depending on the wind speed. Also, it was observed that only 0.5 of the surface of the firebrands was hotter than 300 degreed C when smoldering started. In the presence of wind, this value (0.5) gradually decreases to 0.25; without wind, it rapidly dropped to 0.1.

4.2. Introduction

Surface temperature is understood to be one of the criteria that can result in the ignition a solid [40,77,78]. Two definitions have been assigned to the term “ignition temperature”: (1) the temperature of the air surrounding the specimen, and (2) the surface

temperature of the sample just before ignition [40]. The latter definition is generally more helpful since it is more likely that this temperature does not vary markedly for a material. However, measuring a surface temperature is more difficult than measuring the temperature of the surroundings air [40]. Different techniques have been introduced to measure the temperature of a material, where each one employs a different physical principle. These principals are typically (1) expansion and contraction of a substance due to temperature change, (2) change in electrical resistance of a substance according to the temperature, and (3) employ the relation between temperature and heat radiation emitted from a body [79].

Typically, in order to take advantage of the first two principles, the instrument must be in contact with the medium whose temperature is to be measured. Gas/liquid in glass thermometers, thermocouples, and resistance temperature devices are common invasive instruments. Employing invasive instrument may cause a disturbance in the measurement. When the cold probe comes in contact with the target, it acts like a heat sink and drains away some thermal energy [80]. The resulting error is a function of the relative specific heat capacity of the thermocouple and target as well as the amount of heat being generated/absorbed in the target. If the thermal inertia of the probe and the target are in the same order, the result of the measurement is not reliable. In addition to that, a connection problem is often a source of error. Generally, thermocouples are the best if the target medium is a liquid or gas [81].

The noninvasive techniques work on the principal that all surfaces above absolute zero temperature emit a fraction of black body radiation and this amount is proportional to the temperature of the surface. Pyrometers and infrared cameras are typical devices

that work on this principle. They are equipped with a sensor that transforms the incident IR radiation to an electrical signal, and with accurate calibration, the temperature of the target surface can be precisely measured. Theoretically, these methods are very accurate, but in practice there can be serious obstacles [82]. One of the most important ones is calculating the emissivity.

The rate of energy that leaves a surface, radiosity, is a combination of emitted power and the reflected energy from the surface (radiometry vs thermography). In other words, the surrounding radiation sources influence the amount of radiation that leaves the target surface. Hence, in order to relate the temperature and the emitted energy, one must know what portion of the total radiosity is the reflection of energy from the surrounding and how much is emitted from the surface; this portion is determined by the emissivity of a material.

Both invasive and noninvasive techniques have been employed to measure the surface temperature of burning wood. Evans [83] measured the surface temperature of the cross section of burning cylinders, the dimensions of which were 2.7 cm in diameters and 11.4 in height with a thermocouple, pyrometer, and an IR camera. The thermocouples were implanted at the bottom of the cylinder to measure the internal temperature of the cylinder as a function of the distance to the burning surface. At the same time, a disappearing filament type thermal camera and an infrared pyrometers were aimed at the surface to measure the surface temperature. The study reported that the surface temperature varied nonlinearly in the range of 750 to 1100 C as a function of main stream wind velocity and the emissivity at 43 m/s wind speed and 1055 C was determind to be 0.85.

Kansa et al. [84], developed a one dimensional mathematical model of charring pyrolysis that, considered permeable structural effects. He reported the best regression for charring and virgin material were 0.94 and 0.64, respectively. In order to investigate the radiative ignition mechanism of PMMA and red oak, Kashiwagi conducted two separate studies and reported that for wavelengths greater than 2 micro meters, the emissivity was 0.94. Bennini et al. [85] evaluated the behavior of wood pallets under an intense thermal flux and reported that the best estimate for charring wood was 0.94.

Urbas and Parker [86] compared the recorded values of pyrometer and thermocouples in order to obtain the emissivity of a burning Douglas fir specimen exposed to a heat flux using a the cone calorimeter. The IR pyrometer wavelength band was 8-12 micrometer and was located 750 mm from the surface. In order to have an appropriate contact between the thermocouples and the specimen, two small diameter holes were drilled through the specimen and two 0.127 mm diameter chromel-alumel thermocouples covered with Teflon tubes were passed through the holes in a way that the junction of the thermocouple was located on the specimen. The results showed that the values of the temperature of the thermocouple and pyrometer were in good agreement when the emissivity was set to unity. In a similar study [87], same researchers tested 10 different materials in a vertical cone under 30 and 50 kW/m^2 heat flux. Again it was reported that the emissivity should be set to unity.

The only study which focused on the temperature of the glowing firebrands was Manzello et al. [88]. The temperature of the glowing 10 mm diameter with the length of 76 mm Ponderosa pine firebrands were measured at two wind speeds. It is reported that the higher wind speed raised the temperature by almost 150 c and the average temperature

of the studied firebrands were in the range of 650-700 c in the air flow of 2.4 m/s and 500-600 at the airflow of 1.3. Employing a thermocouple, the temperature recordings with an IR camera were validated and it was reported that the emissivity on the camera for the firebrands should be set to 0.6-0.7 to have a good agreement with the thermocouple data. Table 4.1 summarizes the key points in each study.

Table 4-1. Emissivity values

Experiment	**Details**	**Emissivity**
Evans and Emmons (1976)	Cylinders of American basswood	0.85
Kansa, Perlee & Chaiken (1977)	Mathematical model	0.94
Kashiwagi (1979)	Red oak(horizontal)	0.95
Kashiwagi (1981)	Red oak (vertical)	0.95
Bennini,Castillo&Traverse (1991)	Pressed Poplar wood	0.93
Urbas and Parker (1993)	Douglas fir under the Cone	1
Urbas and Parker (2004)	10 different woods in vertical Cone	1
Manzello, Park and Cleary (2009)	Ponderosa pine firebrands	0.6

In addition to the importance of that the surface temperature in igniting a solid, it can also affect the generation of firebrands. For example, it is understood that it affects the heat release rate during a fire [83]. Heat release rate acts as the driving force of a fire; higher heat release rate equals to faster oxidation and a more intense fire. [89]. Strengthening the convection column, the pressure underneath the roof boosts and leads to the generation of more firebrands with larger size and mass [18]. Also, mechanical properties decrease with temperature, which is more obvious for live woods with higher moisture content [90]. Due to de-polymerization reactions at temperatures greater than 100 C, chemical bonds begin to break [91] and the material gradually loses its strength. Under external forces such as wind pressure, the convective force of the fire etc. it is possible that pieces of the burning material separate from the large body and become lofted.

As explained, only one study has specifically focused on measuring the surface temperature of a firebrand in which the emissivity value was assumed to be in the range of 0.6-0.7 which is not in agreement with other reported values. Thus, there is a certain need to measure the emissivity value of a smoldering firebrand before determining the temperature distribution over the surface.

4.3. Emissivity Measurement

As previously discussed, the emissivity of the burning wood is a controversial issue, which is an important parameter when temperature is recorded using optical instruments. There are tables which present the emissivity values of different materials. However, the emissivity of many materials are still unknown. Emissivity can be defined as the ratio of the emitted energy from a gray body divided by that from a black body and is always less than unity. A black body is a body that absorbs all incident electromagnetic radiation regardless of the wavelength and the incident angle. A gray body, is one that absorbs some of the radiation. Six parameters have been recognized that affect the value of emissivity. The material is considered the most important [82] . The material can be categorized either in non-metal or metal. Other parameters are surface structure, viewing angle, geometry, wavelength and temperature. All of these parameters are sources of uncertainty and affect the measurement process which will be discussed later.

4.3.1. Experimental procedure

Among different techniques that could be used to measure the emissivity, namely tape, paint, hole drilling, and contact thermometer, the last one was chosen for this research. The temperature of a same point was recorded via two different techniques; a pyrometer and three thermocouples. Adjusting the emissivity values on the pyrometer,

the difference between that and the average of the thermocouple recordings was minimized. The temperature varied under the following function with emissivity

$$T_{obj} = \sqrt[n]{\frac{U - CT^{n}_{amb} + C\varepsilon T^{n}_{amb} + CT^{n}_{Pyr}}{C\varepsilon}} \tag{4.1}$$

where U is the detector signal, T is temperature, and obj., amb., and Pyr represent object, ambient and detector respectively. C is the device specific constant (efficiency) and epsilon is the emissivity. The constant n depends on the wavelengths at which the device operates in between. Since the IR thermometers do not cover the whole wavelength range, n varies between 2 and 3 for long wavelengths and between 15 and 17 for short ones [92].

The difficulty in employing the pyrometers was to keep the junction in contact with the surface. During the mass loss, the volume shrank and thus, the connections got loose. Reduction in volume was a non-uniform phenomena and the surface height varied in a chaotic order. Moreover, some fissures might generate in the body, which might lead to improper contact. In order to address this problem, a returning mechanism had been designed to push the tip of the thermocouple downward on the surface; when the surface shrunk, the mechanism exerted a force on the thermocouple to push it towards the body to compensate the burned volume. In this way, we could guarantee that the junction is always in contact with the body. The thermocouples were carefully monitored to touch the surface for the entire testing period. Numerous experiments were abandoned due to sudden cracks in the material. Three Omega thermocouples (diameter 0.125 mm and response time 1.0 second) were used to be able to calculate the uncertainty more accurately and to check the consistency the results. At the same time, a pyrometer (Heitronics KT 19.81 II) which emissivity was set to unity and an IR camera were focused

on the same spot as where the thermocouples were located, and the temperature values were recorded for four minutes. The schematic of the experimental setup is depicted in figure 4.2. A fan was installed 1 meter away from the setup to generate wind (2 m/s) for some periods during the experiment. It was hypothesized that the temperature would increase with wind and we wanted to measure a wide range of temperature.

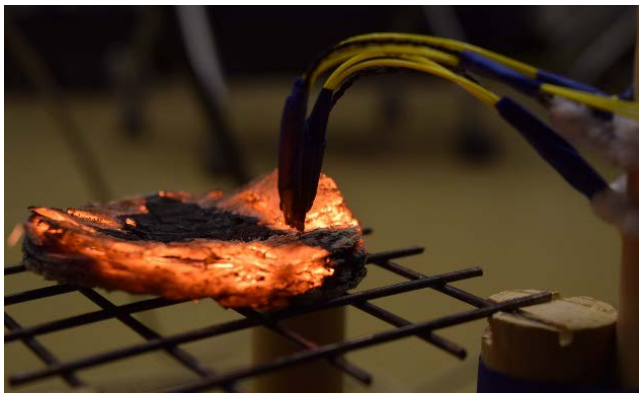

Figure 4-1. Close-up of a measuring process

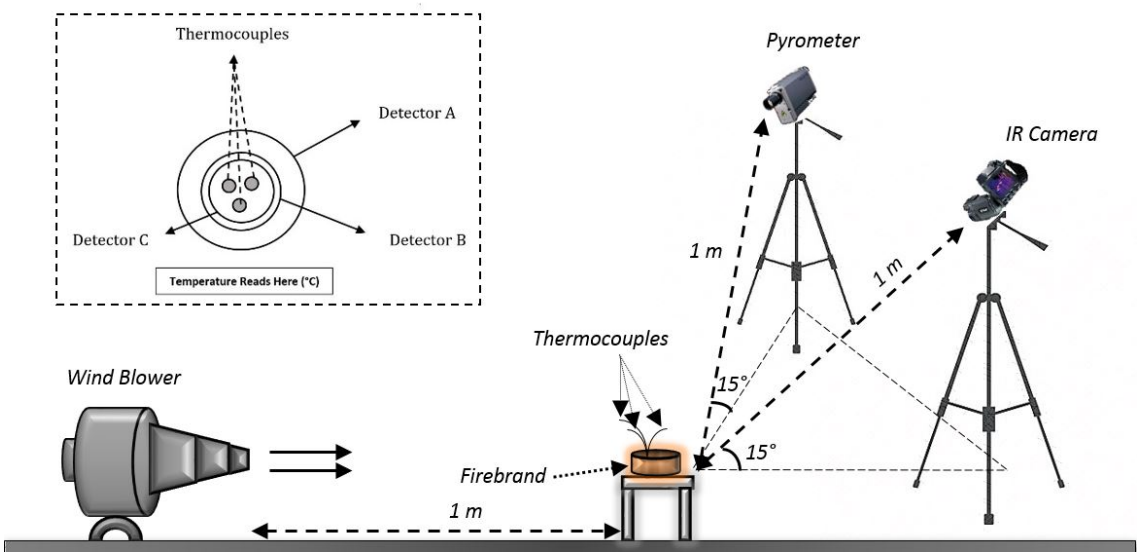

Figure 4-2. Schematic of experimental setup

4.3.2. Analysis of the results

Figure 4.3 and 4.4 show the recorded values of the thermocouples and pyrometer readings and the difference in readings. A total of 15 experiments were conducted to

ensure the repeatability of this experimental setup and procedure. The triangle symbol shows the mean values of the three thermocouples and the red bars are the standard deviation of the three values. As can be seen, there is an acceptable agreement between the instruments which suggest that the emissivity can be approximately assumed to be one. However, only a blackbody radiates all the incoming energy and thus more investigations need to be conducted.

The expected value of any variable can be obtained by integrating the associated PDF. In order to build a PDF, the values of temperature as a function of emissivity must

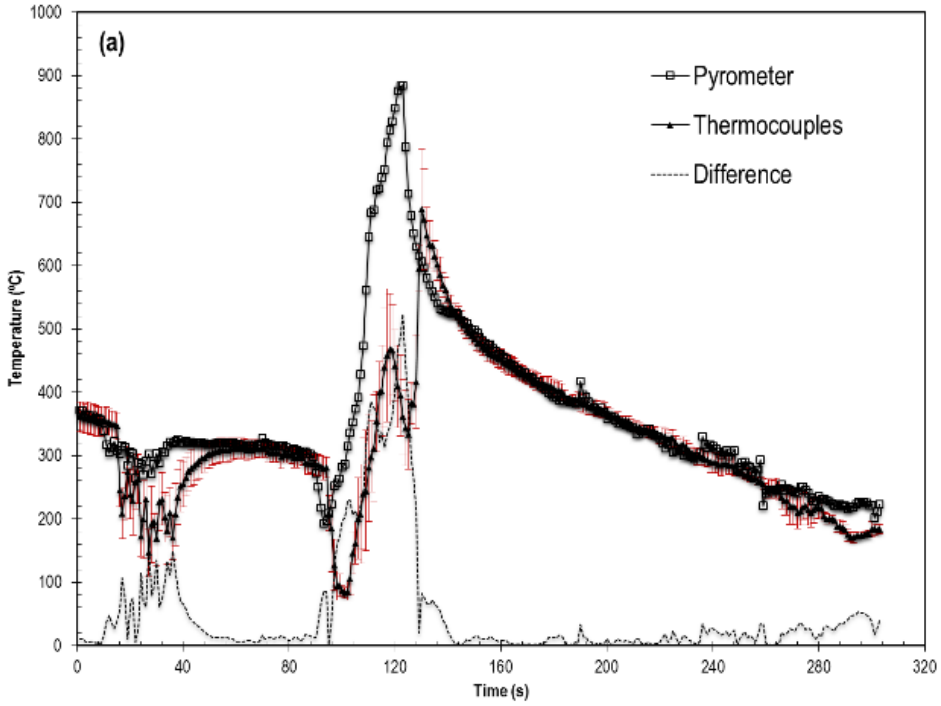

Figure 4-3. Surface temperatures of a smoldering firebrands versus time

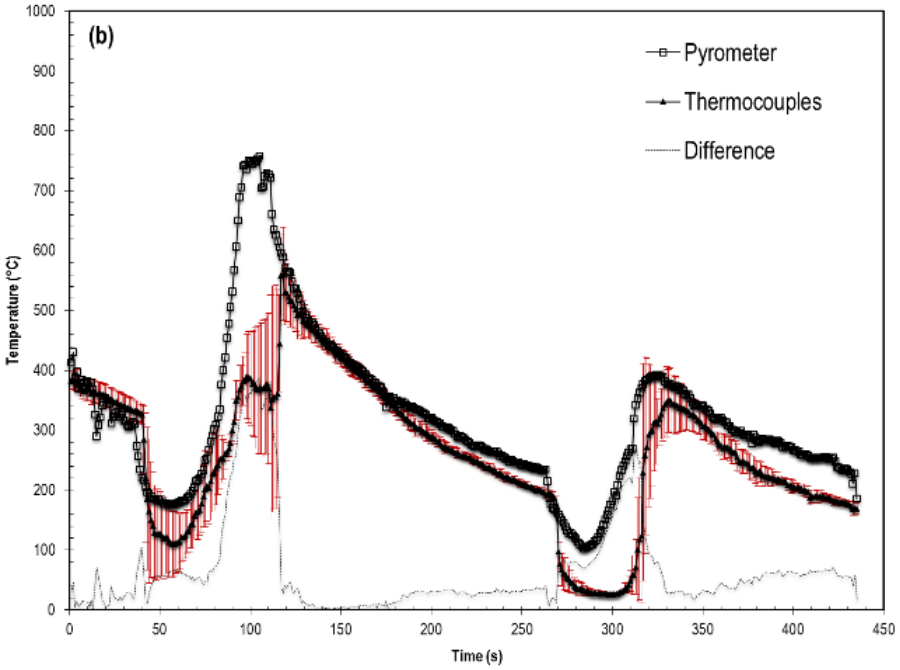

Figure 4-4. Surface temperatures of a smoldering firebrand versus time

be calculated. The FLIR IR camera's software can provide us with that information. The software uses the IR image taken with the camera (FLIR T620) as an input and generates new temperature values for any spot on the image given the user varied the emissivity. Figure 4.5 and 4.6 show the results.

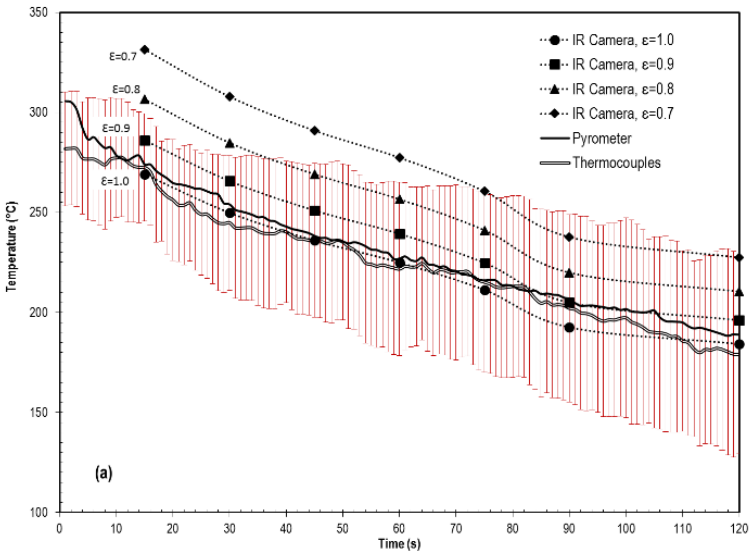

Figure 4-5. Spot temperatures of a smoldering firebrands versus time

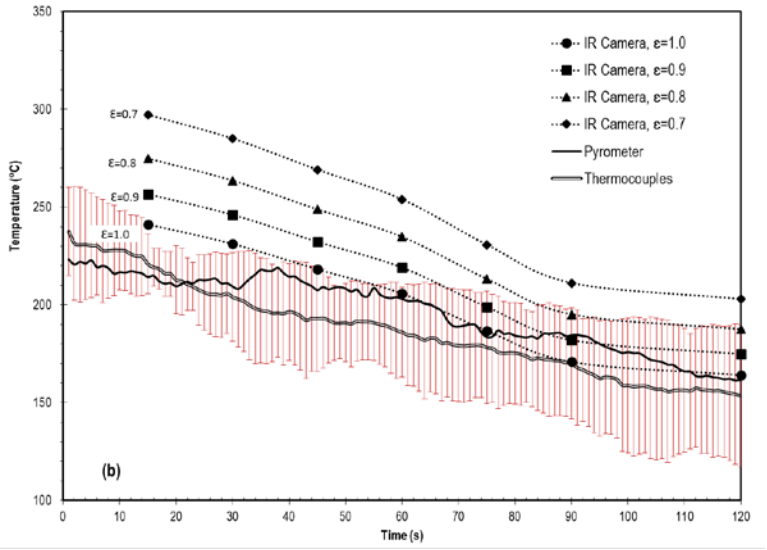

Figure 4-6. Spot temperatures on a smoldering firebrand versus time

Since the emissivity values were decreased by 0.1 intervals, the estimated value can be obtained by a summation as follows

$$\varepsilon = \frac{\sum \varepsilon(\mathrm{i}) PDF(T(\varepsilon(\mathrm{i})))}{\sum PDF((T(\varepsilon(\mathrm{i})))} \qquad (4.2)$$

where *i* is the number of data points. At each point (15 seconds interval), a normal distribution based, on the mean and standard deviation values of the three thermocouple recordings, was constructed. This PDF is a function of temperature. Employing equation 4.1, the value of temperature at each emissivity was calculated and plugged into equation 4.2. Hence, 10 emissivity values have been generated with the mean vale of 0.98 and standard deviation of 0.015. Performing a 99% confidence interval, the emissivity values for the smoldering firebrands were determined to be between 0.95 and 1.00.

It should be noted that both the infrared camera and the pyrometer work in the long infrared band; the IR camera spectral range is 7.8-14 micrometers and the second one's is 8-12 micrometers. Thus, the water vapor and CO_2 emissions do not interfere with the measurement [87].

4.4. Firebrand Temperature Distribution

Squared OSB samples were cut and placed in a small scale firebrand generator. Each sample was allowed to burn until it flamed out. Considering the results of the experiments at IBHS (Table 3-1), the maximum of the average projected areas was 4.87 cm^2; hence, the firebrands were generated in a way that their initial projected area was similar. As can be seen in Figure 4-7, each side of the firebrand was approximately 23 millimeters after the flameout, which results in almost 5 cm^2 projected area.

Figure 4-7. Dimensions of the firebrand after flame out

4.4.1. Experiment Procedure

A T620 FLIR thermal camera was used to measure the surface temperature of smoldering firebrands. The camera has two temperature calibration ranges: 100-650c and 300-2000c that are useful for this experiment. The lower range was chosen for the no wind tests and the upper range was chosen for the 3 and 6 meters per second tests. The smoldering firebrands were then placed on a wire bench which was placed perpendicularly 1 meter beneath the camera. Setting the emissivity to 0.97, every 10 second a frame was recorded until either the firebrand was cold or scattered in the no-wind and wind conditions, respectively. Three samples for each experiment were used. Figure 4-8 shows a recorded frame at 6 m/s wind condition.

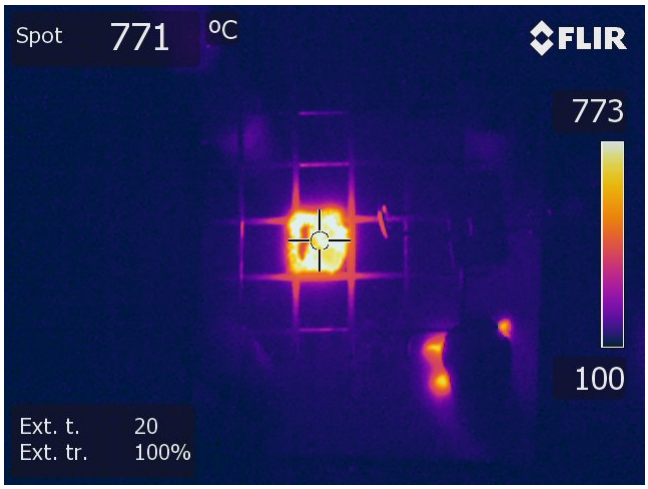

Figure 4-8. A sample recorded from 6 m/s wind tests

4.3.2. Results

Using the FLIR research IR software, a bounding box around the firebrand at each frame was defined and then the temperature values within that box was extracted and saved in a .csv file. During the burning process, firebrands took on an irregular shape; therefore, in each bounding box, several points belong to the background existed. Since the critical surface temperature for wood is 250-300 C, a Matlab code was developed to eliminate any pixel where the temperature was below 300 C. Then, the average temperature of the points on the firebrand (temperature was greater than 300c) at each time was determined and plotted in Figure 4-9. This temperature was chosen since it was reported as the ignition temperature of wood [93]. The error bars represent one standard deviation of three measurements made at each time.

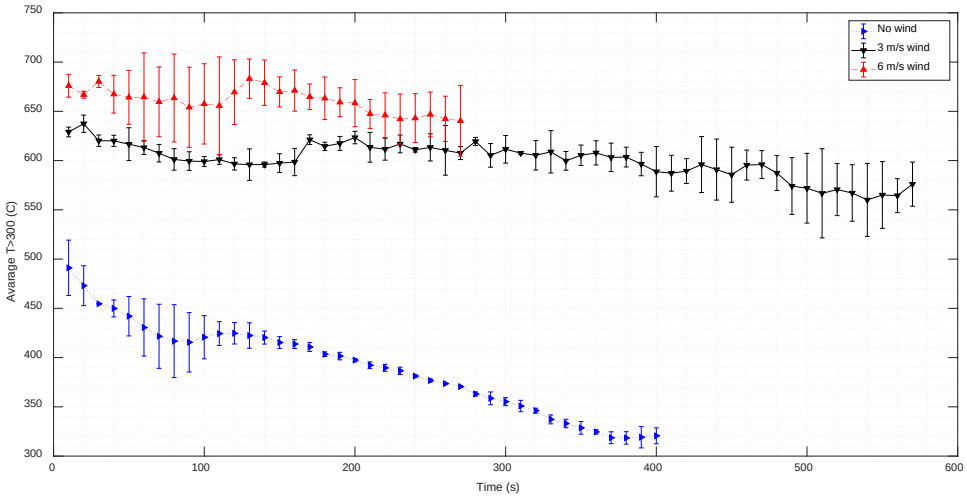

Figure 4-9. Average temperature of the points with T>300 C

Results showed that higher wind resulted in higher surface temperature. Moreover, the average surface temperature in the presence of wind stays almost steady through the test, but without wind, the temperature decreased by 200 degrees in 400 second. The maximum temperature that a firebrand can reach is also an important quantity in assessing the lethality of firebrands which is depicted in Figure 4-10. It can be seen that at 6 m/s wind, the firebrands could reach 1000 c, and mostly fluctuating around 900 C. What is striking about this figure is that medium wind speed was probably the most hazardous one; at the highest wind speed, firebrands rapidly lost mass and burned out in less than 300 seconds. At the lowest wind speed, the temperature drop was dramatic which reduced the possible threat. However, at medium wind, the firebrands could steadily burn at 800 degrees for almost 600 seconds which would generate the maximum heat flux (the area beneath each curve).

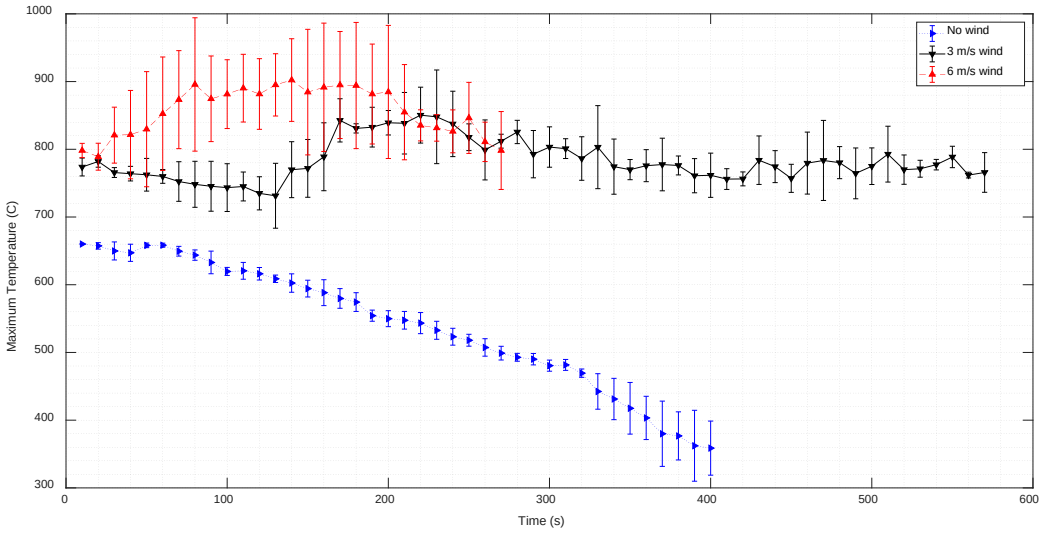

Figure 4-10. Maximum temperature of smoldering firebrands

Figure 4.11 depicts the surface fraction of the firebrands for which temperature is greater than 300 C. It is obvious that for all three wind speeds, at the beginning, only half of the surface is hotter than 300 C. For no wind condition this fraction drops rapidly, conversely, for 3 and 6 m/s wind speeds, the dangerous fraction decreased to almost 0.2. Again, the medium wind speed can be the most hazardous.

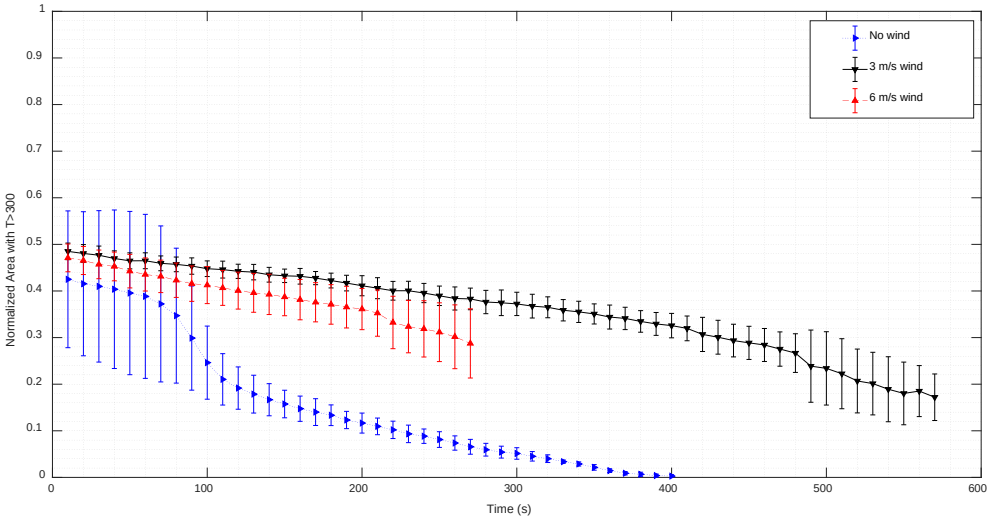

Figure 4-11. The surface fraction with temperature greater than 300C

CHAPTER 5: SUMMARY AND CONCLUSION

The firebrand phenomenon is known as the only mechanism that can initiate a fire at distances further than 60 meters from the original fire. They are typically smoldering pieces of wood carried by wing at their terminal velocity. The lifetime of a firebrand is divided into three phases: generation, transportation and ignition of the fuel bed; among all, the former one is the least explored area. Depending on the original fire properties and the environmental conditions, firebrands may have different levels of lethality. Surface temperature, mass, projected area, and traveling distance are considered influential parameters in assessing the ignition potential of the firebrands.

5.1. Contributions

In this research, in order to characterize the firebrands generated from structural fuels, numerous tests have been conducted at IBHS. Various building assemblies, such as corner and wall assemblies and fences, were ignited in a wind tunnel. Forty two water pans were places downstream of the wind to catch the firebrands. Quenching the firebrands preserves their shape and mass. This information can be extracted later to assess the lethality of the firebrands and theoretical modeling.

After completing the tests, the firebrands were collected and placed in an oven maintain at 104 C to reduce their moisture content to zero. Then, the mentioned quantities of interest (traveling distance, mass and projected area) were measured. Traveling distance can be determined by the position of the pans in which the firebrands land. Mass and projected area, however, are more challenging to measure. For mass, each firebrand must be weighed, and for projected area an image analysis technique can be used. This procedure has been almost the same for the tests conducted in the past 20 years. However,

in some tests, instead of using structural components in a wind tunnel, an entire building was set on fire outside in a real-world condition.

5.2. Novel Objectives and Related Tasks

In the past two decades, the number of firebrands collected from the pans for the post-test processing in structural experiments ranged between 50 and 500. Such small sample sizes may be the result of tediousness of the measurement process. The vital question that may arise is how many firebrands are needed to sufficiently quantify the characteristics of entire population of the firebrands in an experiment? If a statistical test suggests a sample size significantly larger than 500, is the current measurement procedure efficient enough? Moreover, it is not practical to cover the entire space downstream of the wind with water pans; thus, no information can be extracted from the uncovered locations. The second issue that comes to the author's mind is to find a solution for this problem.

In order to fill the knowledge gap, the following objectives were established for this research project:

(1) Perform a thorough statistical analysis on the available data in the literature to estimate the proper probability density functions

(2) Generate firebrands from structural fuels and collect statistically sufficient sample of firebrands for each test

(3) Improve the efficiency of the tedious measurement process, employing machine learning and image processing techniques.

(4) Measure the surface temperature of smoldering firebrands in different conditions

To achieve the first objective, the following tasks were performed: (1) All the raw data from the experiments conducted in the past 50 year was collected. (2) The Bayesian approach was employed to optimize the likelihood function. (3) The most likely probability density functions was suggested, based on the lowest BIC scores. The details about these tasks are presented in chapter two.

The second and third goals were discussed in chapter four because they were closely related. To accomplish the third goal: (1) numerous tests were conducted to generate firebrands from structural fuels. Different building components were set on fire, and the firebrands were collected downstream. (2) Conducting a statistical analysis, the minimum suggested sample size, with a 95% confidence level and a 0.03 margin of error, was 1300. To be even more conservative, for each test at least 1400 firebrands were collected from the pans for further analysis. Since the 40 tests were conducted, the total sample size was 56,000 firebrands which required a significant improvement in the measurement process. In addition, a detailed measurement uncertainty analysis was performed, using both GUM types A and B.

Measuring the mass and projected area were the two challenging tasks, the fourth goal was satisfied by proposing an automated measurement framework. Accordingly, (1) An efficient image processing algorithm was proposed to minimize the human effort in this measurement. Scattering tens of firebrands on a white sheet and taking a photo were the only tasks performed by an operator. The code increased the contrast and detected the edges based on the change in the color intensity at the first step. Then, the debris beyond the borders were cropped out and the noises on the sheet were removed. Finally, the possible holes on the embers were filled and the firebrands were labeled. (2) In order to

facilitate the weighing process, two machine learning algorithms were employed; the Gaussian process regression as a parametric approach and the back propagating neural network as a non-parametric method. Two predictive models were created, which could estimate any quantity of the firebrands, given the other parameters. For example, in providing the traveling distance, surface area, and wind speed, the model could predict the mass within 5% error without physically weighing them. The parametric model, was able to provide a confidence interval for the predicted values. By employing the models, one was able to extract different characteristics of the firebrands even at the uncovered locations.

For the fourth goal, a noninvasive temperature measurement technique was employed, which required a precise measurement of radiation emissivity. Accordingly, (1) A returning mechanism was designed that guaranteed a proper contact between the thermocouples' tip and the surface of a smoldering firebrand. (2) At the same time, the temperature variation of the contact point was monitored with an infrared camera. Adjusting the emissivity on the camera, the difference between the average of thermocouples' recordings and that from thermal the camera was minimized. (3) A confidence interval analysis was performed on the result to find the emissivity. (4) The surface temperature of the firebrands were measured at different wind speeds. Chapter three discusses the related materials.

5.3. Summary of the Results

The results showed that the bivariate truncated normal and bivariate lognormal distributions were the best candidates, among 18 analyzed probability density functions evaluated. Mass and projected area were strongly correlated, but none of them were

heavily correlated with the traveling distance. In addition, the emissivity of the firebrands was observed to be between 0.95 and 1.00 with a 99% confidence. Considering that emissivity equals 0.97, the surface temperature of the firebrands varied between 100 and 1000 C, depending on the wind speed.

In order to have a sample that properly represents the characteristics of the population, the statistical analysis suggested a sample size of at least 1300; however, a sample size of 1400 was chosen to be more conservative. Two regression models (one parametric and one non-parametric) were created and then trained with 70% of the data. The robustness of the models were assessed by comparing the measurement results and the prediction values for the remaining 30%. It was observed that the mass for 1300 firebrands can be predicted within a 5% error without physically weighing them. Employing this predictive model, the sample size could be reduced by 30% (900 instead of 1400 firebrands). Also, mean, standard deviation, and correlation between the parameters could be predicted within 10% error.

5.4. Future Research

This research has raised several questions that need of further investigation, which may start by defining a firebrand explicitly. At the vicinity of the fire, direct flame contact and radiation are the dominant mechanisms that spread a fire. Firebrands are worthy of study because they are the only mechanism that can result in ignition of fuel beds at further distances; thus, traveling distance should be considered in defying the firebrands. Moreover, defining new influential parameters in travel distance and ignition potential of firebrands such as shape and charring level of embers will helpful to estimate the ignition potential.

In addition, recording the experiments with high speed and thermal cameras and then processing the videos, will be extremely insightful. Employing object tracking techniques, one may be able to accurately detect the flying path and traveling distance as well as the surface temperature of the firebrands. Moreover, the generation flux, burning out rate, and temperature variation can be analyzed in real time.

Also, employing a machine learning classification algorithm, one may categorize the firebrands based on key differences in size, mass, traveling distance, or linear combinations of them. This can be beneficial in classifying the hazard that firebrands with different characteristics create.

REFERENCES

1. Cohen JD Reducing the wildland fire threat to homes: where and how much? In: Proceedings of the symposium on fire economics, planning, and policy: bottom lines, 1999. pp 189-195
2. Cohen JD (2000) Preventing disaster: home ignitability in the wildland-urban interface. Journal of forestry 98 (3):15-21
3. Cohen J (2008) The wildland-urban interface fire problem: a consequence of the fire exclusion paradigm.
4. Caton SE, Hakes RSP, Gorham DJ, Zhou A, Gollner MJ (2017) Review of Pathways for Building Fire Spread in the Wildland Urban Interface Part I: Exposure Conditions. Fire Technology 53 (2):429-473. doi:10.1007/s10694-016-0589-z
5. Wells RW (1968) Fire at Peshtigo. Prentice Hall,
6. Fernandez-Pello A, Lautenberger C, Rich D, Zak C, Urban J, Hadden R, Scott S, Fereres S (2015) Spot fire ignition of natural fuel beds by hot metal particles, embers, and sparks. Combustion science and technology 187 (1-2):269-295
7. Manzello SL, Cleary TG, Shields JR, Maranghides A, Mell W, Yang JC (2008) Experimental investigation of firebrands: generation and ignition of fuel beds. Fire Safety Journal 43 (3):226-233
8. Hylton JH, G. (2016) Fire Loss in the United States During 2015. NFPA,
9. Zhou A (2015) Fire Ember production From Wildland and Structural Fuels. JFSP, University of North Carolina at Charlotte
10. Glaeser EL (1998) Are Cities Dying? The Journal of Economic Perspectives 12 (2):139-160
11. Stewart S, Radeloff V, Hammer R, Fried J, Holcomb S, McKeefry J (2005) Mapping the wildland urban interface and projecting its growth to 2030: Summary statistics. USDA Forest Service North Central Research Station: Evanston, IL, USA
12. Goverse T, Hekkert MP, Groenewegen P, Worrell E, Smits REHM (2001) Wood innovation in the residential construction sector; opportunities and constraints. Resources, Conservation and Recycling 34 (1):53-74. doi:https://doi.org/10.1016/S0921-3449(01)00093-3
13. Vodvarka F (1969) FIREBRAND FIELD STUDIES. IIT RESEARCH INST CHICAGO ILL ENGINEERING MECHANICS DIV, CHICAGO
14. Vodvarka F (1970) URBAN BURNS - FULL-SCALE FIELD STUDIES. IIT RESEARCH INST CHICAGO ILL ENGINEERING MECHANICS DIV, CHICAGO
15. Suzuki S, Manzello SL, Lage M, Laing G (2012) Firebrand generation data obtained from a full-scale structure burn. International Journal of Wildland Fire 21 (8):961-968. doi:https://doi.org/10.1071/WF11133
16. Yoshioka H, Hayashi Y, Masuda H, Noguchi T (2004) Real-Scale Fire Wind Tunnel Experiment on Generation of Firebrands from a House on Fire. Fire Science and Technology 23 (2):142-150. doi:10.3210/fst.23.142

17. Suzuki S, Brown A, Manzello SL, Suzuki J, Hayashi Y (2014) Firebrands generated from a full-scale structure burning under well-controlled laboratory conditions. Fire Safety Journal 63:43-51. doi:http://dx.doi.org/10.1016/j.firesaf.2013.11.008
18. Waterman TE, Laboratory NRD, Defense OoC (1969) Experimental Study of Firebrand Generation - Final Technical Report. IIT Research Institute. Engineering Mechanics Division,
19. Suzuki S, Manzello SL, Hayashi Y (2013) The size and mass distribution of firebrands collected from ignited building components exposed to wind. Proceedings of the Combustion Institute 34 (2):2479-2485. doi:http://dx.doi.org/10.1016/j.proci.2012.06.061
20. Suzuki S, Manzello SL (2016) Firebrand production from building components fitted with siding treatments. Fire Safety Journal 80:64-70. doi:http://dx.doi.org/10.1016/j.firesaf.2016.01.004
21. Manzello SL, Foote EID (2014) Characterizing Firebrand Exposure from Wildland–Urban Interface (WUI) Fires: Results from the 2007 Angora Fire. Fire Technology 50 (1):105-124. doi:10.1007/s10694-012-0295-4
22. Maranghides A, Mell W (2011) A Case Study of a Community Affected by the Witch and Guejito Wildland Fires. Fire Technology 47 (2):379-420. doi:10.1007/s10694-010-0164-y
23. Manzello SL, Shields JR, Cleary TG, Maranghides A, Mell WE, Yang JC, Hayashi Y, Nii D, Kurita T (2008) On the development and characterization of a firebrand generator. Fire Safety Journal 43 (4):258-268. doi:https://doi.org/10.1016/j.firesaf.2007.10.001
24. Zhou K, Suzuki S, Manzello SL (2015) Experimental Study of Firebrand Transport. Fire Technology 51 (4):785-799. doi:10.1007/s10694-014-0411-8
25. Manzello SL, Hayashi Y, Yoneki T, Yamamoto Y (2010) Quantifying the vulnerabilities of ceramic tile roofing assemblies to ignition during a firebrand attack. Fire Safety Journal 45 (1):35-43. doi:https://doi.org/10.1016/j.firesaf.2009.09.002
26. Himoto K, Tanaka T Transport Of Disk-shaped Firebrands In A Turbulent Boundary Layer. In: Fire Safety Science Proceedings of the 8th International Symposium, 2005. p 11
27. Barr BW, Ezekoye OA (2013) Thermo-mechanical modeling of firebrand breakage on a fractal tree. Proceedings of the Combustion Institute 34 (2):2649-2656. doi:http://dx.doi.org/10.1016/j.proci.2012.07.066
28. Tohidi A, Kaye N, Bridges W (2015) Statistical description of firebrand size and shape distribution from coniferous trees for use in Metropolis Monte Carlo simulations of firebrand flight distance. Fire Safety Journal 77:21-35. doi:http://dx.doi.org/10.1016/j.firesaf.2015.07.008
29. Hemmati V, Plumer M, Whitehead J, Southern B (2012) Monte Carlo simulations of magnetic ordering in the fcc kagome lattice. Physical Review B 86 (10):104419
30. TARIFA CS, NOTARIO PP, MORENO FG, VILLA AR (1967) Transport and combustion of firebrands, Report of U. S. department of agriculture and forest service. INSTITUTO NACIONAL DE TECNICA AEROESPACIAL, Madrid
31. Tarifa CS, Notario PPd, Moreno FG (1965) On the flight paths and lifetimes of burning particles of wood. Symposium (International) on Combustion 10 (1):1021-1037. doi:http://dx.doi.org/10.1016/S0082-0784(65)80244-2

32. Muraszew A, Fedele J (1976) Statistical Model for Spot Fire Hazard. The Aerospace Corporation, El Segundo, CA
33. Muraszew A, Kuby W, Fedele J (1975) Firebrand investigation. Aerospace Corporation,
34. Muraszew A, Operations ACES (1974) Firebrand Phenomena. Aerospace Corporation,
35. Clements H (1977) Lift-off of forest firebrands [Pinus]. USDA Forest Service Research Paper SE (USA) no 159
36. Ellis PF (2011) The aerodynamic and combustion characteristics of eucalypt bark: a firebrand study.
37. Woycheese JP (2000) Brand lofting and propagation from large-scale fires. University of California, Berkeley,
38. Manzello SL, Suzuki S (2017) Generating wind-driven firebrand showers characteristic of burning structures. Proceedings of the Combustion Institute 36 (2):3247-3252. doi:https://doi.org/10.1016/j.proci.2016.07.009
39. Manzello SL, Suzuki S, Yamada T, Foote EI, Lage M, Laing G, Hayashi Y, Hamins AP, Averill JD, Gann RG (2012) Exposing Wood Decking Assemblies to Continuous Wind-Driven Firebrand Showers. US Department of Commerce, National Institute of Standards and Technology,
40. Babrauskas V (2003) Ignition Handbook: Principles and Applications to Fire Safety Engineering, Fire Investigation, Risk Management and Forensic Science. Fire Science Publishers,
41. Hogg R, McKean J, Craig A (2005) Introduction to mathematical statistics. 6 edn. Pearson, N J
42. Schwarz G (1978) Estimating the dimension of a model. Annals of Statistics 6 (2):4
43. Posada D, Buckley TR (2004) Model Selection and Model Averaging in Phylogenetics: Advantages of Akaike Information Criterion and Bayesian Approaches Over Likelihood Ratio Tests. Systematic Biology 53 (5):793-808. doi:10.1080/10635150490522304
44. Kass RE, Raftery AE (1995) Bayes Factors. Journal of the American Statistical Association 90 (430):773-795. doi:10.2307/2291091
45. Kirkup L, Frenkel RB (2006) An Introduction to Uncertainty in Measurement: Using the GUM (Guide to the Expression of Uncertainty in Measurement). Cambridge University Press,
46. Balakrishnan N, Lai CD (2009) Continuous bivariate distributions. Springer, Dordrecht; London
47. Yue S (2002) The bivariate lognormal distribution for describing joint statistical properties of a multivariate storm event. ENV Environmetrics 13 (8):811-819
48. Kocherlakota S (1986) The bivariate inverse gaussian distribution: an introduction. Communications in Statistics - Theory and Methods 15 (4):1081-1112. doi:10.1080/03610928608829171
49. Raban DR, Rabin E The power of assuming normality. In: Proceedings of European and Mediterranean Conference on Information Systems 2007, 2007.
50. Koo E, Linn RR, Pagni PJ, Edminster CB (2012) Modelling firebrand transport in wildfires using HIGRAD/FIRETEC. International Journal of Wildland Fire 21 (4):396-417. doi:https://doi.org/10.1071/WF09146

51. Koo E, Pagni PJ, Weise DR, Woycheese JP (2010) Firebrands and spotting ignition in large-scale fires. International Journal of Wildland Fire 19 (7):818-843. doi:https://doi.org/10.1071/WF07119
52. Ganteaume A, Guijarro M, Jappiot M, Hernando C, Lampin-Maillet C, Pérez-Gorostiaga P, Vega JA (2011) Laboratory characterization of firebrands involved in spot fires. Annals of Forest Science 68 (3):531
53. Manzello SL, Maranghides A, Mell WE (2007) Firebrand generation from burning vegetation<xref ref-type="fn" rid="FN1">1</xref>. International Journal of Wildland Fire 16 (4):458-462. doi:https://doi.org/10.1071/WF06079
54. Ellis P (2013) Firebrand characteristics of the stringy bark of messmate (Eucalyptus obliqua) investigated using non-tethered samples. International journal of wildland fire 22 (5):642-651
55. Manzello SL, Suzuki S (2013) Experimentally Simulating Wind Driven Firebrand Showers in Wildland-urban Interface (WUI) Fires: Overview of the NIST Firebrand Generator (NIST Dragon) Technology. Procedia Engineering 62 (Supplement C):91-102. doi:https://doi.org/10.1016/j.proeng.2013.08.047
56. Manzello SL, Suzuki S, Hayashi Y (2012) Enabling the study of structure vulnerabilities to ignition from wind driven firebrand showers: A summary of experimental results. Fire Safety Journal 54:181-196. doi:http://dx.doi.org/10.1016/j.firesaf.2012.06.012
57. de Vries PG (1986) Stratified random sampling. In: Sampling theory for forest inventory. Springer, pp 31-55
58. Cohen J (1992) Statistical power analysis. Current directions in psychological science 1 (3):98-101
59. Hedayati F, Zhou A Statistical analysis on firebrand generation from structural fuels. In: Fire and Materials, San Francisco, USA, 2017. Proceedings of the 15th International Conference on Fire and Materials, pp 656-667
60. Carbonell JG, Michalski RS, Mitchell TM (1983) An overview of machine learning. In: Machine learning. Springer, pp 3-23
61. Schmidhuber J (2015) Deep learning in neural networks: An overview. Neural networks 61:85-117
62. Delalleau O, Bengio Y Shallow vs. deep sum-product networks. In: Advances in Neural Information Processing Systems, 2011. pp 666-674
63. Bahrani B, Hemmati V, Zhou A, Quarles SL (2018) Effects of natural weathering on the fire properties of intumescent fire-retardant coatings. Fire and Materials
64. Bernardo J, Berger J, Dawid A, Smith A (1998) Regression and classification using Gaussian process priors. Bayesian statistics 6:475
65. Williams CK, Rasmussen CE Gaussian processes for regression. In: Advances in neural information processing systems, 1996. pp 514-520
66. Rasmussen CE, Williams CK (2006) Gaussian processes for machine learning, vol 1. MIT press Cambridge,
67. Rasmussen CE, Williams CK (2004) Gaussian processes in machine learning. Lecture notes in computer science 3176:63-71
68. Semary NA, Tharwat A, Elhariri E, Hassanien AE (2015) Fruit-based tomato grading system using features fusion and support vector machine. In: Intelligent Systems' 2014. Springer, pp 401-410

69. Refaeilzadeh P, Tang L, Liu H (2009) Cross-validation. In: Encyclopedia of database systems. Springer, pp 532-538
70. Safavian SR, Landgrebe D (1991) A survey of decision tree classifier methodology. IEEE transactions on systems, man, and cybernetics 21 (3):660-674
71. Tetko IV, Livingstone DJ, Luik AI (1995) Neural network studies. 1. Comparison of overfitting and overtraining. Journal of chemical information and computer sciences 35 (5):826-833
72. Gibbs MN (1998) Bayesian Gaussian processes for regression and classification. Citeseer,
73. Djolonga J, Krause A, Cevher V High-dimensional gaussian process bandits. In: Advances in Neural Information Processing Systems, 2013. pp 1025-1033
74. Neal RM (2012) Bayesian learning for neural networks, vol 118. Springer Science & Business Media,
75. Denil M, Shakibi B, Dinh L, De Freitas N Predicting parameters in deep learning. In: Advances in neural information processing systems, 2013. pp 2148-2156
76. Bashiri M, Geranmayeh AF (2011) Tuning the parameters of an artificial neural network using central composite design and genetic algorithm. Scientia Iranica 18 (6):1600-1608
77. Hemmati V (2017) Investigation of weathering effects on performance of intumescent coatings used in fire protection of wood structures. ProQuest Dissertations Publishing,
78. Bahrani B (2015) Effects of weathering on performance of intumescent coatings for structure fire protection in the wildland-urban interface. The University of North Carolina at Charlotte,
79. Childs PRN, Childs PRN, Greenwood JR, Greenwood JR, Long CA, Long CA (2000) Review of temperature measurement. Review of Scientific Instruments 71 (8)
80. Beck JV, Hurwicz H (1960) Effect of Thermocouple Cavity on Heat Sink Temperature. Journal of Heat Transfer 82 (1):27-36. doi:10.1115/1.3679876
81. Bradley D, Matthews KJ (1968) Measurement of High Gas Temperatures with Fine Wire Thermocouples. Journal of Mechanical Engineering Science 10 (4):299-305. doi:10.1243/jmes_jour_1968_010_048_02
82. Vollmer M, Klaus-Peter M (2010) Infrared thermal imaging: fundamentals, research and applications. John Wiley & Sons,
83. Evans DD, Emmons HW (1977) Combustion of wood charcoal. Fire Safety Journal 1 (1):57-66. doi:http://dx.doi.org/10.1016/0379-7112(77)90008-X
84. Kansa EJ, Perlee HE, Chaiken RF (1977) Mathematical model of wood pyrolysis including internal forced convection. Combustion and flame 29:311-324
85. Bennini S, Castillo S, Traverse J (1991) Effects of an intense thermal flux on a lignocellulosic material. Journal of analytical and applied pyrolysis 21 (3):305-314
86. Urbas J, Parker WJ (1993) Surface temperature measurements on burning wood specimens in the cone calorimeter and the effect of grain orientation. Fire and Materials 17 (5):205-208
87. Urbas J, Parker WJ, Luebbers GE (2004) Surface temperature measurements on burning materials using an infrared pyrometer: accounting for emissivity and reflection of external radiation. Fire and materials 28 (1):33-53

88. Manzello SL, Park S-H, Cleary TG (2009) Investigation on the ability of glowing firebrands deposited within crevices to ignite common building materials. Fire Safety Journal 44 (6):894-900. doi:http://dx.doi.org/10.1016/j.firesaf.2009.05.001
89. Hurley MJ, Gottuk DT, Hall Jr JR, Harada K, Kuligowski ED, Puchovsky M, Torero JL, Watts Jr JM, Wieczorek CJ (2016) SFPE Handbook of Fire Protection Engineering.
90. Mortensen A (2006) Concise Encyclopedia of Composite Materials. Elsevier Science,
91. White RH, Dietenberger MA (2001) Wood Products: Thermal Degradation and Fire A2 - Buschow, K.H. Jürgen. In: Cahn RW, Flemings MC, Ilschner B, Kramer EJ, Mahajan S, Veyssière P (eds) Encyclopedia of Materials: Science and Technology (Second Edition). Elsevier, Oxford, pp 9712-9716. doi:https://doi.org/10.1016/B0-08-043152-6/01763-0
92. Basic principles of non-contact temperature measurement. www.optris.com/optris-downloads
93. Babrauskas V (2002) Ignition of wood: a review of the state of the art. Journal of Fire Protection Engineering 12 (3):163-189